M A S T E R ' S T H E S I S

D I P L O M A R B E I T

Artificial ground freezing in cohesive soils at the underground station "Schottenring" – experimental study on ice-lens formation

Künstliche Bodenvereisung in bindigen Böden bei der U-Bahn Station "Schottenring" – Experimentelle Untersuchung der Eislinsenbildung

ausgeführt zum Zwecke der Erlangung des akademischen
Grades eines Diplom-Ingenieurs

unter der Leitung von
Univ.Doz. Dipl.-Ing. Dr.techn. Roman Lackner
E202 - Institut der Mechanik für Werkstoffe und Strukturen (IMWS)
der Technischen Universität Wien (TU Wien)

eingereicht an der Technischen Universität Wien
Fakultät für Bauingenieurwesen

von

Elisabeth Gudrun Aigner
Matr.-Nr.: 0025507
Meissnergasse 8/2/14
A - 1220 Wien

Wien, im September 2005 . . . . . .

Unser Wissen ist kritisches Raten.
Sir Karl Raimund Popper

Danksagung

Im Folgenden möchte ich einer Vielzahl von Personen danken, die wesentlich an der Entstehung dieser Diplomarbeit beteiligt waren.
Diese Diplomarbeit stellt eine Fortsetzung der Arbeit von Dipl.-Ing. Andreas Kloiber dar. Er hat wesentlich zur Entwicklung und zum Bau der Prüfmaschine für die in dieser Diplomarbeit durchgeführten Versuche beigetragen und mich am Anfang der Versuchsserie tatkräftig unterstützt.
O.Univ.Prof Dipl.-Ing. Dr.techn. Dr.h.c.mult. Herbert Mang Ph.D., Univ.Prof. Dipl.-Ing. Dr.techn. Josef Eberhardsteiner und Univ.Doz. Dipl.-Ing. Dr.techn. Roman Lackner möchte ich danken, dass ich am Institut für Mechanik der Werkstoffe und Strukturen der TU Wien meine Diplomarbeit verfassen konnte. Meinem Betreuer, Univ.Doz. Dipl.-Ing. Dr.techn. Roman Lackner, gebührt besondern Dank, seine Vorschläge und Ideen lieferten einen wichtigen Beitrag für das Gelingen dieser Arbeit.
Motiviert durch die Durchführung der Bodenvereisung im Zuge der Verlängerung der U-Bahnlinie U2/1 "Schottenring", Wien, sollte im Rahmen dieser Diplomarbeit die Bildung von Eislinsen untersucht werden, was durch die Unterstützung von Herrn Hon.-Prof. Dipl.-Ing. Dr.techn. Lothar Martak, Herrn Dipl.-Ing. Thomas Herzfeld und Frau Dipl.-Ing. Petra Drucker auch reibungslos gelang. Sie ermöglichten mir einen Einblick in das Bauvorhaben zu gewinnen, halfen bei der Entnahme der zu untersuchenden Bodenproben auf der Baustelle, und bei der Entwicklung des Versuchsprogrammes. Insbesondere möchte ich Herrn Hon.-Prof. Dipl.-Ing. Dr.techn. Lothar Martak danken, der mir bei etwaigen Fragen und sonstigen Anliegen immer tatkräftig zur Seite stand.
Während meiner Arbeit im Labor unterstützten mich Dipl.-Ing Dr.techn. Martin Fleischmann, Ing. Christian Schmid, und das Laborpersonal des Institutes für Mechanik der Werkstoffe und Strukturen. Diese Zeit möchte ich nicht missen.

Ein großes Dankeschön gilt meiner Familie, auf dessen Unterstützung ich immer zählen konnte. Besonders meine Eltern Gertrude und Ing. Mag. Dr. Johann Aigner trugen wesentlich zu meiner akademischen und beruflichen Entwicklung bei.
Meinem Freund Andreas Kratochvill danke ich ganz besonders. Er begleitete mich durch die wesentlichen Jahre meines Studiums und stand mir immer mit Rat und Tat zur Seite. Bei ihm konnte ich die nötige Erholung und Ruhe finden um mich immer wieder neu zu motivieren.
Dank gilt auch all jenen Personen, die mir, in welcher Form auch immer, hilfreich zur Seite standen, hier jedoch nicht namentlich erwähnt wurden.

Kurzfassung

Durch das Gefrieren von Porenwasser in gesättigten bzw. teilweise gesättigten Böden kommt es zu einer Verbesserung der mechanischen Eigenschaften (Steifigkeit, Festigkeit, Kriechverhalten) des Bodens. Die dadurch erhaltene erhöhte Belastbarkeit wird zum Beispiel bei der künstlichen Bodenvereisung im Zuge von Tunnelvortrieben genutzt. Hierbei stellt der gefrorene Bodenkörper eine temporäre Stützmaßnahme dar, die nach Fertigstellung der Tunnelröhre durch Auftauen wieder entfernt wird. Bei der künstlichen Bodenvereisung in feinkörnigen (tonig/schluffigen) Böden kommt es aufgrund der erhöhten Kapillarwirkung zur Bildung von Eislinsen, die zu beachtlichen Hebungen führen können. Zusätzlich zu den, am Beginn der Gefrierarbeiten unbekannten Hebungen kann die erhebliche Konsistenzverringerung des aufgetauten Bodens zu ungewollten Setzungen führen.
Im Rahmen dieser Diplomarbeit wurden die Hebungs- und Setzungseigenschaften von gefrierenden und auftauenden tonigen Schluffen, die an der Baustelle U2/1 "Schottenring" (Wien) entnommen wurden, experimentell untersucht. Neben dem experimentellen Teil der Diplomarbeit wurden die maßgebenden Vorgänge im Boden während der Gefrierphase beschrieben, wobei besonders auf zeitliche Prozesse, wie Abkühlrate, Wärmeleitung, Wassertransport und die jeweiligen charakteristischen Zeitmaßstäbe eingegangen wurde.

Mit den auf der Baustelle entnommenen Bodenproben wurden Frost- und Tauversuche mit einer am Institut der Mechanik der Werkstoffe und Strukturen der TU Wien entwickelten Apparatur durchgeführt. Die Abkühlung der unbelasteten Proben erfolgte an der Oberseite der Probe, wobei die Temperatur an der Unterseite konstant auf +11 °C gehalten wurde.
Zusätzlich zu Abkühlversuchen, bei denen die Temperatur an der Oberseite der Probe mit verschiedenen Abkühlraten $\dot{T}$ [°C/h] reduziert wurde, wurden Frost/Tau-Versuche durchgeführt.
Während der Versuchsdurchführung wurde die vertikale Verformung (Frosthebung) der Bodenprobe über einen Wegaufnehmer gemessen. Zusätzlich wurden Temperatursensoren in regelmäßigen Abständen über die Probenhöhe eingebaut um die Temperaturentwicklung in der Probe und somit die aktuelle Lage der 0 °C Isotherme während des Versuchs verfolgen zu können.
Änderungen in den Abkühlraten zeigten deutliche Unterschiede in der zeitlichen Entwicklung der Frosthebung und in der Temperaturverteilung über die Probenhöhe. Letztere war bei schnellem Abkühlen durch einen höheren räumlichen Gradienten im Bereich der Oberseite der Probe gekennzeichnet. Dieser erhöhte Gradient, der sich im Zuge des Versuchs abschwächte, spiegelte sich

in der Hebungsentwicklung wieder. So kam es am Beginn des Gefrierens zu einem rasanten Anstieg der Hebung (hohe Hebungsrate), die sich jedoch im Laufe des Versuches ebenfalls abschwächte. Bei langsamen Kühlraten war ein linearer Anstieg der Frosthebung zu beobachten. Das Abklingen der Frosthebung, das auch bei langsamen Kühlraten beobachtet wurde, konnte durch das Verschieben der 0 °C Isotherme in die Eislinse zufolge Hebung (geometrischer Effekt) erklärt werden.
Dem beobachteten Zusammenhang zwischen Temperaturgradient und Frosthebung wurde durch die Bestimmung des Segregationspotentials SP für die untersuchten Böden Rechnung getragen. In der Tat ergab die Auswertung von SP zu dem Zeitpunkt an dem die letzte (dicke) Eislinse in der Probe zu wachsen beginnt - dieser Zeitpunkt entspricht dem Zeitpunkt des Erreichens der stationären Temperaturverteilung in der Probe - für die untersuchten Böden ähnliche Ergebnisse für verschiedene Abkühlraten. Die abschließend durchgeführte Dimensionsanalyse für den Vereisungsversuch ergab erste Einblicke über den möglichen Zusammenhangs zwischen dem empirisch gefundenen SP und bodenspezifischer Parameter.

Abstract

Freezing of pore water in saturated and partially saturated soil results in an improvement of the mechanical properties (stiffness, strength, creep behavior) of soil. This increased load-carrying capacity of the frozen soil is exploited during artificial ground freezing in underground excavation. Hereby, the frozen soil serves as temporary support, which is removed on completion of the tunnel tube by thawing. During artificial ground freezing in cohesive (clayey/silty) soils, the high capillary action results in the formation of ice lenses, leading to severe frost heave. In addition to the unknown frost heave at the beginning of freezing, the reduction of the soil consistency during thawing may led to unwanted settlements.
In this thesis, the heave and settlement behaviour of clayey silt subjected to freezing and thawing was investigated. The soil samples were extracted at the construction site U2/1 "Schottenring" (Vienna). In addition to the experimental work, the essential processes in freezing soil were described, focusing on transient processes, such as cooling, temperature and water flow, as well as on their characteristic time scales.

The soil samples extracted from the construction site were used to conduct freezing and thawing experiments on a setup developed at the Institute for Mechanics of Materials and Structures at TU Wien. Cooling of the unloaded samples was performed at the top surface, while the temperature at the bottom surface of the cylindrical sample was held constant at +11 °C.
In addition to the freezing experiments characterized by a reduction of the temperature at the top surface of the sample by different cooling rates, freez/thaw experiments were conducted.
During the experiment, the vertical displacement of the top surface (frost heave) of the soil sample was measured. Moreover, the temperature was monitored by four sensors located at different heights within the soil sample. A modification of the cooling rate resulted in differences in the history of the frost-heave and in the temperature distribution over the sample height. At fast cooling rates, the latter was characterized by a high spatial gradient in the top area of the sample. This rather high gradient, which decreased in the course of the experiment, was reflected in the evolution of the frost heave, characterized by a significant increase in the frost heave at the beginning of freezing (high heave rate). At low cooling rates, on the other hand, a linear increase of frost heave was observed until the stationary temperature state in the sample was reached. The decrease of the frost-heave rate, also observed for low cooling rates, was explained by the movement of the 0 °C isotherm into the ice lens as a result of heave (geometrical effect).

The observed correlation between the temperature gradient and the frost heave motivated the determination of the segregation potential SP for the investigated soils. In fact, the analysis of SP at the time instant when the final (thicker) ice lens starts to form - i.e., this time instant when the temperature distribution in the sample reaches the stationary state - gave similar results for various cooling rates. Finally, the conducted dimensional analysis of the performed freezing experiment provided first insights into the correlation between the empirically introduced SP and soil-specific parameters.

Contents

1 Motivation **1**

2 Basics **4**
2.1 The unfrozen water content 4
2.2 Water flow in freezing soil 9
2.3 The segregation potential 13

3 Frost-heave experiments **15**
3.1 State of the art 15
3.2 Testing equipment at the IMWS at TU Wien 23
3.3 Materials 23
3.4 Presentation of results 28

4 Discussion **36**
4.1 Temperature distribution in soil sample 36
4.2 Water transport within soil sample 42
4.3 Segregation potential 43

5 Summary and concluding remarks **52**

Chapter 1

Motivation

Freezing of capillary water in porous media, such as soil, is observed in permafrost regions, where the temperature remains below 0 °C for two or more years, during seasonal frost characterized by frost/thaw cycles in overlying ground-surface layers, and during artificial ground freezing. The latter is used for groundwater control and as (temporary) excavation support in ground construction work. It takes advantage of the increasing mechanical strength and decreasing permeability in consequence of freezing of the capillary water. Soil is a composite material composed of solid particles, water, and air. When subjected to temperatures below 0 °C, ice is introduced as fourth material phase, while some water remains liquid in the shape of thin water films surrounding the soil particles. This amount of unfrozen water decreases with decreasing temperature and depends on the soil properties such as the specific surface. In addition to the change of mechanical and transport properties during freezing, the 9 % volume increase of water during freezing results in macroscopic dilation. This dilation, however, is marginal compared to deformations caused by the formation of ice lenses with thicknesses up to several centimeters, causing frost heave and damage on surface infrastructure (see Figure 1.1).
The formation of ice lenses results from the continuous transport of water towards the area where freezing takes place (see Figure 1.2). This transport depends on the change in the flow potential at the location of freezing and the transport properties of the unfrozen soil. As regards e.g. pavement

(a)  (b) 

Figure 1.1: Damage of pavement caused by (a) the formation of ice lenses and (b) frost/thaw cycles

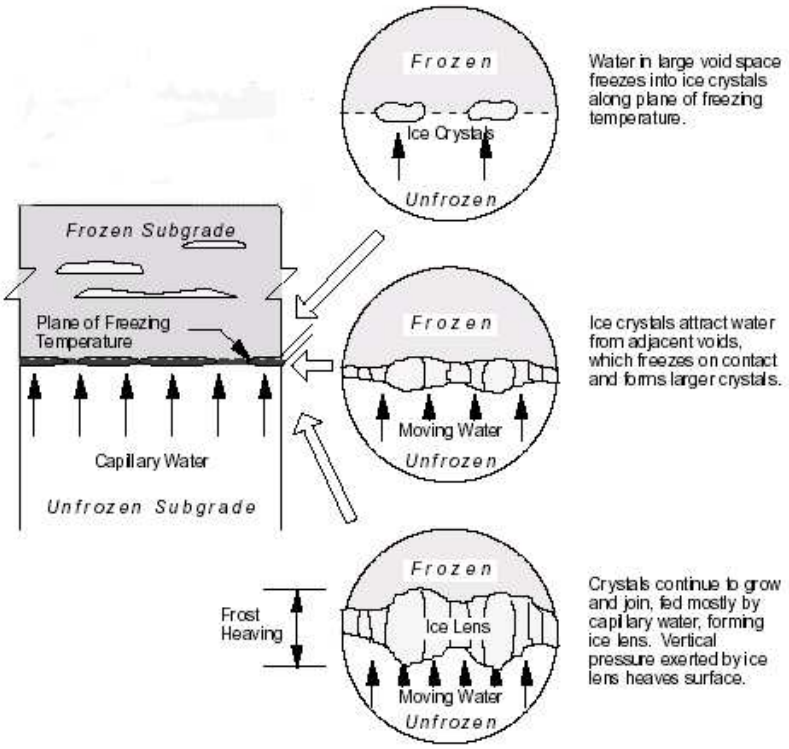

Figure 1.2: Illustration of ice-lens formation in soils (WAPA 2002)

engineering, the Casagrande criterion [1] and the mineral criterion [2] are standardly used for assessing the risk of ice-lens formation. Whereas the materials used for pavement construction may be adopted to meet the mentioned criteria, the material composition is defined by the geological conditions met at construction sites in case of artificial ground freezing. As regards the latter, only the freezing rate (temperature history in the freezing pipes) can be optimized with respect to minimization of ice-lens formation. So far, the effect on the freezing rate on the ice-lens formation and, hence, the specification of an optimal temperature history in the freezing pipes is still unsolved and a topic of ongoing research.
In this thesis, the effect of the cooling rate and the properties of cohesive soil on the ice-lens formation is investigated experimentally. The following chapter provides the basics for freezing of water in porous media, comprising the unfrozen water content and the transport of water in the course of ice-lens formation. Chapter 3 contains a description of the experimental work performed within this thesis, starting with an overview of frost-heave experiments reported in the literature. Thereafter, the experimental setup available at the laboratory of the IMWS at TU Wien is described and the obtained results are presented. In Chapter 4, the obtained results are discussed, highlighting the factors influencing the formation of ice lenses. Finally, a summary and concluding remarks on the freezing work at the underground construction site "Schottenring" are given in Chapter 5.

[1] The Casagrande criterion for identifying potentially frost susceptible soils states that under natural freezing conditions and with sufficient water supply considerable ice segregation could be expected in (a) non-uniform soils containing more than 3% of grains smaller 0.02 mm and (b) very uniform soils containing more than 10% of grains smaller 0.02 mm. No ice segregation takes place in soils with less than 1% of grains smaller 0.02 mm.

[2] The mineral criterion is an important part of the evaluation process of frost susceptibility concerning base materials for road construction in Austria. As a function of the grain-size distribution, it defines mineralogical limiting values for the grain fraction smaller than 0.02 mm.

Chapter 2

Basics

2.1 The unfrozen water content

The unfrozen water content is the amount of liquid water in a soil at a given sub-zero temperature. Even when cooled below 0 °C, some water in porous media remains unfrozen in the form of thin, liquid layers on the particle surfaces. Accordingly, frozen soil becomes a four-phase medium, consisting of soil particles, water, air, and ice.
The presence of this layer of unfrozen water is explained by the interfacial free energies for ice-solid γ_{is}, ice-water γ_{iw}, and water-soil γ_{ws}, with

$$\gamma_{is} > \gamma_{iw} + \gamma_{ws} \ [\mathrm{J/m^2}] \ . \tag{2.1}$$

The thickness of the aforementioned layers of unfrozen water and, thus, the amount of unfrozen water depends on the temperature and decreases with decreasing temperature. In addition to the temperature, soil properties such as the pore-size distribution and the specific surface area influence the amount of unfrozen water. The smaller the particles and, thus, the higher specific surface area, the higher the amount of unfrozen water. Several techniques have been developed to determine the unfrozen water content:

1. **Differential scanning calorimetry (DSC):**

   Differential scanning calorimetry allows determination of enthalpy changes associated with freezing/thawing processes. The unfrozen water content is obtained by integrating the area between an interpolated base line and the peak of the thermogram and comparison with the absorbed energy of 1 mg melting water (see Figure 2.1).

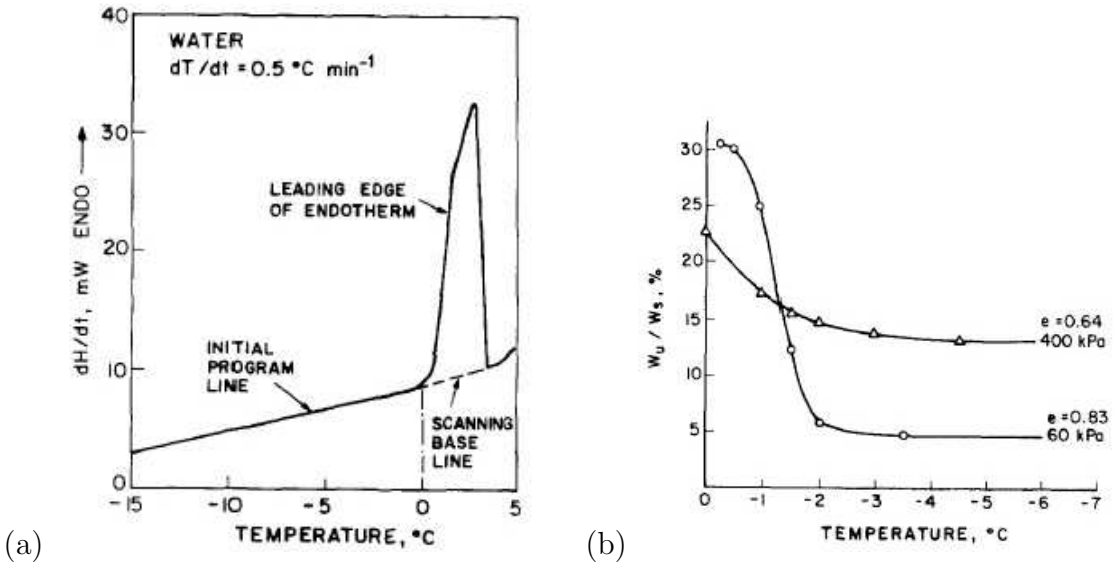

(a) (b)

Figure 2.1: (a) DSC thermogram for pure water and (b) unfrozen water content as a function of the temperature for Devon clayey silt with two different void ratios e (Konrad 1990)

2. **Pulsed nuclear magnetic resonance (NMR):**

   The proton of water bears a slight magnetic moment originating from its spin and acts as magnet that tends to align along a fixed external magnetic field. The magnetic moment re-orients when a pulse is applied to a sample set in a fixed magnetic field and it returns to the initial direction when the pulse is eliminated. During NMR, the change in magnetic field is measured by voltage decay with time, referred to as free-induction decay (FID). The FID peak value is proportional to the number of protons of water and ice in the sample. The FID signal resulting from ice, however, decreases much faster than the signal corresponding to liquid water, giving access to the amount of liquid water (see Figure 2.2).

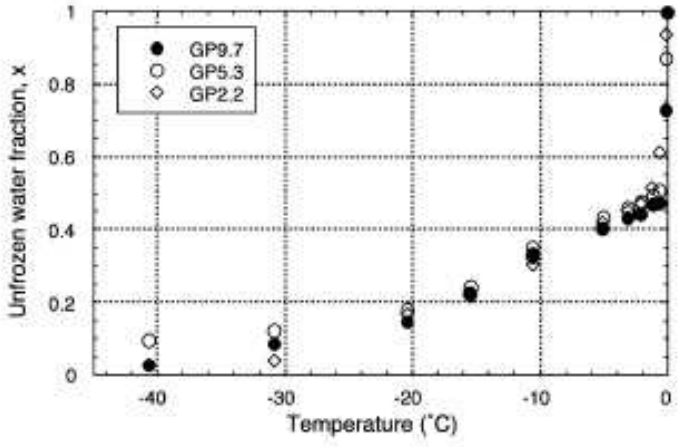

Figure 2.2: Unfrozen water fraction in glass powders with an initial water content of 80 % (Watanabe et al. 2002)

3. **Capacitive method:**

   The capacity method exploits the difference between the dielectric constant of liquid water, air, and minerals (Fen-Chong at al. 2004).

   The local spatial redistribution of polarized electrical charges in a material sample under an applied electric field is characterized by its dielectric constant. The dielectric property describes the ability to store electrical potential energy under the influence of an electrical field, relative to that of air:

$$\epsilon* = \epsilon - i\epsilon_r, \tag{2.2}$$

   where the real part ϵ [F/m, Farad per meters] behaves like an ideal insulator and characterizes the degree of electric polarisability of the material. The imaginary component ϵ_r [F/m], on the other hand, is associated with the electric energy dissipation into heat. The dielectric constants of water, air, and minerals are considered to be constant, and equal to 1 for water and air, and range from 2 to 10 for solids.

   A linear calibration curve between the resonant frequency $\overline{\nu}$ [MHz] and the capacity C [F] is obtained from different commercial ceramic capacitors. For each sample of known geometry and water content, $\overline{\nu}$ is recorded and turned into C [F]. C is related to the sample dielectric constant using the relation $C = F\epsilon$, where F [m] is a geometrical factor, which in case of a plate condensator equals $F = A/d$, where A

is the area of the plates arranged by a distance d. Finally, the dielectric constant gives access to the amount of liquid water in the sample (see Figure 2.3).

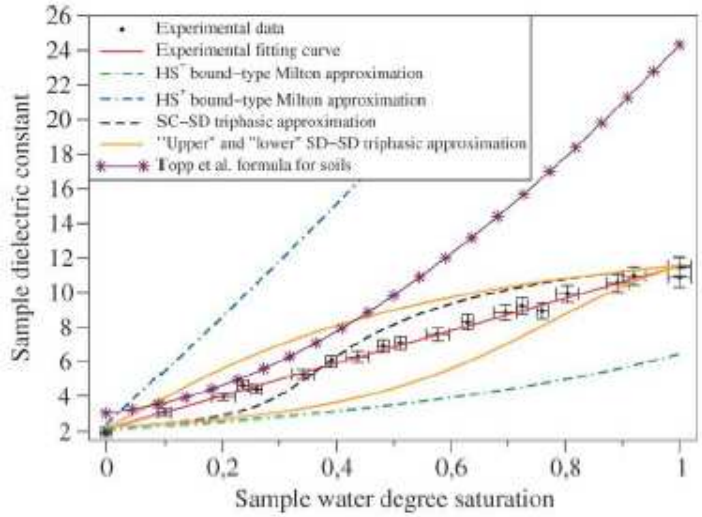

Figure 2.3: Sample dielectric constant ϵ [F/m] as a function of water saturation (Fen-Chong et al. 2004).

4. **Time domain reflectrometry (TDR):**

   This method also relies on the dielectric constant. However, in contrast to the determination of the dielectric constant by the capacitive method, it is determined from the propagation velocity of electromagnetic waves through the sample. The pulse generator of the TDR unit provides a small step voltage with a rise time of 110 picoseconds. The dielectric constant is determined from the TDR trace. The dielectric constant is measured for various temperatures. A variation in this constant is a response to the accompanying variation in unfrozen water content (see Figure 2.4).

All described measurement techniques are used to establish empirical relations for the unfrozen water content, e.g.,

$$w_u = \alpha |T|^{\beta} \ [\%], \tag{2.3}$$

where α and β are soil parameters and T [°C] is a sub-zero temperature. Typical values for α and β are given in (Andersland 1994) and (Jessberger and Jagow-Klaff 2001), see also Figure 2.5.

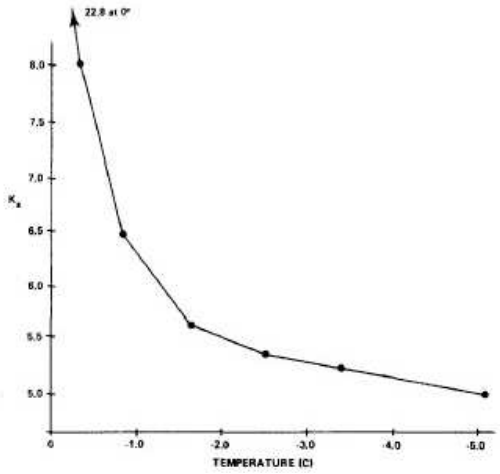

Figure 2.4: Variation of dielectric constant with temperature for Castor silt (Patterson and Smith 1980)

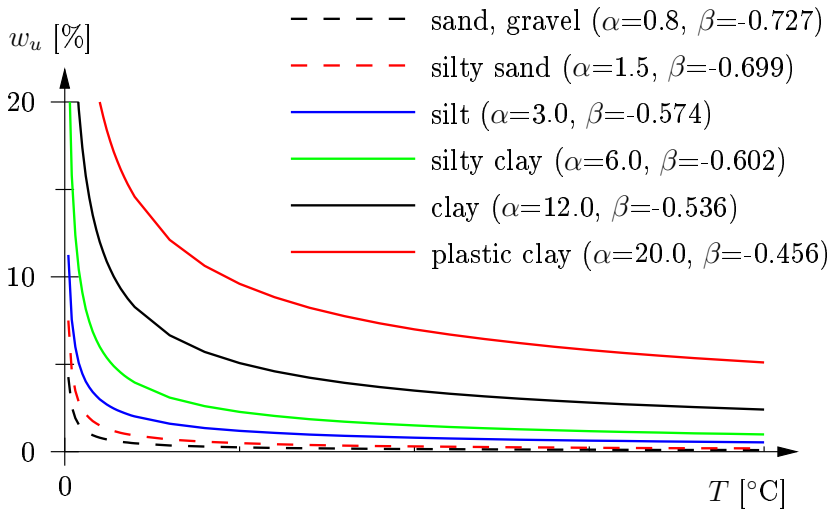

Figure 2.5: Unfrozen water content w_u [%] for different types of soil according to (Jessberger and Jagow-Klaff 2001)

2.2 Water flow in freezing soil

Within freezing soil, three regions are standardly distinguished: (i) the completely frozen zone, (ii) the unfrozen zone, and (iii) a partially frozen region between them, referred to as the frozen fringe (see Figure 2.6).

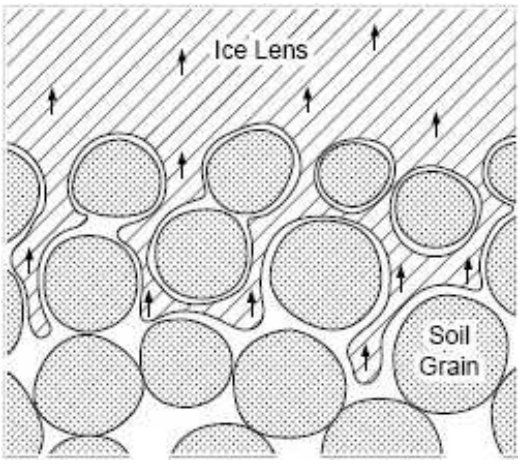

Figure 2.6: Schematic illustration of the frozen fringe [after (O'Neill and Miller 1985)]

For the formation of ice lenses, the water flow within the unfrozen soil towards the frozen fringe is of essential importance. This water flow may be described by a modified form of Darcy's law, reading

$$v_w = -k\frac{\partial \Psi}{\partial z}, \tag{2.4}$$

where v_w [m/s] is the flow velocity of water, k [m/s] is the hydraulic conductivity, and Ψ [m] is the total potential for the water flow.
The total potential for water flow consists of the total water potential Φ and the chemical potential μ, reading

$$\Psi = \Phi + \mu \ . \tag{2.5}$$

The total water potential itself consists of the gravitational potential Φ_g, the pressure potential Φ_p, the osmotic potential Φ_o, and the capillary potential Φ_{cap}.

$$\Phi = \Phi_g + \Phi_p + \Phi_o + \Phi_{cap} \ \ [\text{Pa}] \ , \tag{2.6}$$

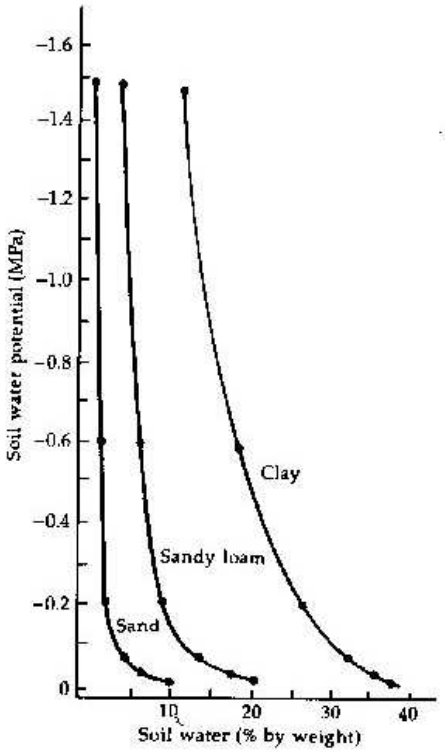

Figure 2.7: Plot of total soil water potential as a function of the water content (University of Colorado 2004)

Figure 2.7 shows the total water potential for various soil types as a function of the water content [1]. The different contributions to the total potential appearing in Equation (2.6) and their impact in the case of freezing soil are described in the following:

1. **Gravitational potential**

   The gravitational potential is related to the vertical position z [m], reading

   $$\Phi_g(z) = \rho_w \times g \times z \quad [\text{Pa}] \,, \tag{2.7}$$

   with $\rho_w = 1.00$ kg/m^3 as the density of water and $g = 9.81$ m/s^2 as the gravitation.

[1] The dimensions of the total water potential appearing in Equations (2.4) and (2.5) is either [Pa] or [m]. The dimensions are easily changed using 1 Pa = 0.102 m.

2. **Pressure potential**

The pressure potential considers the water flow in consequence of pressure variations within the water phase, with

$$\Phi_p[p(z)] = p(z_1) - p(z_2) \text{ [Pa]} , \tag{2.8}$$

where $p(z_1)$ is the pressure at a coordinate z_1, and $p(z_2)$ is the pressure at a coordinate z_2. At atmospheric pressure, the water potential equals zero.

3. **Osmotic potential**

The osmotic potential takes the presence of solutes in soil water into account, reading

$$\Phi_o = - RT \times C_s \text{ [Pa]} \tag{2.9}$$

where $R = 8.314$ [J/(mol K)] is the universal gas constant, T [K] is the absolute temperature, and C_s [mol/m^3] is the solute concentration.

4. **Capillary potential**

Capillarity is an effect associated with molecular forces at the interface between phases and is the major driving force of water flow towards the frozen fringe. The pressure difference between two phases α and β connected to an interface is given by the Laplace equation:

$$p_\alpha - p_\beta = \frac{2\gamma_{\alpha\beta}}{r_{\alpha\beta}} , \tag{2.10}$$

with $\gamma_{\alpha\beta}$ [J/m^2] is the surface tension and $1/r_{\alpha\beta}$ [1/m] represents the curvature of the interface. In the course of freezing, new interfaces, i.e., the water-ice interfaces are introduced, starting with a rather small radius during nucleation of ice crystalls (see Figure 2.8). According to Equation (2.10), the pressure difference between ice and water becomes

$$p_i - p_w = \frac{2\gamma_{iw}}{r_{iw}} \tag{2.11}$$

with $\gamma_{iw} = 28 \times 10^{-3}$ J/m^2 is the surface tension at the ice-water interface [see, e.g., (Luo et al.2005)].

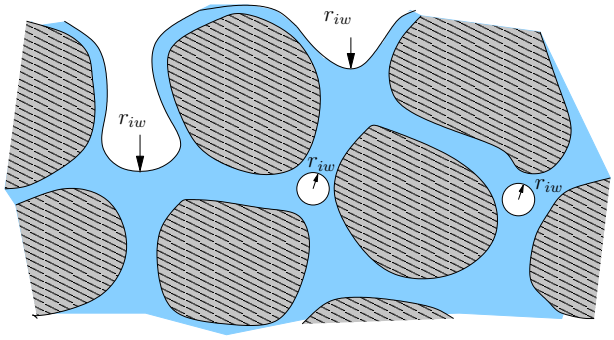

Figure 2.8: Introduction of new interfaces in the course of freezing

5. Chemical potential

Fluid flow takes place from regions of high chemical potential to regions with low chemical potential. Figure 2.9 shows the chemical potential as a function of temperature. Water has a higher chemical potential than ice and a flow into the cold region takes place.

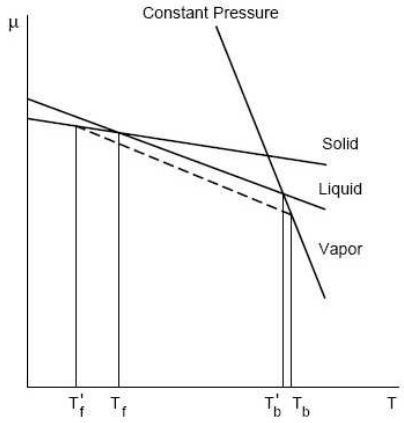

Figure 2.9: Chemical potential μ [J/mol] as a function of temperature for a pure solvent (solid lines) and in case a solute is present (dashed line) (Castellan 1998).

The concept of soil water potential is limited. Potential, for example, takes no explicit account of the effect of temperature on the total energy change of a system. Fortunately another function, called "free energy", was invented in the fields of thermodynamics. This new field relates to a new potential, called chemical potential. Freezing results in a change of the Gibbs free energy ΔG [kJ/kg], reading

$$\Delta G = \Delta H - T\Delta S, \tag{2.12}$$

with an enthalpy change ΔH of -334 kJ/(kg water). In Equation (2.12), T [°C] is the temperature, and S [kJ/°C kg] is the entropy. In highly exothermic reactions, such as freezing, the term $T\Delta S$ has little influence on the change of Gibbs free energy.

The chemical potential μ_j [J/mol] represents the ability of the substance j to activate physical and chemical processes and corresponds to the change in Gibbs free energy by the relation

$$\mu_i = \left(\frac{\partial G}{\partial n_i}\right)_p \tag{2.13}$$

where n [mol] is an infinitesimal amount of substance, p is the pressure.

2.3 The segregation potential

In 1980, Konrad and Morgenstern presented a frost-heave model, assuming the frozen soil behind the ice lens as passive with regard to water flow and taking the flow of water towards the frozen fringe into account. They introduced the so-called segregation potential SP [m^2/s/°C], which relates moisture migration rate v [m/s] to the temperature gradient in the frozen soil near the 0 °C isotherm, reading

$$v = SP \text{ grad } T. \tag{2.14}$$

The situation at the frozen fringe is illustrated in Figure 2.10, showing characteristic distributions fot the temperature T [°C], the permeability k [m/s], and the suction p [Pa]. Hereby p_w and p_u consider the suction at the bottom of the ice-lens or rather at the frost front, and T_i and T_{so} are the temperatures at the bottom of the ice lens and at the frost front respectively.

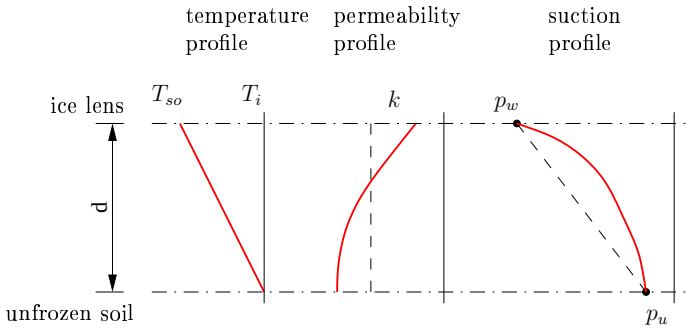

Figure 2.10: Distribution of temperature, permeability, and suction in the frozen fringe (solid lines: correct distributions; dashed lines: simplified distributions) after (Konrad and Morgenstern 1980)

Chapter 3

Frost-heave experiments

3.1 State of the art

The main difficulty in frost-heave experiments lies in the monitoring of the different processes taking place and their interaction described by in thermo-hygro-chemo-mechanical couplings (see Figure 3.1).

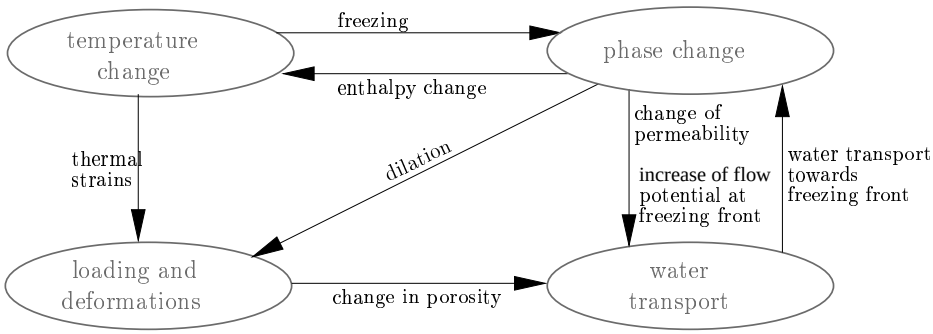

Figure 3.1: Illustration of processes and couplings taking place during frost-heave experiments

Basically, frost-heave experiments reported in the literature can be divided into two categories: On the one hand, experiments aim to reproduce on-site conditions as good as possible by taking the different processes and couplings into account. On the other hand, experiments are designed to focus on one or two couplings, leaving not involved processes aside (e.g., unloaded experiments neglecting the effect of mechanical loading).
Results from loaded freezing experiments are reported in (Hermansson 2004). The employed setup (see Figure 3.2) consists of two Perspex tubes with an inner diameter of 122 mm. One of the tubes, the suction tube, is 480 mm long and the other tube, the cap, is 200 mm long. A sample is placed into

the suction tube and the cap is put over the suction tube such that the lid of the cap rests on the sample. A cooling element is situated on the lid of the cap. The suction tube rests in a water bath with constant temperature. In order to simulate ground pressure, weights are placed on the top of the cooling element.

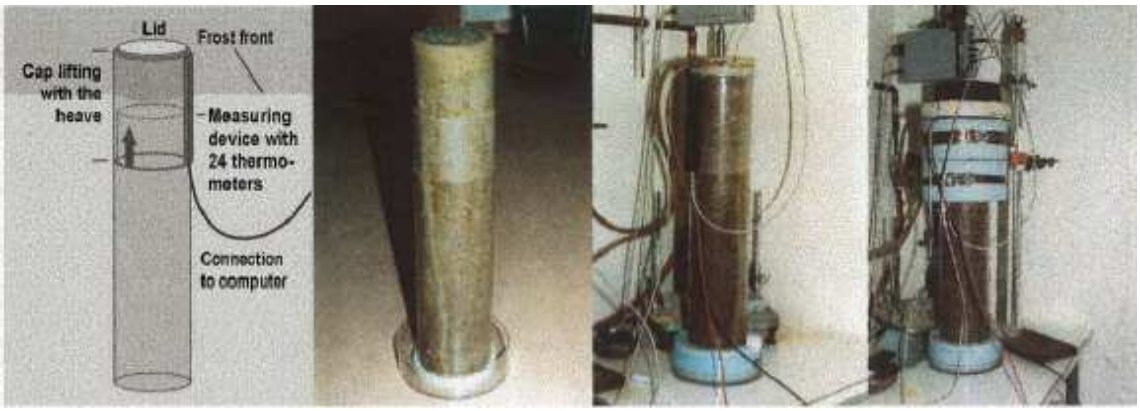

Figure 3.2: Experimental setup proposed in (Hermansson 2004)

Results of two experiments on undisturbed naturally saturated silt are reported in (Hermansson 2004):

1. The first experiment, characterized by frost-penetration rates between 20 and 50 mm/day for the different freeze/thaw-cycles shows that frost depth and frost heave increase almost linearly as the temperature is reduced in the cooling element (see Figure 3.3 and Table 3.1). By increasing the temperature after cooling, the sample returns to approximately the same height after every cycle. The large variation in frost penetration rate monitored during the experiments is only slightly reflected by the heave rate, which is about 0.22 mm/h for a frost penetration rate of 20 mm/day and 0.25 mm/h for a frost penetration rate of 50 mm/day.

2. The second experiment, characterized by a change of the cooling rate every fifth hour between a high and a low level, shows that the changes in the cooling rate influence the heave rate (see Figure 3.4).

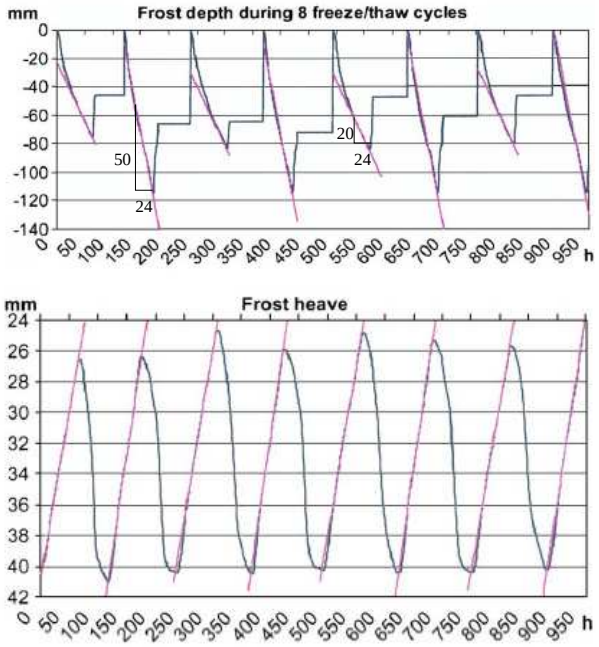

Figure 3.3: History of frost depth [mm] and frost heave [mm] for different frost penetration rates for eight freeze/thaw cycles reported in (Hermansson 2004) (frost penetration rate = 20 and 50 mm/day)

cycle no.	frost-penetration rate [mm/day]	heave rate [mm/h]
1	20	0.215
2	50	0.245
3	20	0.220
4	50	0.255
5	20	0.220
6	50	0.255
7	20	0.215
8	50	0.245

Table 3.1: Rate of frost penetration and heave reported in (Hermansson 2004)

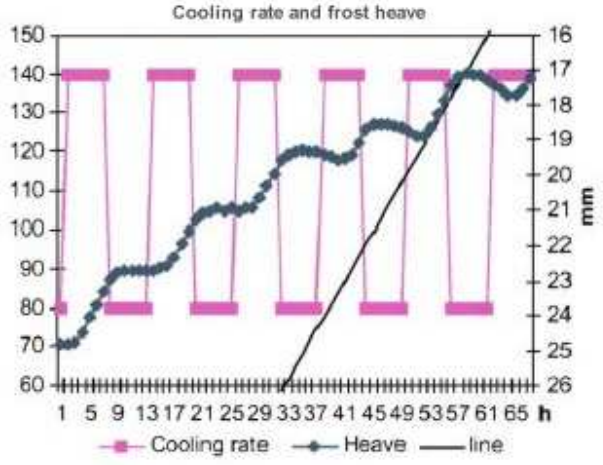

Figure 3.4: History of cooling rate [°C/day] and frost heave [mm] reported in (Hermansson 2004) (slope of line corresponds to heave rate of 0.4 mm/h)

In (Penner, 1986), a test equipment, originally designed at Northern Engineering Services in Calgary with heat exchangers at both ends of the sample is described (see Figure 3.5). The setup consists of a frost cell with a diameter and height of 100 mm. Water is supplied from the top of the cell and cooling is performed at the bottom. Freezing of the sample takes place from the bottom upwards.
Results obtained from the freezing experiments employing this frost cell are shown in Figure 3.6 for soils with a clay content of 29 and 41 mass-% [1] . The starting temperatures at the bottom and the top of the sample were -0.35 °C and 0.55 °C, respectively. X-ray was used to determine the position of the ice lenses. The cooling rates for the experiments were 0.000417, 0.00083, 0.002083, and 0.00417 °C/h, giving a progress of the 0 °C isotherm of 0.0458, 0.0917, 0.229, and 0.458 mm/h. Only the frost penetration rates of 0.0458 and 0.0917 mm/h resulted in the formation of ice lenses of a suitable size for X-ray photographs. The results show that both heave rate and water intake changed during the growth period of a lens. The growth rate increased rapidly at the beginning of the experiment, followed by a protected period of decreasing growth.
A similar experimental setup was used by Konrad (1988), focusing on the effect of the cooling history on frost heave. Figure 3.7 shows the history of the frost heave for a step-like (constant temperature at both the bottom and the

[1]The soils considered in the experimental study of this thesis have a clay content of 27% (see Table 3.4).

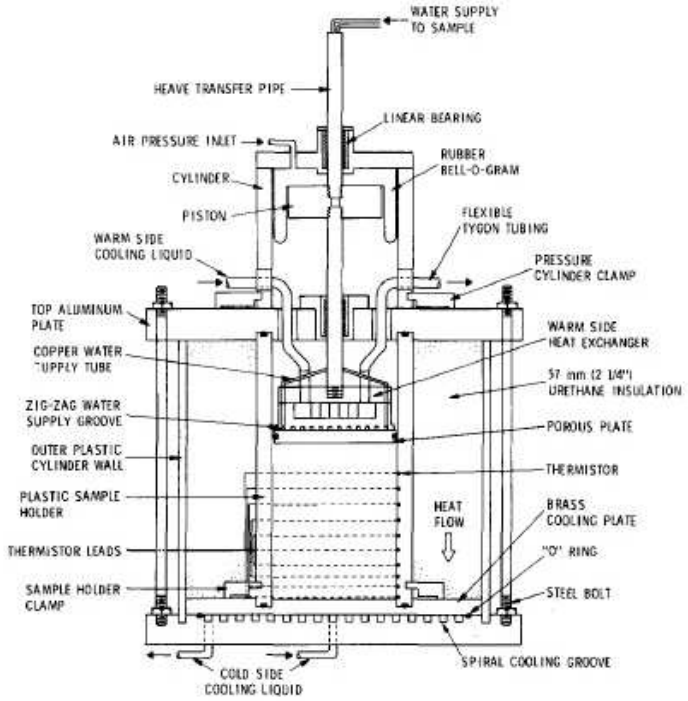

Figure 3.5: Frost cell according to Penner (1986)

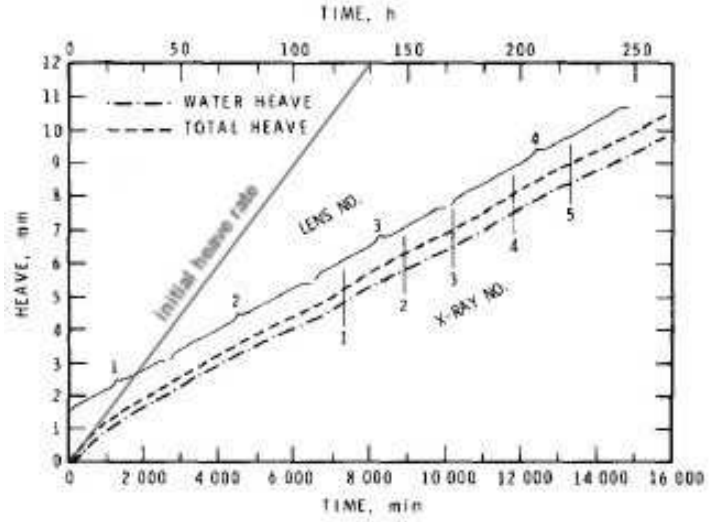

(a)

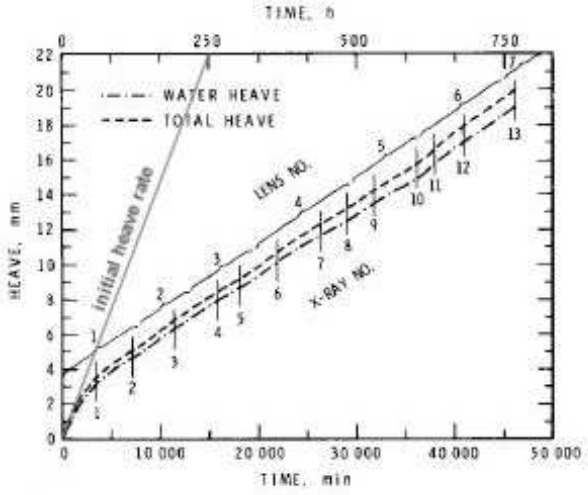

(b)

Figure 3.6: History of frost heave [mm] reported in (Penner 1986): soil with a clay content of (a) 29 mass-% (cooling rate = 0.02 °C/day) and (b) 41 mass-% (cooling rate = 0.01 °C/day) (specimen height = 100 mm)

top of the soil sample) and a continuous (ramped) decrease of the temperature at the bottom of the sample. The test conditions are summarized in Table 3.2. The results show that the highest heave rate is obtained for step freezing. However, as the temperature distribution approaches the stationary situation (with grad T reducing to 0.06 °C/mm), the heave rate decreases. In case of ramp cooling with 0.035 °C/h and 0.0208 °C/h, the temperature at the bottom side of the sample continuously decreases, resulting in an increasing temperature gradient and, thus, in an increasing heave rate. For a smaller cooling rate, characterized by smaller frost penetration rates, the heave rate decreases and becomes almost constant for a cooling rate of 0.00083 °C/h.

test Nr.	type of cooling	cooling rate [°C/h]	grad T [°C/mm]	frost-penetration rate [mm/h]
1	ramped	0.035	0.033	1.458
2	ramped	0.0208	0.012	1.417
3	ramped	0.00083	0.0095	0.0917
4	step	variable	variable	variable

Table 3.2: Freezing-test conditions reported in (Konrad 1988) (for the step-like decrease, the temperatures are - 4 °C and 2 °C at the cold and warm side of the sample, respectively)

Padilla et al. (1997) also used a similar apparatus to verify a finite element (FE) calculation with laboratory data. The FE program, developed by Padilla and Villeneuve (1992), takes water flow, and heat and solute transport in saturated and non-saturated soils into account, and allows simulation of the formation of ice lenses in granular and clayey soils. The unknowns of the underlying FE formulation are the capillary pressure, the temperature, and the solute concentration in the liquid water. After having reached a saturated state, the samples with a height of 160 mm were subjected to a temperature of -6 °C at the top and +4 °C at the bottom. Characteristic curves for this experiments are shown in Figure 3.8. The growth rate of each sample decreases with time.

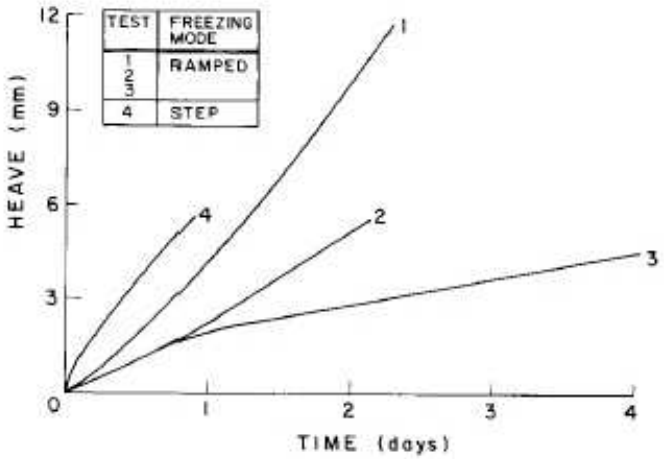

Figure 3.7: History of frost heave of clayey silt with 29 mass-% clay content according to Konrad (1988) (specimen height = 100 mm)

(a)

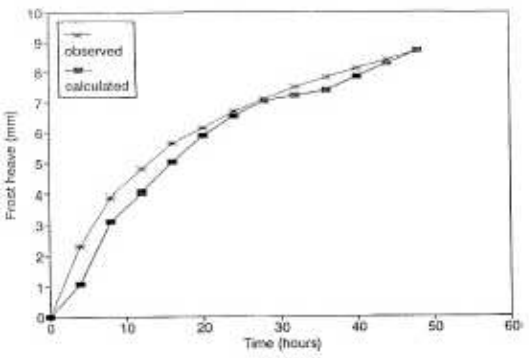

(b)

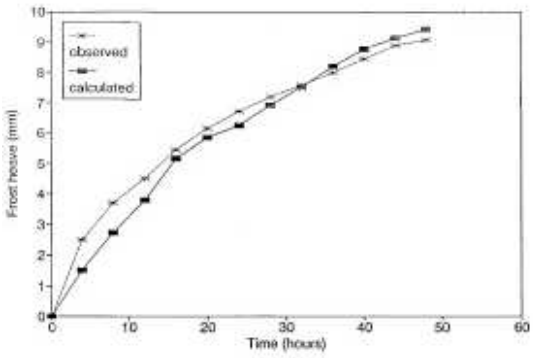

Figure 3.8: History of frost heave for a granular fill with a porosity of (a) 12 % and (b) 33 % and varying grading curves according to Padilla et al. (1997) (specimen height = 160 mm).

3.2 Testing equipment at the IMWS at TU Wien

In contrast to the previously described experimental setups, the testing equipment employed in this thesis was used to conduct unloaded experiments, thus eliminating the effect of stresses on thermal, hygral, and phase-change processes. Hereby, soil samples with a diameter of 50 mm and a height of 100 mm (Figure 3.9) were isolated in the radial direction by styrodur. The sample is placed on a non-woven material, with its bottom face submerged into a water bath with constant temperature. The top surface of the specimen is connected to a cooling device. The latter is used to simulate the temperature change in the freezing pipes during artificial ground freezing. The temperature in the samples is continuously monitored by four temperature sensors located 20, 40, 60, and 80 mm above water level (see Figure 3.10). The frost heave is measured by a displacement gauge fixed to the cooling plate at the top of the specimen.

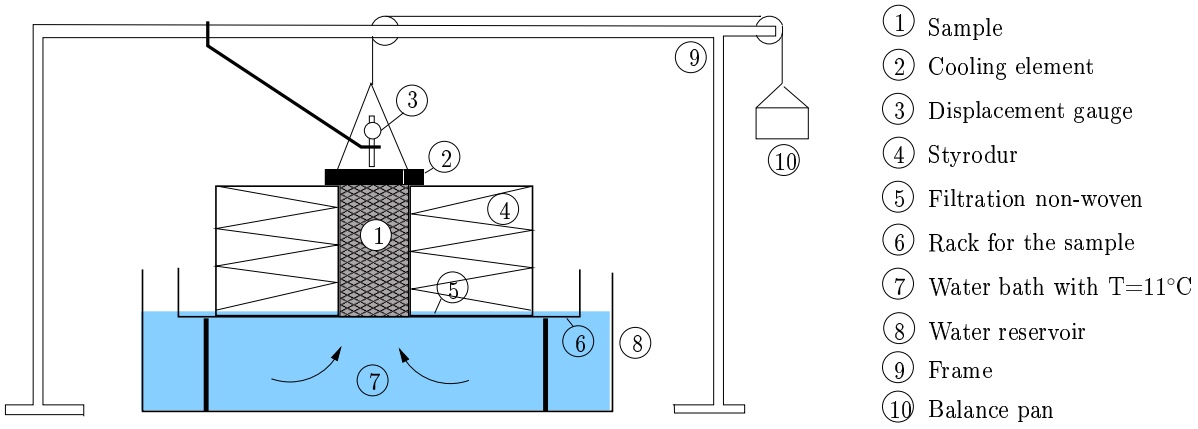

Figure 3.9: Setup for unloaded frost-heave experiments conducted in this thesis

3.3 Materials

The material investigated in this thesis was provided by the construction site U2/1 "Schottenring", Vienna, where artificial ground freezing was performed in order to minimize surface settlements during tunnel excavation and, hence, to avoid damage of historical buildings (see Figure 3.11).
For the experimental work, material was extracted three times from different locations within the two silt layers indicated in Figure 3.12 (in the following

(a)  (b) 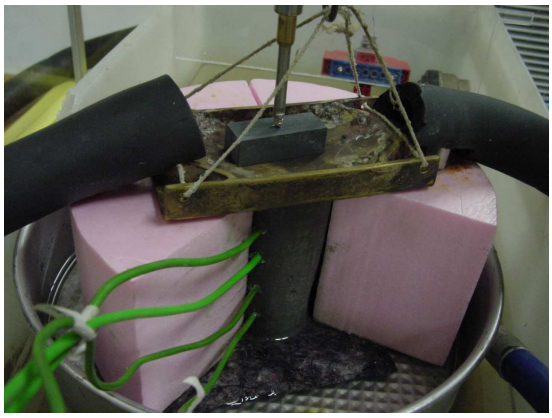

Figure 3.10: (a) Preparation of soil specimen after Kloiber (2004) and (b) specimen with temperature sensors placed onto non-woven material

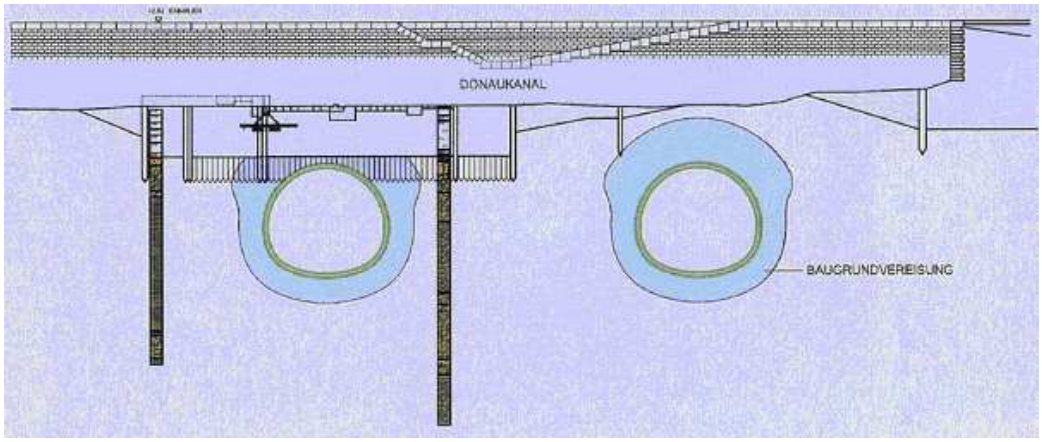

Figure 3.11: Cross-section of the ground freezing construction site U2/1 "Schottenring", Vienna, Austria

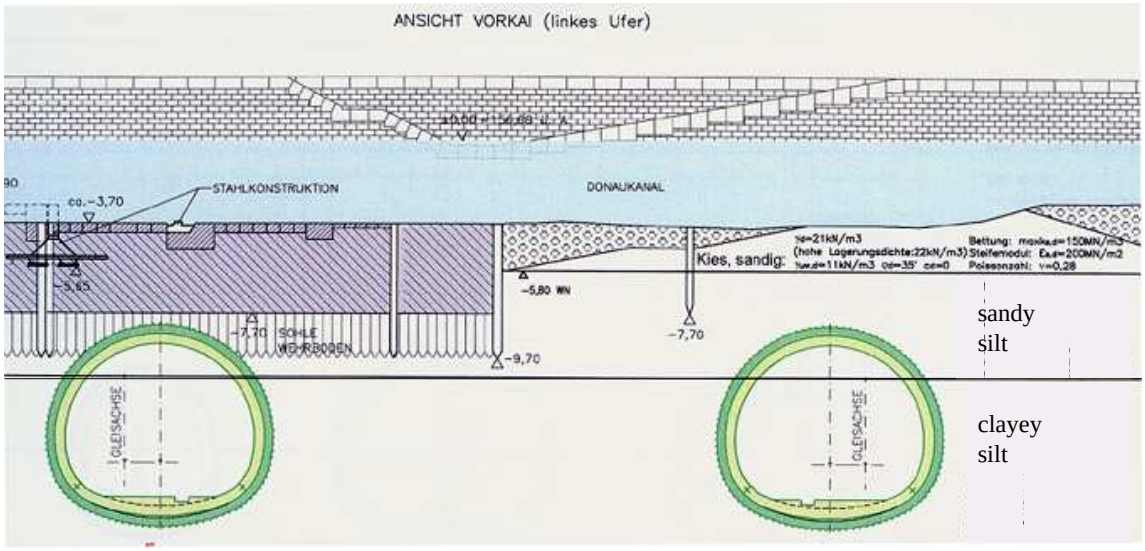

Figure 3.12: Geological conditions at the construction site

referred to as "silt 1" to "silt 3"). In these layers, soil freezing is performed prior and during excavation of the underground station tubes. Characteristic values of the extracted materials are listed in Table 3.3. The respective grading curves are depicted in Figure 3.13. In addition to the characteristic values of the soil and the grading curves, the mineralogy was analyzed in cooperation with Prof. Ottner and Karl Potz (both from the University of Natural Resources and Applied Life Sciences, Vienna), see Table 3.4. The clay fraction of all silts is characterized by a high smectite [2] content.

[2]Smectite is a three-layer silicate. The electrostatic forces between the layers are able to store water. The mineral is able to swell, with a volume increase up to eight times of its initial volume.

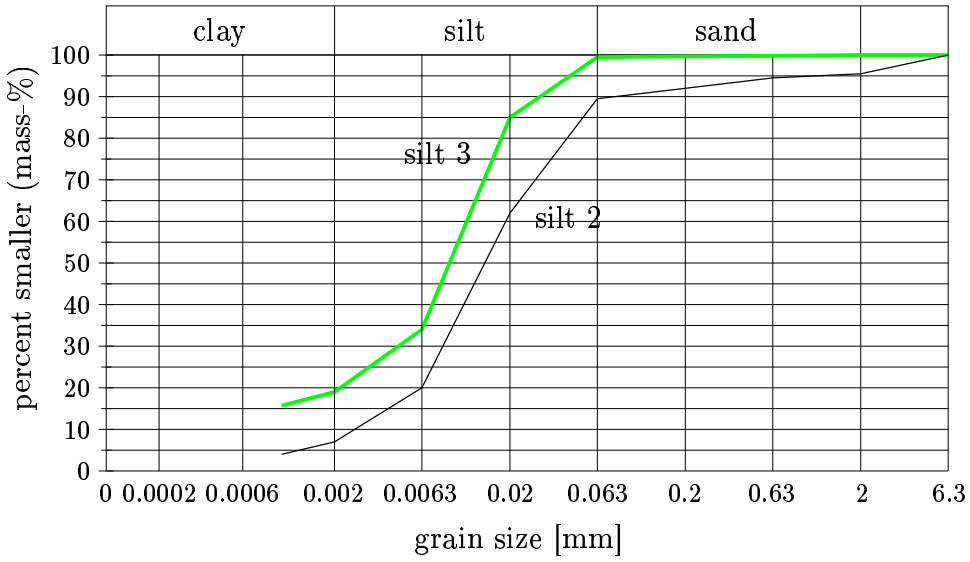

(a)

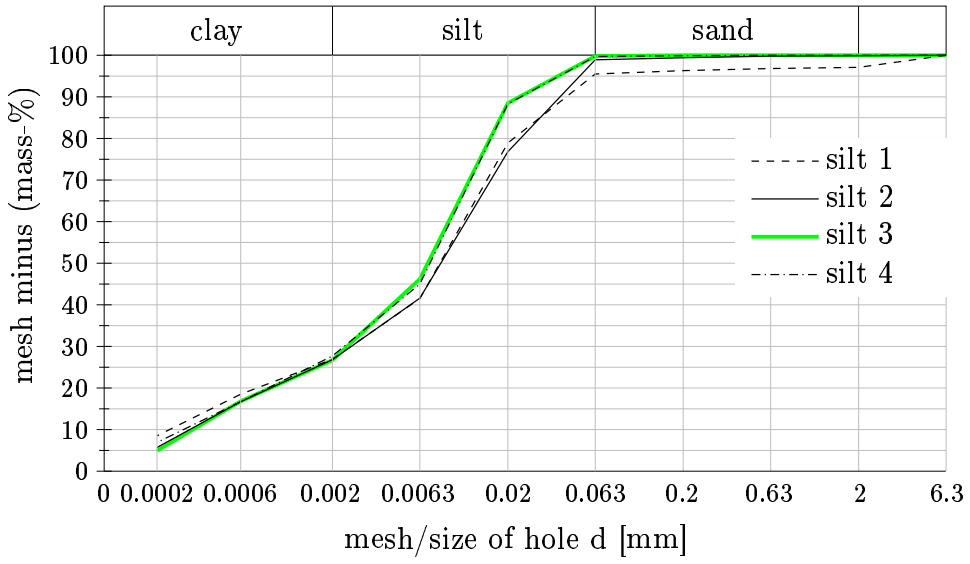

(b)

Figure 3.13: Grading curves of investigated silts obtained at (a) TU Wien and (b) University of Natural Resources and Applied Life Sciences, Vienna

	silt 1	silt 2	silt 3
density of solid particles ρ_s	2.74 g/cm^3	2.73 g/cm^3	2.74 g/cm^3
density ρ	2.02 g/cm^3	1.96 g/cm^3	2.02 g/cm^3
density of dry soil ρ_d	1.63 g/cm^3	1.61 g/cm^3	1.63 g/cm^3
water content w	24.0 %	22.0 %	24.0 %
porosity $n = 1$ - ρ_d/ρ_s	0.405	0.410	0.405
liquid limit w_l	46.0 %	49.5 %	46.0 %
plasticity limit w_p	27.0 %	28.0 %	27.0 %
plasticity index I_p	19.0 %	21.5 %	19.0 %

Table 3.3: Characteristic values for the investigated silts

silt	mass-% of clay	mass-% in the whole sample			
	in the whole sample	smectite	illite	kaolinite	chlorite
1	26.9 %	16 %	5 %	3 %	3 %
2	26.8 %	16 %	6 %	3 %	3 %
3	26.7 %	17 %	5 %	2 %	2 %

silt	mass-% in the clay fraction			
	smectite	illite	kaolinite	chlorite
1	60.0 %	20.0 %	10.0 %	10.0 %
2	58.0 %	22.0 %	10.0 %	10.0 %
3	62.0 %	20.0 %	9.0 %	9.0 %

Table 3.4: Mineralogy of the investigated silts and mineralogy within clay fraction of the investigated silts according to Potz (2005)

3.4 Presentation of results

In order to investigate the influence of the cooling procedure on the ice-lens formation and on the permanent deformations after a frost/thaw cycle, three types of freezing experiments were conducted in the course of this thesis. While the temperature of the water bath was always kept constant at +11 °C (which corresponds to the average water temperature at the bottom of the Danube channel, see Subsection 3.3), the temperature at the top of the sample was prescribed, depending on the type of experiment (see also Data-Sheets in Appendix A);

1. **One-step cooling experiments:**

   The temperature in the cooling element is reduced from +11 °C to −15 °C with a specified cooling rate $\dot{T}$ [°C/h] and, thereafter, held constant for 48 hours. Experiments with cooling rates of 50 °C/h, 1 °C/h, and 0.4 °C/h were conducted.

   For a cooling rate of 50 °C/h, high heave rates $\dot{u}$ [mm/h] are observed when the frost front penetrates into the soil sample (see Figure 3.14 and Table 3.8), followed by a period of decreasing growth. The decrease of the frost heave rate, as indicated in Figure 3.14, is explained by the shift of the 0 °C isotherm towards the ice lens as the soil sample gains height and the temperatures at the bottom and the top of the sample remain constant. For the theoretical case of the 0 °C isotherm being always at the lower boundary of the ice lens, the ice lens should grow constantly. The frost-heave history obtained for the three tested silts is comparable (see Figures 1 to 7, Figures 9 to 13, Figures 20 to 23, and Figure 27 in Appendix A). The properties of Silt 2, however, result in a delay in the ice-lens formation. Some samples (mainly for Silt1 and Silt 3) show significant radial deformations in the unfrozen (bottom) part of the sample, resulting in a collapse which is reflected by a decrease of the frost heave (see Figures 2, 5, 18, 21, and 24 in Appendix A). Although the initial water content for all considered soils are at the same level, the final water content for the frozen part of the sample is higher for Silt 1 and Silt 3 (see Figure 3.15), corresponding to the observed heave rates.

   The frost heave obtained from freezing experiments with small cooling rates (0.4 and 1 °C/h) increase almost linearly with time, characterized by the formation of several thin ice lenses. After reaching the stationary

(linear) temperature state in the sample, the growth of one thicker ice lens begins and the heave rate decreases in consequence of the afore mentioned shift of the 0 °C isotherm.

2. **Two-step cooling experiments:**

   The temperature in the cooling element is reduced from +11 °C to −10 °C within 30 minutes (cooling rate: 50 °C/h), held constant for 24 hours, reduced to −15 °C and, finally, held constant for another 24 hours.

   Two-step experiments were conducted in order to observe the formation and position of ice lenses for varying locations of the 0 °C isotherm (see Data-Sheets for Samples 12, 19, 21, and 32). The obtained results show the formation of thick ice lenses at each location of the 0 °C isotherm of the stationary temperature distribution corresponding to each of the two sub-zero temperature levels at the top of the samples. Thus, two thick ice lenses developed. The heave in consequence of the formation of the second thick ice lens adds to the heave curve of the first ice lens. The heave rates at the beginning of the freezing process and at the stationary case are given in Figure 3.14 and Table 3.6.

3. **Freeze/thaw experiments:**

   The temperature in the cooling element is reduced from +11 °C to −15 °C within 40 minutes (cooling rate: 50 °C/h), held constant for 72 hours, raised to +11 °C and, finally, held constant for 48 hours (see Data-Sheets for soil samples 13 to 17, 22, and 31 in Appendix A).

   Whereas the freezing process is similar to the one-step experiments, the thawing process causes melting of the formed ice lens within a few hours. During the thawing process, the height of the soil sample decreases almost linearly. After melting of the entire sample, a deformation of 2 to 4 mm remained, which is explained by extensive swelling of clayey phases in the lower part of the sample. In the bottom (unfrozen) part of the soil samples exhibiting a freeze/thaw cycle, the consistency number [3] decreases significantly in consequence of the

[3]The consistency number $I_C = (w_L - w)/I_P$ (w_L: liquid limit, I_P: plasticity index) defines the condition of the soil, with $I_C \leq 0$: liquid, $0 \leq I_C \leq 0.5$: mushy, $0.5 \leq I_C \leq 0.75$: soft, $0.75 \leq I_C \leq 1$: stiff, $1 \leq I_C \leq S$: semisolid, $S \leq I_C$: compact.

water intake during ice-lens formation. In the upper part, the blocking of water transport by the frozen soil and the ice lens yielded a lower reduction of the consistency number (see Table 3.5).

Figures 9 to 13, 18, and 27 show the temperature history in the sample during thawing. The endotherm process of the melting process, resulting in a delay of the temperature increase, can be clearly seen in the temperature records of the sensors.

sample no. (silt)	water content w [%]	liquid-limit [%]	plastic-limit [%]	plasticity-index [%]	consistency-number
13(2)	28.0 / 32.7 / 34.1	49.5	28.0	21.5	1.00 / 0.78 / 0.72
14(2)	26.3 / 30.3 / 31.0	49.5	28.0	21.5	1.08 / 0.90 / 0.86
15(2)	27.2 / 30.6 / 33.3	49.5	28.0	21.5	1.04 / 0.88 / 0.76
16(2)	27.4 / 32.4 / 32.9	49.5	28.0	21.5	1.03 / 0.79 / 0.77
17(2)	27.7 / 33.9 / 32.9	49.5	28.0	21.5	1.01 / 0.72 / 0.77
22(3)	24.7 / 30.3 / 36.6	46.0	27.0	19.0	1.12 / 0.83 / 0.50
31(3)	26.8 / 31.2 / 36.2	46.0	27.0	19.0	1.01 / 0.78 / 0.52

Table 3.5: Variation of the consistency number I_C for freeze/thaw experiments [before freezing / after thawing (top) / after thawing (bottom)]

sample no. (silt)	type of experiment (cooling rate [°C/h])	heave rate $\dot{u}_1$ [mm/h] (t_1 [h])	$\dot{u}_2$ [mm/h] (t_2 [h])
12 (2)	two-step experiment (50)	0.95 (0.6)	0.14 (18)
19 (2)	two-step experiment (50)	0.97 (0.5)	0.17 (18)
21 (3)	two-step experiment (50)	1.85 (0.6)	0.45 (18)
32 (3)	two-step experiment (50)	1.41 (0.5)	0.38 (18)

Table 3.6: Heave rate at the beginning of ice formation ($\dot{u}_1$) and after having reached the stationary (linear) temperature distribution ($\dot{u}_2$) for two-step experiments with a cooling rate of 50 °C/h

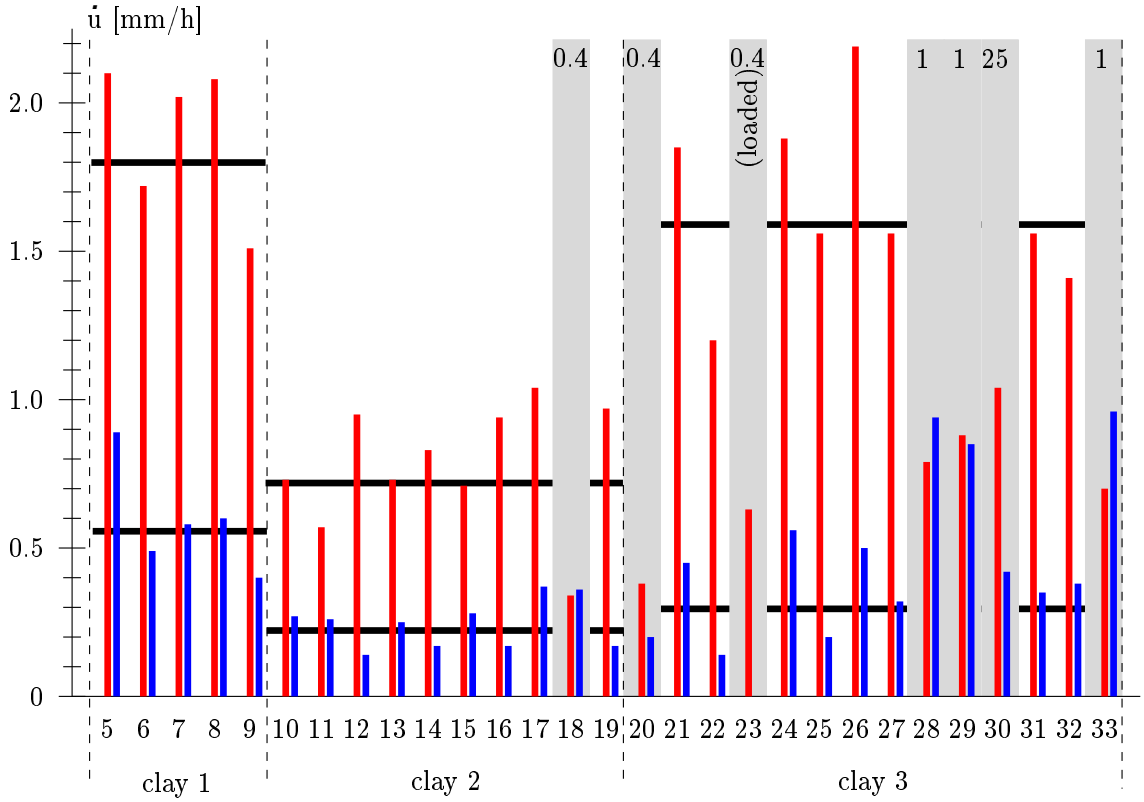

Figure 3.14: Heave rate $\dot{u}$ [mm/h] at the onset of freezing (red) and when the temperature has reached its final (linear) distribution (blue)

sample no. (silt)	type of experiment (cooling rate [°C/h])	heave rate $\dot{u}_1$ [mm/h] (t_1 [h])	$\dot{u}_2$ [mm/h] (t_2 [h])
28 (3)	one-step experiment (1.0)	0.79 (12.7)	0.94 (29)
29 (3)	one-step experiment (1.0)	0.88 (12.7)	0.85 (29)
33 (3)	one-step experiment (1.0)	0.70 (12.7)	0.96 (29)

Table 3.7: Heave rate at the beginning of ice formation ($\dot{u}_1$) and after having reached the stationary (linear) temperature distribution ($\dot{u}_2$) for one-step experiments with a cooling rate of 1 °C/h

sample no. (silt)	type of experiment (cooling rate [°C/h])	heave rate $\dot{u}_1$ [mm/h] (t_1 [h])	$\dot{u}_2$ [mm/h] (t_2 [h])
5 (1)	one-step experiment (50)	2.10 (0.4)	0.89 (18)
6 (1)	one-step experiment (50)	1.72 (0.5)	0.49 (18)
7 (1)	one-step experiment (50)	2.02 (0.6)	0.58 (18)
8 (1)	one-step experiment (50)	2.08 (0.3)	0.60 (18)
9 (1)	one-step experiment (50)	1.51 (0.1)	0.40 (18)
10 (2)	one-step experiment (50)	0.73 (0.1)	0.27 (18)
11 (2)	one-step experiment (50)	0.57 (0.1)	0.26 (18)
13 (2)	freeze/thaw-experiment (50)	0.73 (0.5)	0.25 (18)
14 (2)	freeze/thaw-experiment (50)	0.83 (0.5)	0.17 (18)
15 (2)	freeze/thaw-experiment (50)	0.71 (0.6)	0.28 (18)
16 (2)	freeze/thaw-experiment (50)	0.94 (0.5)	0.28 (18)
17 (2)	freeze/thaw-experiment (50)	1.04 (0.5)	0.37 (18)
24 (3)	one step experiment (50)	1.88 (0.5)	0.56 (18)
25 (3)	one step experiment (50)	1.56 (0.5)	0.20 (18)
26 (3)	one step experiment (50)	2.19 (0.5)	0.50 (18)
27 (3)	one step experiment (50)	1.56 (0.5)	0.32 (18)
31 (3)	freeze/thaw-experiment (50)	1.56 (0.5)	0.35 (18)

Table 3.8: Heave-rate at the beginning of ice formation ($\dot{u}_1$) and after having reached the stationary (linear) temperature distribution ($\dot{u}_2$) for one-step experiments and freeze/thaw-experiments with a cooling rate of 50 °C/h

sample no. (silt)	type of experiment (cooling rate [°C/h])	heave rate $\dot{u}_1$ [mm/h] (t_1 [h])	$\dot{u}_2$ [mm/h] (t_2 [h])
18 (2)	one-step experiment (0.4)	0.34 (34)	0.36 (68)
20 (3)	one-step experiment (0.4)	0.33 (34)	0.24 (68)

Table 3.9: Heave rate at the beginning of ice formation ($\dot{u}_1$) and after having reached the stationary (linear) temperature distribution ($\dot{u}_2$) for one-step experiments with a cooling rate of 0.4 °C/h

In order to determine the water intake during the freezing experiments, the weight of each soil sample was measured prior and after the experiment. As regards the latter, the weight of the frozen and unfrozen part was measured separately. After drying at 105 °C, the dry weight of the soil sample m_d is obtained, finally giving access to the initial water content,

$$w = \frac{m(\text{prior to freezing}) - [m_d(\text{frozen part}) + m_d(\text{unfrozen part})]}{m_d(\text{frozen part}) + m_d(\text{unfrozen part})} \quad , \quad (3.1)$$

and the water content of the frozen and unfrozen part after the experiment:

$$w_{frozen} = \frac{m_f(\text{frozen part}) - m_d(\text{frozen part})}{m_d(\text{frozen part})} \quad (3.2)$$

and

$$w_{unfrozen} = \frac{m_f(\text{unfrozen part}) - m_d(\text{unfrozen part})}{m_d(\text{unfrozen part})} \; . \quad (3.3)$$

In Equations (3.1) to (3.3), m [g], m_d [g], and m_f [g] represent the initial mass, the dry mass, and the wet mass of the soil. The so-obtained water contents are summarized in Table 3.10 and Figure 3.15.

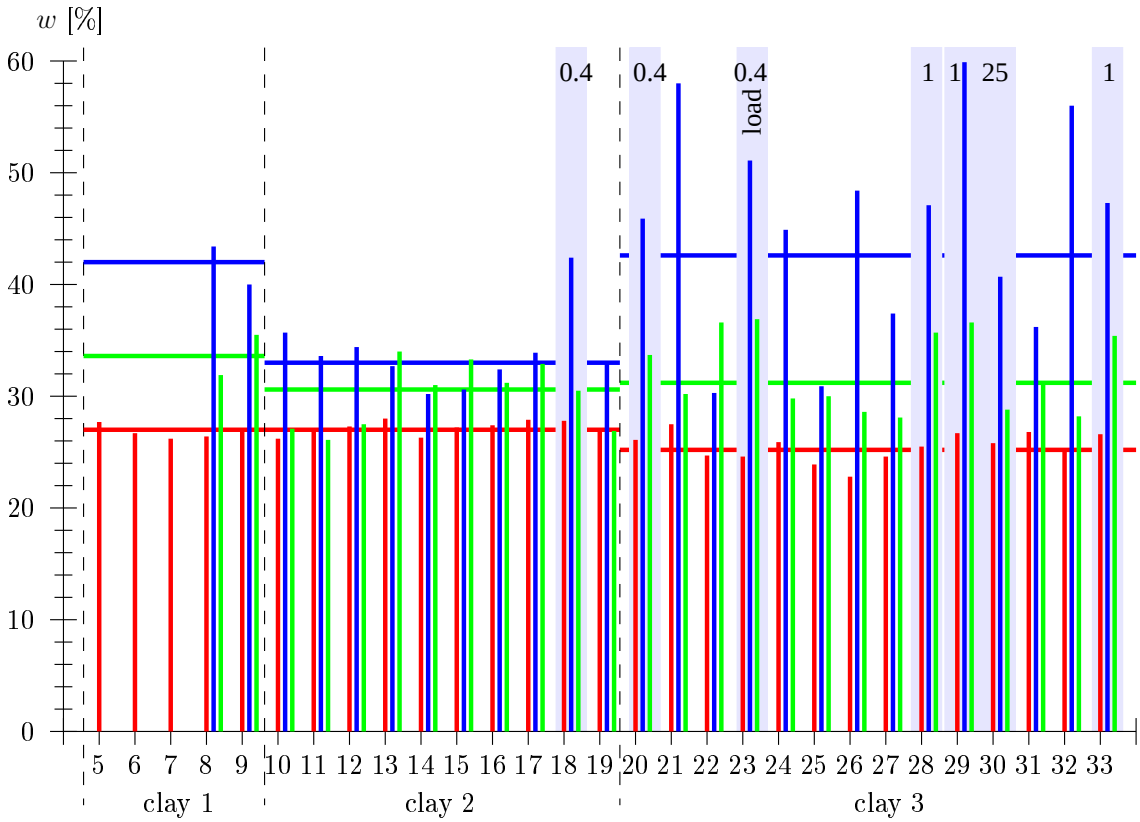

Figure 3.15: Water content w [%] (red: initial water content; blue: water content in the frozen (top) part after the freezing experiment; green: water content in the unfrozen (bottom) part after the freezing experiment)

sample no. (silt)	type of experiment (cooling rate [°C/h])	temperature of cooling device [°C]	water content w [%]
5 (1)	one-step experiment (50)	-15	27.7 / – / –
6 (1)	one-step experiment (50)	-15	26.7 / – / –
7 (1)	one-step experiment (50)	-15	26.2 / – / –
8 (1)	one-step experiment (50)	-15	26.4 / 43.4 / 31.9
9 (1)	one-step experiment (50)	-15	27.1 / 40.0 / 35.5
10 (2)	one-step experiment (50)	-15	26.2 / 35.7 / 27.1
11 (2)	one-step experiment (50)	-15	27.1 / 33.6 / 26.1
12 (2)	two-step experiment (50)	-10 / -15	27.3 / 34.4 / 27.5
13 (2)	freeze/thaw-experiment (50)	-15 / 11	28.0 / 32.7 / 34.0
14 (2)	freeze/thaw-experiment (50)	-15 / 11	26.3 / 30.2 / 31.0
15 (2)	freeze/thaw-experiment (50)	-15 / 11	27.2 / 30.6 / 33.3
16 (2)	freeze/thaw-experiment (50)	-15 / 11	27.4 / 32.4 / 31.2
17 (2)	freeze/thaw-experiment (50)	-15 / 11	27.9 / 33.9 / 32.9
18 (2)	one-step experiment (0.4)	-15	27.8 / 42.4 / 30.5
19 (2)	two-step experiment (50)	-10 / -15	27.1 / 33.1 / 26.9
20 (3)	one-step experiment (0.4)	-15	26.1 / 45.9 / 33.7
21 (3)	two-step experiment (50)	-10 / -15	27.5 / 58.0 / 30.2
22 (3)	freeze/thaw-experiment (50)	-15 / 11	24.7 / 30.3 / 36.6
23 (3)	one-step experiment (0.4)	-15	24.6 / 51.6 / 36.9
24 (3)	one-step experiment (50)	-15	25.9 / 44.9 / 29.8
25 (3)	one-step experiment (50)	-15	23.9 / 30.9 / 30.0
26 (3)	one-step experiment (50)	-15	22.8 / 48.4 / 28.6
27 (3)	one-step experiment (50)	-15	24.6 / 37.4 / 28.1
28 (3)	one-step experiment (1.0)	-15	25.5 / 47.1 / 35.7
29 (3)	one-step experiment (1.0)	-15	26.7 / 59.9 / 36.6
30 (3)	one-step experiment (25)	-15	25.8 / 40.7 / 28.8
31 (3)	freeze/thaw-experiment (50)	-15 / 11	26.8 / 36.2 / 31.2
32 (3)	two-step experiment (50)	-10 / -15	25.1 / 56.0 / 28.2
33 (3)	one-step experiment (1.0)	-15	26.6 / 47.3 / 35.4

Table 3.10: Parameters for freezing experiments (Samples 5 to 33) (water content is given for the initial condition / the frozen (top) part / the unfrozen (bottom) part)

Chapter 4

Discussion

4.1 Temperature distribution in soil sample

In addition to the temperature prescribed at the top surface of the cylindrical soil sample, the temperature distribution over the sample height depends on the heat propagation through the specimen. The temperature at the top surface is specified by the cooling rate $\dot{T}$ [°C/h], where the time scale associated with cooling is set equal to the time needed for the cooling device to reduce the temperature from 11 °C to the target temperature, reading

$$\tau_c = \frac{\text{target temperature} - \text{initial temperature}}{\text{cooling rate}} = \frac{\Delta T}{\dot{T}} \ , \qquad (4.1)$$

with the initial temperature equal to +11 °C.
The so-obtained time scale related to cooling of the top surface ranges from 36 min for $\dot{T} = 50$ °C/h, 26 h for $\dot{T} = 1$ °C/h, to 65 h for $\dot{T} = 0.4$ °C/h (see Figure 4.1 for the case of $\dot{T} = 50$ °C/h).
The time scale describing the heat flow over the specimen height, on the other hand, is given by (Ulm and Coussy 2001)

$$\tau_h = \frac{l^2}{D_T}, \qquad (4.2)$$

where l=0.1 m is the height of the cylindrical soil sample and D_T is the thermal diffusity, given by

$$D_T = \frac{k}{\rho \ c} \qquad (4.3)$$

with k [kJ/(°C h m)] as the thermal conductivity, ρ [kg/m^3] as the density, and c [kJ/(kg °C)] as the specific heat capacity.

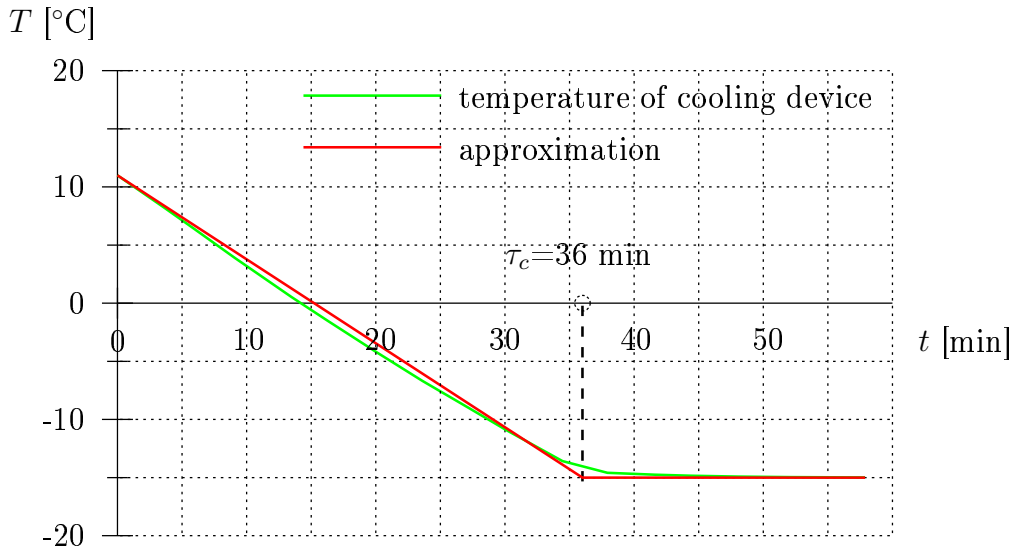

Figure 4.1: τ_c for the experiments with a cooling rate of 50 °C/h

Using values for k, c, and ρ given in (Jessberger and Jagow-Klaff 2001) for wet silt [k=6.84 kJ/(°C h m), $C = \rho c$=3000 kJ/(m^3 °C)], τ_h is obtained as

$$\tau_h = \frac{0.1^2}{6.84/3000} = 4.4 \text{ h} .$$

For $\tau_c \gg \tau_h$, i.e., for a cooling process at the top of the soil sample significantly slower than the temperature transport through the sample, a nearly linear temperature distribution over the sample height is obtained (see also numerical results for $\dot{T}$=1 and 0.4 °C/h in Figures 4.4 and 4.5). For $\tau_c < \tau_h$, on the other hand, the temperature distribution over the sample height becomes nonlinear (see Figure 4.3). For the numerical simulation, a one-dimensional finite-element program accounting for the enthalpy change in consequence of freezing and thawing (ΔH = 334 kJ/(kg water)) was employed (see (Lackner, Amon, Lagger 2005)):

- Hereby, the degree of freezing ξ, with $\xi = w_f/w_{f,\infty}$, where w_f is the frozen water content and $w_{f,\infty}$ is the final frozen water content for $T \ll T_f$ (T_f represents the freezing temperature), is linked to the temperature by

$$\xi = 1 - \exp\left[-\frac{(T - T_f)^2}{\bar{T}^2}\right] , \tag{4.4}$$

with a freezing temperature $T_f = 0$ °C and a constant calibration parameter $\bar{T} = 2$ °C. The latter was computed from experimental results of freezing clayey silt reported in (Konrad, 1990).

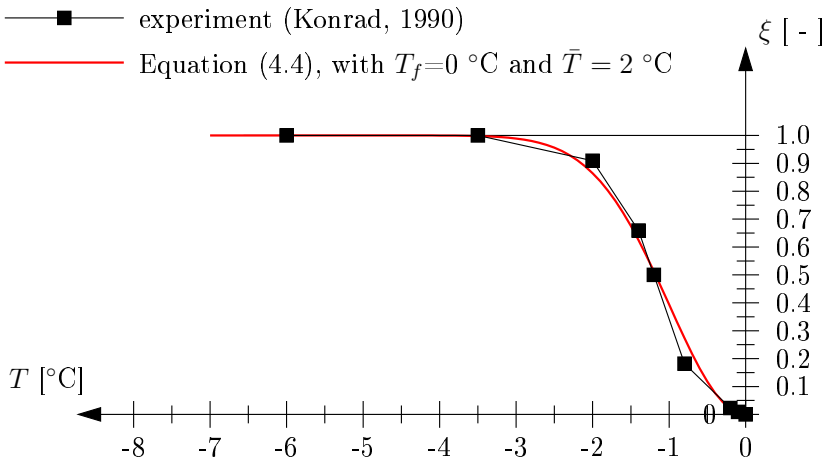

Figure 4.2: Degree of freezing ξ computed from experimental results of freezing clayey silt reported in (Konrad, 1990) (w=27 % and $w_{f,\infty}$=22 %) and $\xi(T)$ according to Equation (4.4)

- The enthalpy change in consequence of freezing/thawing is considered in the numerical simulations by the latent heat of freezing, given by

$$l_\xi = 334 \times \rho_w \times f_{i,\infty} \ [\mathrm{kJ/m^3}] \ , \tag{4.5}$$

where ρ_w [kg/m^3] is the density of water and $f_{i,\infty}$ is the final volume fraction of ice for $T \ll T_f$. The latter is given by the water content $w = 40$ % and the frozen water content for $T \ll T_f$, $w_{f,\infty}$, reading

$$f_{i,\infty} = f_w \times \frac{w_{f,\infty}}{w} \ .$$

In the numerical simulations, w and $w_{f,\infty}$ were set equal to 40 % and 22 %, respectively.

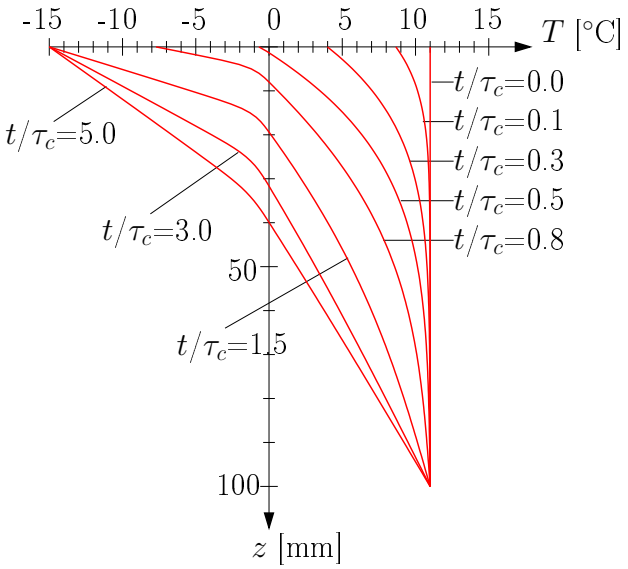

Figure 4.3: Thermal analysis for a cooling rate of 50 °C/h, $\tau_c/\tau_h = 0.14$ [used parameters: k=6.84 kJ/(°C h m), ρc=3000 kJ/(m^3 °C), $w = 40$ %=constant]

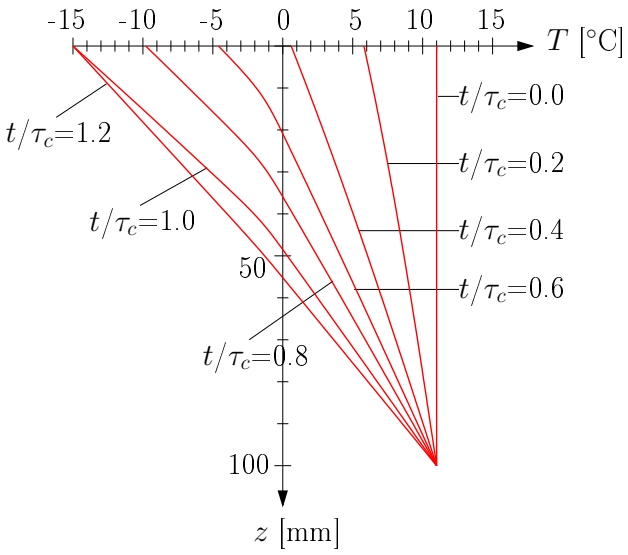

Figure 4.4: Thermal analysis for a cooling rate of 1 °C/h, $\tau_c/\tau_h = 5.9$ [used parameters: k=6.84 kJ/(°C h m), ρc=3000 kJ/(m^3 °C), $w = 40$ %=constant]

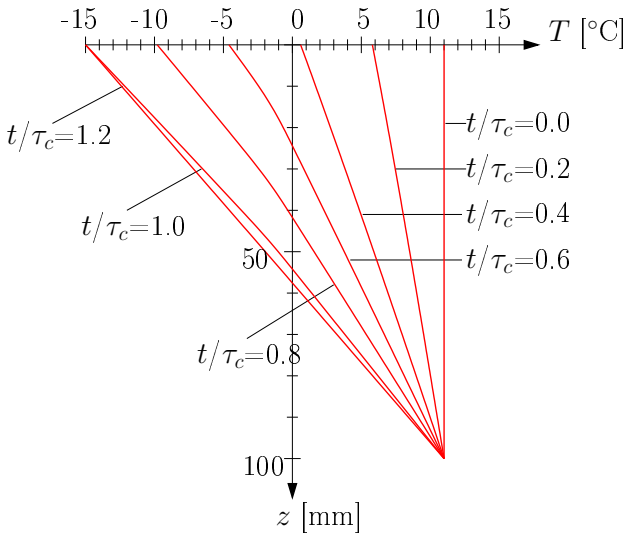

Figure 4.5: Thermal analysis for a cooling rate of 0.4 °C/h, $\tau_c/\tau_h = 14.8$ [used parameters: k=6.84 kJ/(°C h m), ρc=3000 kJ/(m^3 °C), $w = 40$ %=constant]

Freeze/thaw experiments were conducted with a cooling rate of $\dot{T} = 50$ °C/h until the temperature at the top surface of the soil sample reached -15 °C. In the numerical analysis, the thawing process is simulated by a temperature increase in the cooling device from -15 °C to +11 °C within approximately 10 minutes. When prescribing this boundary conditions, the numerically obtained temperature profiles over the sample height (Figure 4.6) and the temperature history at the temperature sensors (Figure 4.7) clearly confirm the experimentally observed delay of the heating process caused by melting of the frozen soil.

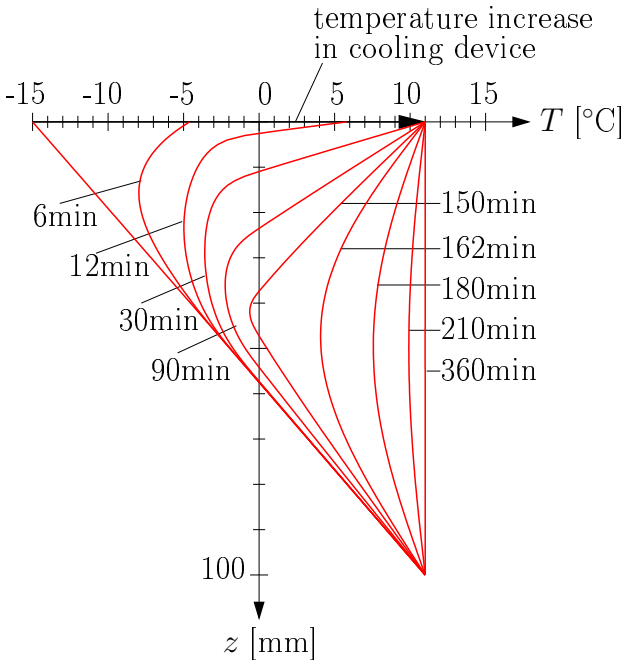

Figure 4.6: Temperature profiles over the sample height for the thawing process [used parameters: k=6.84 kJ/(°C h m), ρc=3000 kJ/(m^3 °C), w = 40 %=constant]

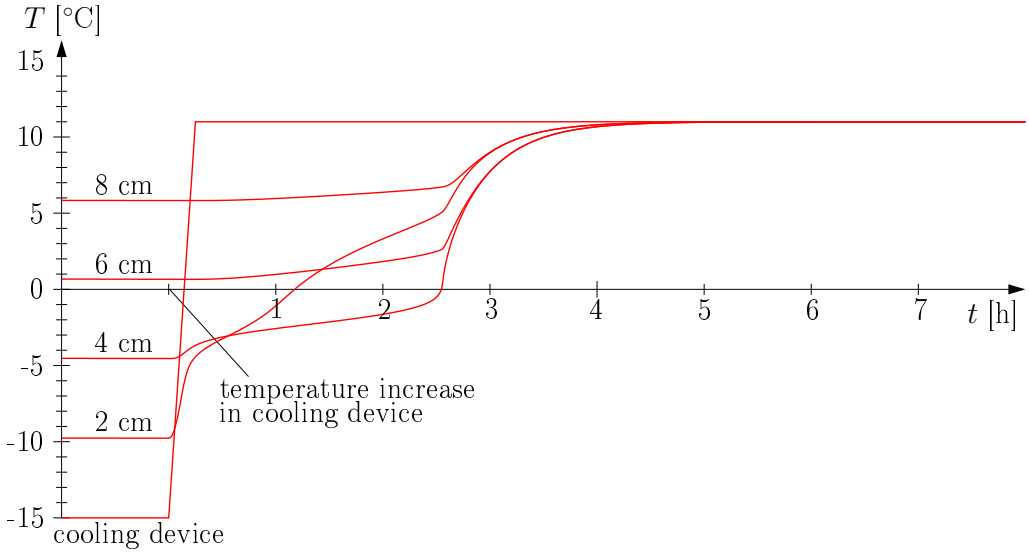

Figure 4.7: Thermal analysis for the thawing process [used parameters: k=6.84 kJ/(°C h m), ρc=3000 kJ/(m^3 °C), w = 40 %=constant]

4.2 Water transport within soil sample

The increase of the water content and the formation of ice lenses reported in Section 3 are associated with a significant water flux into the soil sample. This water flux v [m/s] is standardly related to the potential Ψ [m] using Darcy's law, reading

$$v = k_h \frac{d\Psi}{dz}, \tag{4.6}$$

where k_h [m/s] represents the hydraulic conductivity. In Equation (4.6), the potential Ψ is composed of the water potential $\Phi = \Phi_g + \Phi_p + \Phi_o + \Phi_{cap}$ and the chemical potential.
For the case of the experiments conducted in this thesis, the following assumptions regarding the water potential Φ are made:

1. $\Phi_g = 0$; the vertical dimension of the specimen is rather small, with the gravitational potential Φ_g having no significant effect on the water transport,

2. $\Phi_p = 0$; the low influence of the potential associated with fluid pressure is explained by the zero pressure gradient in the sample associated with external loading (unloaded experiments), and

3. $\Phi_o = 0$; in the absence of solutes, no potential associated with different solute concentrations within the soil sample is present.

Accordingly, the capillary potential Φ_{cap} and the chemical potential become the major driving forces for the water flux into the soil sample.
Similar to the temperature flow through the soil sample (Ulm and Coussy 2001), a time scale for the water transport is introduced, reading

$$\tau_t = \frac{L_w^2}{D_H}, \tag{4.7}$$

where L_w [m] is the distance from the water source at the bottom surface of the soil sample to the frost front and D_H [m^2/s] is the hydraulic diffusity. The latter is given by (Fairhurst and Platten, 1997)

$$D_H = k_h \, \frac{\partial \Psi}{\partial w} \, , \tag{4.8}$$

with w [%] as the actual water content in the unfrozen zone of the soil sample. The dependency of the hydraulic diffusivity on the actual water content in the case of water transport in nonsaturated porous media may also be considered

by replacing the permeability k_h appearing in Equation (4.6) by $\kappa/\eta \times k_{rw}$, where κ [m^2] is the intrinsic permeability, η [N s/m^2] is the dynamic viscosity of water, and $k_{rw}(S_w)$ [-] accounts for the relative permeability with regard to the water saturation S_w: $k_{rw}(0)$=0 and $k_{rw}(1)$=1.

4.3 Segregation potential

Applying Equation (2.14) to the results obtained from the conducted freezing experiments, the segregation potential SP [m^2/(°C h)] is obtained as [see, e.g., (Jessberger et al. 2001)]

$$SP = \frac{\dot{u}}{\text{grad } T} \ , \tag{4.9}$$

with $\dot{u}$ [m/h] as the frost-heave rate monitored in the experiments and grad T as the gradient of the spatial distribution of the temperature at the 0 °C isotherm.
SP is a parameter frequently used to describe the frost susceptibility of fine-grained soils. In addition to the determination of SP at the time instant related to the onset of formation of the final ice lens (see (Konrad and Morgenstern, 1980)), SP is determined in this thesis for different time instants. Hereby, a nearly constant evolution for SP was found for the experiments with a cooling rate of $\dot{T}$ = 50 °C/h (see Table 4.1 and Figures 4.8 and 4.9). For slow cooling rates ($\dot{T}$ = 1.0 °C/h and 0.4 °C/h), on the other hand, the segragation potential decreases with time and approaches a constant value at the time instant when the thicker ice lens begins to form (see Figure 4.10).

sample no. (silt)	type of experiment (cooling rate [°C/h])	segregation potential [$m^2/(°C\ h)$]
5 (1)	one step experiment (50)	3.02×10^{-2}
6 (1)	one step experiment (50)	1.59×10^{-2}
7 (1)	one step experiment (50)	2.18×10^{-2}
8 (1)	one step experiment (50)	2.28×10^{-2}
9 (1)	one step experiment (50)	1.70×10^{-2}
10 (2)	one step experiment (50)	8.6×10^{-3}
11 (2)	one step experiment (50)	8.2×10^{-3}
12 (2)	two step experiment (50)	8.2×10^{-3}
13 (2)	freeze/thaw-experiment (50)	8.0×10^{-3}
14 (2)	freeze/thaw-experiment (50)	6.3×10^{-3}
15 (2)	freeze/thaw-experiment (50)	6.1×10^{-3}
16 (2)	freeze/thaw-experiment (50)	7.7×10^{-3}
17 (2)	freeze/thaw-experiment (50)	1.03×10^{-2}
18 (2)	one step experiment (0.4)	6.3×10^{-3}
19 (2)	two step experiment (50)	7.3×10^{-3}
20 (3)	one step experiment (0.4)	7.2×10^{-3}
21 (3)	two step experiment (50)	1.60×10^{-2}
22 (3)	freeze/thaw-experiment (50)	sample broken
23 (3)	one step experiment (0.4)	loaded sample
24 (3)	one step experiment (50)	2.15×10^{-2}
25 (3)	one step experiment (50)	1.01×10^{-2}
26 (3)	one step experiment (50)	1.80×10^{-2}
27 (3)	one step experiment (50)	1.53×10^{-2}
28 (3)	one step experiment (1.0)	1.65×10^{-2}
29 (3)	one step experiment (1.0)	1.59×10^{-2}
30 (3)	one step experiment (25)	2.13×10^{-2}
31 (3)	freeze/thaw-experiment (50)	1.44×10^{-2}
32 (3)	two step experiment (50)	2.04×10^{-2}
33 (3)	one step experiment (1.0)	1.52×10^{-2}

Table 4.1: Segregation potential calculated at the time instant when the final ice lens begins to form

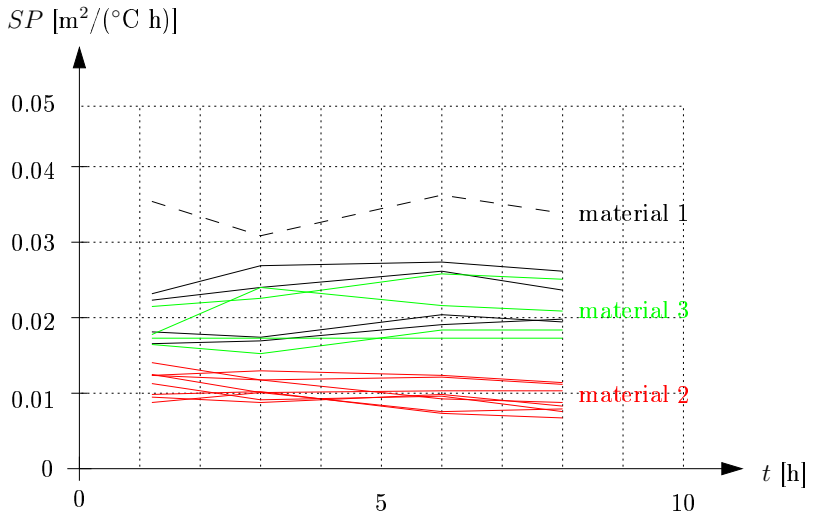

Figure 4.8: Segregation potential SP for one-step experiments and freeze/thaw experiments with a cooling rate of 50 °C/h

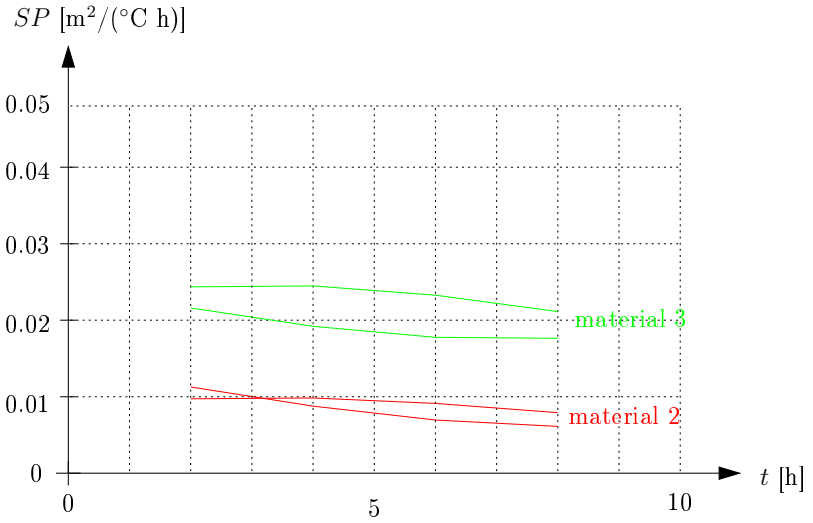

Figure 4.9: Segregation potential SP for two-step experiments with a cooling rate of 50 °C/h

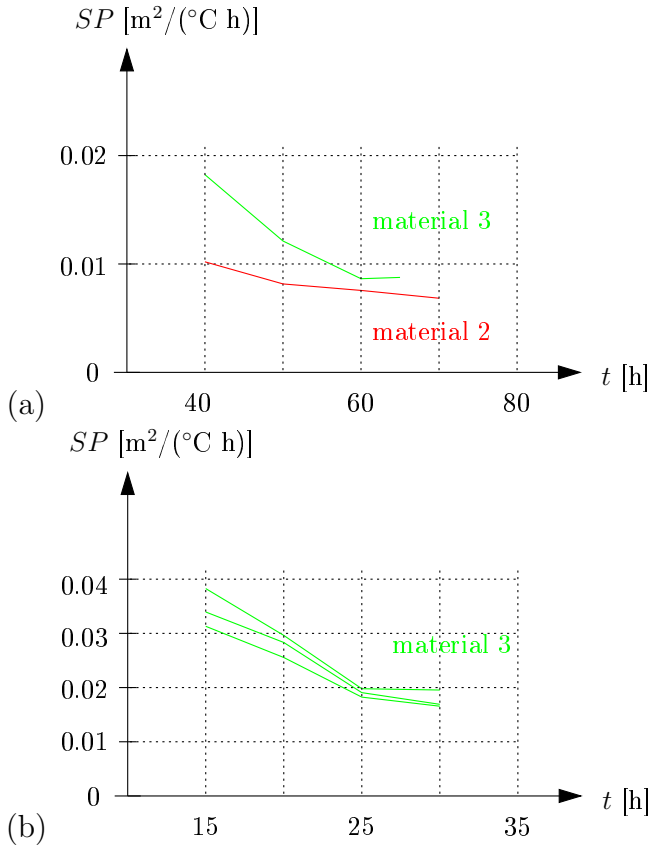

Figure 4.10: Segregation potential for frost heave experiments with a cooling rate of (a) 0.4 °C/h and (b) 1.0 °C/h

In order to relate the segregation potential obtained from the empirical relation (4.9) to the potentials introduced in Subsection 4.2 and, thus, to physically sound properties, dimensional analysis is employed. Hereby, the following variables are selected to describe the freezing experiments performed in this thesis (see also Table 4.2):

- L [m]: height of soil sample,
- L_w [m]: distance from bottom surface of soil sample to the actual location of the 0 °C isotherm,
- p_c [Pa/m]: capillary pressure in the soil sample (representing the water potential Φ),
- grad T [°C/m]: temperature gradient at the location of the 0 °C isotherm,
- τ_t [h]: time scale for water transport,
- τ_h [h]: time scale for temperature flow,
- τ_c [h]: time scale associated with cooling at the top surface of the soil sample,
- $\bar{T}$ [°C]: parameter controlling freezing in sub-zero temperatures,
- $\dot{T}$ [°C/h]: cooling rate,
- $\dot{u}$ [m/h]: frost-heave rate,
- κ/η [m^3 h/kg]: ratio of intrinsic permeability and dynamic viscosity.

	$[L]$	$[L_w]$	$[p_c]$	[grad T]	$[\tau_t]$	$[\tau_h]$	$[\tau_c]$	$[\bar{T}]$	$[\dot{T}]$	$[\dot{u}]$	$[\kappa/\eta]$
length	1	1	-1	-1						1	3
mass			1								-1
time			-2		1	1	1		-1	-1	1
temperature				1				1	1		

Table 4.2: Dimensional matrix of parameters describing the freezing experiment conducted in this thesis

As mentioned before, SP is standardly determined at the time instant of onset of the formation of the final ice lens. For this specific time instant the temperature distribution has reached its final (stationary) distribution.

Thus, all variables associated with the control of the temperature in the sample ($\dot{T}$, τ_c, τ_h) are not considered in the following.
The rank [1] of the so-obtained dimensional matrix [4 × 8] is four; therefore, four dimensionally independent variables are chosen. Namely, L, τ_t, $\bar{T}$, and κ/η. The remaining quantities, L_w, p_c, grad$T$, and $\dot{u}$, are expressed in a dimensionless manner, using the selected dimensionally independent variables, reading e.g. for $\dot{u}$ as

$$\Pi = \frac{\dot{u}}{L^a \times \tau_t^b \times \bar{T}^c \times (\kappa/\eta)^d}$$

where the constant values for a, b, c, and d need to be determined.
From this procedure, the following dimensionless parameters are obtained:

$$\Pi = \frac{\dot{u}}{\tau_t^{-1} \times L} \ , \tag{4.10}$$

$$\Pi_1 = \frac{\mathrm{grad}T}{L^{-1} \times \bar{T}} \ , \tag{4.11}$$

$$\Pi_2 = \frac{p_c}{(\kappa/\eta)^{-1} \times \tau_t^{-1} \times L^2} \ , \tag{4.12}$$

$$\Pi_3 = \frac{L_w}{L} \ . \tag{4.13}$$

Based on the Buckingham Pi-Theorem, the dimensionless frost heave rate Π is given in the form

$$\Pi = F(\Pi_1, \Pi_2, \Pi_3) \ . \tag{4.14}$$

Using the form of the empirical relation (4.9), Equation (4.14) may be simplified to

$$\Pi = \bar{F}(\Pi_2, \Pi_3) \times \Pi_1 \ , \tag{4.15}$$

where $\bar{F}$ is directly related to SP. Since SP is assumed to be exclusively controlled by soil properties, Π_3, describing the location of the 0 °C isotherm, is eliminated, giving

$$\Pi = \alpha \times \Pi_2^{\beta} \times \Pi_1 \ . \tag{4.16}$$

with the constant values α and β still unknown. Inserting Equations (4.10) to (4.13) into Equation (4.16), one gets

[1] The rank of the exponent matrix (see Table 4.2) is the maximum number of linearly independent rows or columns.

$$\frac{\dot{u}\ \tau_t}{L} = \alpha\ \ \frac{p_c^{\beta}\ (\kappa/\eta)^{\beta}\ \tau_t^{\beta}}{L^{2\beta}} \times \frac{\mathrm{grad}T\ L}{\bar{T}}\ . \tag{4.17}$$

Reformulating Equation (4.17) gives

$$\dot{u} = \alpha\ \ \frac{L^{2(1-\beta)}\ p_c^{\beta}\ (\kappa/\eta)^{\beta}}{\tau_t^{1-\beta}\ \bar{T}} \times \mathrm{grad}T\ . \tag{4.18}$$

Comparing Equation (4.18) with the empirical relation (4.9), SP is obtained as

$$SP = \alpha\ \ \frac{L^{2(1-\beta)}\ p_c^{\beta}\ (\kappa/\eta)^{\beta}}{\tau_t^{1-\beta}\ \bar{T}}\ . \tag{4.19}$$

Since SP is assumed to depend on soil parameters only, the sample height L must be eliminated in Equation (4.19), giving β=1.
Hence, using the experimentally obtained values for SP (see Table 4.1) and [2] $\eta = 1.55 \times 10^{-3}$ N s/m^2, $\kappa = 1 \times 10^{-13}$ m^2, and $\bar{T}$=2 °C, $\alpha\ p_c$ can be calculated from

$$\alpha\ p_c = \frac{SP \times \bar{T}}{\kappa/\eta}\ . \tag{4.20}$$

Figure 4.11 and Table 4.3 contain the so-obtained values for $\alpha\ p_c$ during ice-lens formation for the investigated types of soil.

[2]The dynamic viscosity η changes with temperature. At 0 °C , $\eta = 1.78 \times 10^{-3}$ N s/m^2, and at 10 °C, $\eta = 1.31 \times 10^{-3}$ N s/m^2. The temperature in the unfrozen part of the soil sample ranged from +11 °C to 0 °C.

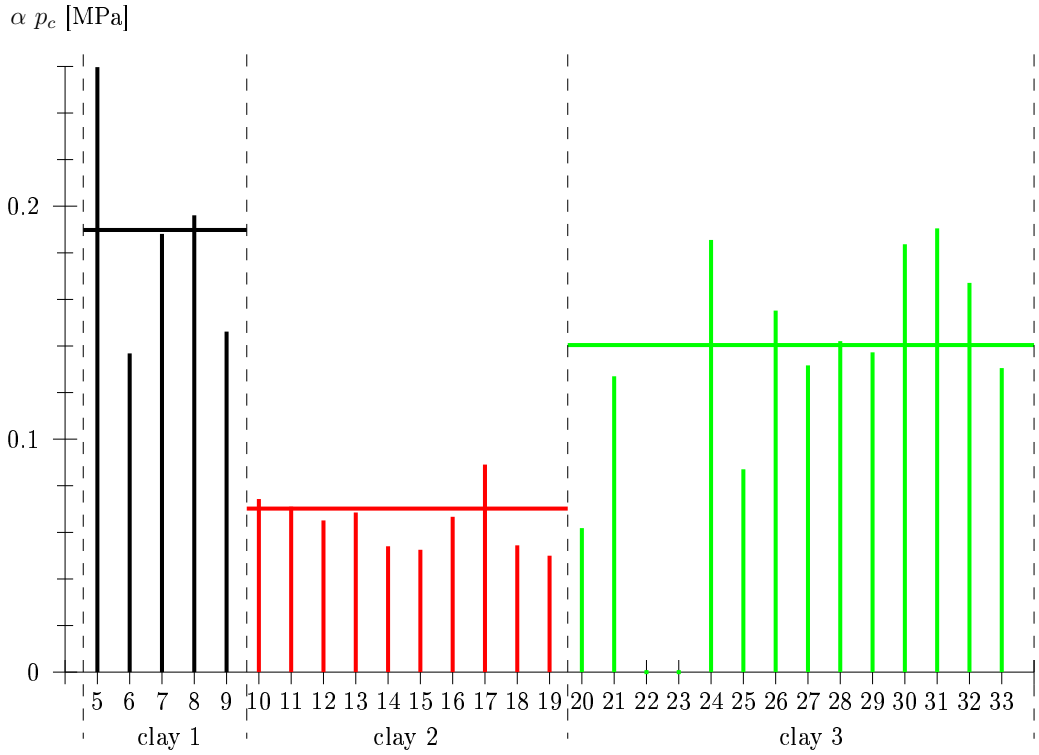

Figure 4.11: Values for $\alpha\ p_c$ [MPa] determined from SP obtained at the time instant when the final ice lens begins to form

sample no. (silt)	type of experiment (cooling rate [°C/h])	$\alpha\ p_c$ [MPa]
5 (1)	one step experiment (50)	0.2597
6 (1)	one step experiment (50)	0.1368
7 (1)	one step experiment (50)	0.1881
8 (1)	one step experiment (50)	0.1961
9 (1)	one step experiment (50)	0.1462
10 (2)	one step experiment (50)	0.0743
11 (2)	one step experiment (50)	0.0710
12 (2)	two step experiment (50)	0.0651
13 (2)	freeze/thaw-experiment (50)	0.0685
14 (2)	freeze/thaw-experiment (50)	0.0540
15 (2)	freeze/thaw-experiment (50)	0.0525
16 (2)	freeze/thaw-experiment (50)	0.0667
17 (2)	freeze/thaw-experiment (50)	0.0891
18 (2)	one step experiment (0.4)	0.0544
19 (2)	two step experiment (50)	0.0500
20 (3)	one step experiment (0.4)	0.0618
21 (3)	two step experiment (50)	0.1270
22 (3)	freeze/thaw-experiment (50)	sample broken
23 (3)	one step experiment (0.4)	sample loaded
24 (3)	one step experiment (50)	0.1855
25 (3)	one step experiment (50)	0.0871
26 (3)	one step experiment (50)	0.1552
27 (3)	one step experiment (50)	0.1317
28 (3)	one step experiment (1.0)	0.1421
29 (3)	one step experiment (1.0)	0.1373
30 (3)	one step experiment (25)	0.1837
31 (3)	freeze/thaw-experiment (50)	0.1905
32 (3)	two step experiment (50)	0.1671
33 (3)	one step experiment (1.0)	0.1305

Table 4.3: Values for $\alpha\ p_c$ calculated for the time instant when the final ice lens begins to form

Chapter 5

Summary and concluding remarks

A new test setup for the assessment of ice-lens formation in cohesive soils was designed and installed at the laboratory of the Institute for Mechanics of Materials and Structures (TU Wien). This test setup was designed to conduct unloaded freezing experiments, eliminating the effect of stress on thermal, hygral, and phase-change processes. Hereby, the temperature at the top surface of the cylindrical soil samples was controlled by a cooling device and the temperature at the bottom surface was kept constant at +11 °C. The continuous water supply in the course of freezing was established by a water bath, in which the soil sample was slightly submerged.
In the course of this thesis, three types of freezing experiments were performed:

1. One-step cooling experiments, where the temperature at the top surface was reduced from +11 °C to −15 °C and, thereafter, held constant for 48 hours,

2. two-step cooling experiments, where the temperature at the top surface was reduced from +11 °C to −10 °C within 30 minutes, held constant for 24 hours, reduced to −15 °C and, finally, held constant for another 24 hours, and

3. freeze/thaw experiments, where the temperature at the top surface was reduced from +11 °C to −15 °C, held constant for 72 hours, raised to +11 °C and, finally, held constant for 48 hours.

Based on the frost heave monitored at the top surface of the soil samples and the temperature evolution at four temperature sensors, the following conclusions can be drawn:

- As observed in the temperature histories obtained from both the experiments and numerical analysis using the finite element method, the temperature distribution remains linear for low cooling rates, following the prescribed temperature at the top surface by keeping T=+11 °C at the bottom surface of the soil sample.

  For high cooling rates, on the other hand, the rapid temperature decrease at the top surface resulted in a nonlinear temperature distribution over the sample height, characterized by high temperature gradients near the top surface of the soil sample. This effect was explained by the different time scales related to cooling of the top surface and to the temperature flow within the sample.

- As regards the frost heave, an almost linear increase was obtained for low cooling rates, caused by the subsequent formation of several thin layers of ice. When the target temperature was reached at the top surface of the sample (stationary temperature state), a thicker ice lens began to form and the frost-heave rate, which was constant during cooling, began to decline. This reduction of the heave rate was explained by a geometrical effect: for a constant temperature at the top and the bottom surface (stationary state), an increase of the sample height by the formation of the ice lens results in a shift of the 0 °C isotherm into the ice lens.

  For high cooling rates, the earlier mentioned high temperature gradient near the top surface became smaller with time as the temperature distribution approached the final, stationary situation. This reduction of the temperature gradient was reflected by the heave rate which also decreased with time.

- In fact, the correlation between the temperature gradient at the location of the freezing front and the heave rate is described by the so-called segregation potential SP. SP was found to be constant for the experiments with a high cooling rate. The calculation of SP at four time instants gave almost similar values.

  The linear heave observed in the experiments with a low cooling rate, on the one hand, and the increasing temperature gradient during cooling, on the other hand, led to a reduction of the value of SP with time for the freezing experiments with a low cooling rate.

  However, the values of SP obtained for the time instant related to the onset of the final ice-lens formation were almost similar for both slow and fast cooling rates.

- Finally, SP was related to results from dimensional analysis. Assuming that the relation used for determination of SP from the frost-heave rate and the temperature gradient holds, SP was related to soil-specific parameters controlling ice-lens formation.

  E.g., capillary pressure, which was related to the values for SP obtained from the freezing experiments, showed significant differences for the investigated types of soil. Silt 1 and Silt 3 gave capillary pressures two times higher than Silt 2, explaining the difference in the frost heave monitored in the performed freezing experiments.

Bibliography

[1] Andersland B.O., Ladanyi B. (1994). *An introduction to frozen ground engineering*. Chapman & Hall, Bonn.

[2] Atkins P.W. (2002). *Kurzlehrbuch Physikalische Chemie*. WILEY-VCH, Weinheim. In German.

[3] Castellan G.W. (1998). *Physical chemistry. Third edition*. Benjamin/Cummings, Menlo Park.

[4] Dash J.G., Fu H., Wettlaufer J.S. (1995). *The premelting of ice and its environmental consequences*. Rep. Prog. Phys. 58:115-167.

[5] Efimov S.S., Kozhevnikov N.N., Kurilko A.S., Nikitina M., Stepanov A.V. (1981). *Influence of cyclic freezing-thawing on heat and mass transfer characteristics of clay soil*. Engineering Geology, 18:147-152.

[6] Fairhurst J., Platten A.K. (1997) *Moisture distribution and the hydraulic diffusivity in hardened cement pastes modified by partial replacement with condensed silica-fume*. International Conference on Maintenance and Durability of Concrete Structures, 17-20.

[7] Fen-Chong T., Fabbri A., Guilbaud J.-P., Coussy O. (2004). *Determination of liquid water content and dielectric constant in porous media by the capacitive method*. C.R. Mecanique, 332:639-645.

[8] Fowler A.C., Noon C.G. (1993). *A simplified numerical solution of the Miller model of secondary frost heave*. Cold Regions Science and Technology, 21:327-336.

[9] Henry K.S. (2000). *A review of the thermodynamics of frost heave*. Cold Regions Research and Engineering Laboratory.

[10] Hermansson A. (2004). *Laboratory and field testing on rate of frost heave versus heat extraction*. Cold Regions Science and Technology, 38:137-151.

[11] Hermansson A., Guthrie W.S. (2005). *Frost heave and water uptake rates in silty soil subject to variable water table height during freezing*. Cold Regions Science and Technology, In print.

[12] Hohmann M. (1997). *Soil freezing-the concept of soil water potential. State of the art*. Cold Regions Science and Technology, 25:101-110.

[13] Hopke S.W. (1980). *A model for frost heave including overburden*. Cold Regions Science and Technology, 3:111-127.

[14] Jessberger H.-L., Jagow-Klaff R. (2001). Article 2.4 (*Bodenvereisung*). In *Grundbautaschenbuch Teil 2: geotechnische Verfahren*. Sixth edition, Ernst & Sohn, Berlin. In German.

[15] Kloiber A.P. (2004). *Experimentelle Untersuchung und mikrimechanische Modellierung des Kriechverhaltens von gefrohrenem Boden*. Diploma thesis, Vienna University of Technology, Vienna, Austria. In German.

[16] Konrad J.-M. (1988). *Influence on freezing mode on frost heave characteristics*. Cold Regions Science and Technology, 15:161-175.

[17] Konrad J.-M. (1989). *Influence of cooling rate on the temperature of ice lens formation in clayey silts*. Cold Regions Science and Technology, 16:25-36.

[18] Konrad J.-M. (1990). *Unfrozen water as a function of void ratio in a clayey silt*. Cold Regions Science and Technology, 18:49-55.

[19] Konrad J.-M., Morgenstern R. (1981). *The segregation potential of a freezing soil*. Canadian Geotechnical Journal, 18:482-491.

[20] Konrad J.-M., Shen M. (1996). *2-D frost action modeling using the segregation potential of soils*. Cold Regions Science and Technology, 24:263-278.

[21] Lackner R., Amon A., Lagger H. (2005). *Artificial ground freezing of fully-saturated soil: Thermal problem*. Journal of Engineering Mechanics (ASCE), 131(2):211-220.

[22] van Loon W. K. P. (1991). *Heat and mass transfer in frozen porous media*. Ph. D. thesis, Agricultural University Wageningen, Wageningen, Netherlands.

[23] Lottmann A. (2003). *Tragfähigkeit und Frostempfindlichkeit von kalkbehandelten bindigen Böden im Planumsbereich von Verkehrsflächen*. Doctoral thesis, Cottbus University of Technology, Cottbus, Germany. In German.

[24] Luo S.-N., Strachan A., Swift D.C. (2005). *Deducing solid-liquid interfacial energy from superheating and supercooling: application to H_2O at high pressures*. Modelling and Simulation in Materials Science and Engineering, 13:321-328

[25] Matsuoka N., Abe M., Ijiri M. (2003). *Differential frost heave and sorted patterned ground: field measurements and laboratory experiment*. Geomorphology, 52:73-85.

[26] Nixon J.F. (1982). *Field frost heave predictions using the segregation potential concept*. Canadian Geotechnical Journal, 19:526-529.

[27] Noon C. (1996). *Secondary frost heave in freezing soils*. Doctoral thesis, University of Oxford, Oxford, U.K..

[28] Or D., Tuller M., Wraith J.M. (2005). *Water potential*. Water Potential, 270-277.

[29] Ozawa H., Kinosita S. (1989). *Segregated ice growth on a microporous filter*. Journal of Colloid and Interface Science, 132 (1):113-124.

[30] Padilla F., Villeneuve J.-P. (1992). *Modeling and experimental studies of frost heave including solute effects*. Cold Regions Science and Technology, 20:183-194.

[31] Padilla F., Villeneuve J.-P., Stein J. (1997). *Simulation and analysis of frost heaving in subsoils and granular fills of roads*. Cold Regions Science and Technology, 13:91-100.

[32] Patterson D.E., Smith M.W. (1980). *The use of time domain reflectrometry for the measurement of unfrozen water content in frozen soils*. Cold Regions Science and Technology, 3:205-210.

[33] Penner E. (1986). *Aspects of ice lens growth in soils*. Cold Regions Science and Technology, 25:89-99.

[34] Penner E., Walton T. (1979). *Effects of temperature and pressure on frost heaving*. Engineering Geology, 13:29-39.

[35] Potz K. (2005). *Frost action in soft soils*. Diploma thesis, University of Natural Resources and Applied Life Sciences, Vienna, Austria. In preparation.

[36] Pusch R. (1979). *Unfrozen water as a function of clay microstructure*. Engineering Geology, 13:157-162.

[37] Talamucci F. (2003). *Freezing Processes in Porous Media: Formation of Ice lenses, Swelling of the Soil*. Mathematical and Computer Modelling, 37:595-602.

[38] Ulm F.-J., Coussy O. (2001). *What is a massive concrete structure at early ages? Some dimensional arguments*. Journal of Engineering Mechanics (ASCE), 127(5):512-522.

[39] Vignes M., Dijkema K.M. (1974). *A model for freezing of water in a dispersed medium*. Journal of Colloid and Interface Science, 49(2):165 ff.

[40] Watanabe K. (1999). *Ice Lensing Mechansim during Soil Freezing*. Doctoral thesis, Mie University, Japan.

[41] Watanabe K. (2002). *Relationship between growth rate and supercooling in the formation of ice lenses in a glass powder*. Journal of Crystal Growth, 237-239 Part3:pp 2194-2198.

[42] Watanabe K., Mizoguchi M. (2002). *Amount of unfrozen water in frozen porous media saturated with solution*. Cold Regions Science and Technology, 34:103-110.

[43] Zeiml M. (2004). *Analytical and numerical modeling of heat and water-vapour transport in concrete subjected to fire loading*. Diploma thesis, Vienna University of Technology, Vienna, Austria.

[44] WAPA-Washington Asphalt Pavement Association (2002). Seattle, www.asphaltwa.com.

[45] University of Colorado at Boulder (2004). Colorado, http://www.colorado.edu/eeb/courses/4140bowman/lectures/4140-07.html.

Data-Sheets for conducted frost-heave experiments

The obtained results for all frost-heave experiments and the temperature evolution at the sensors are given, using one data sheet for each experiment. The first diagram shows the heave curve and the temperature curves for the four sensors in the sample, while the other diagrams show critical phases of temperature or heave evolution in detail. At the bottom of each data sheet, illustrative pictures are provided.

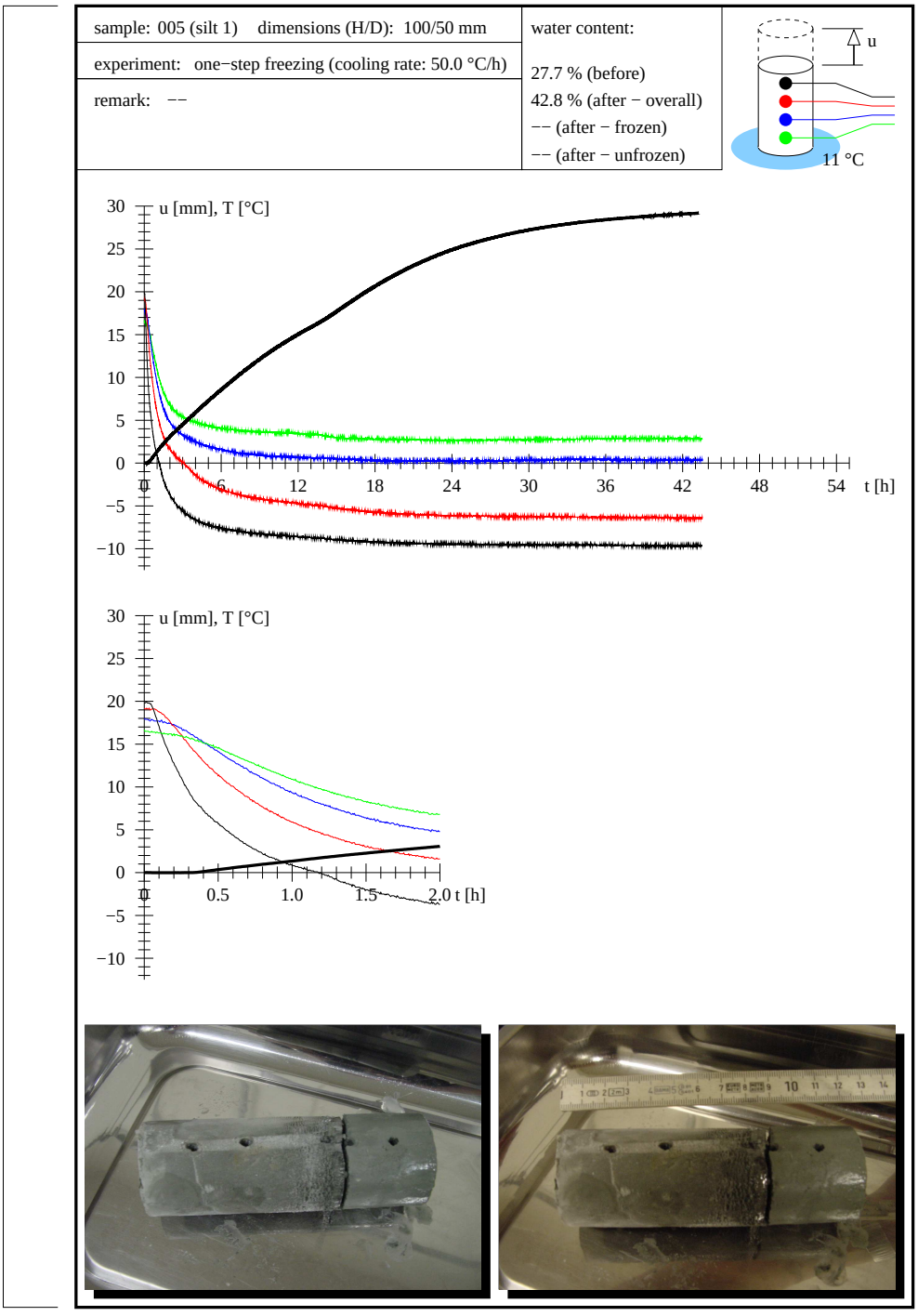

Figure 1: Results for experiment 5

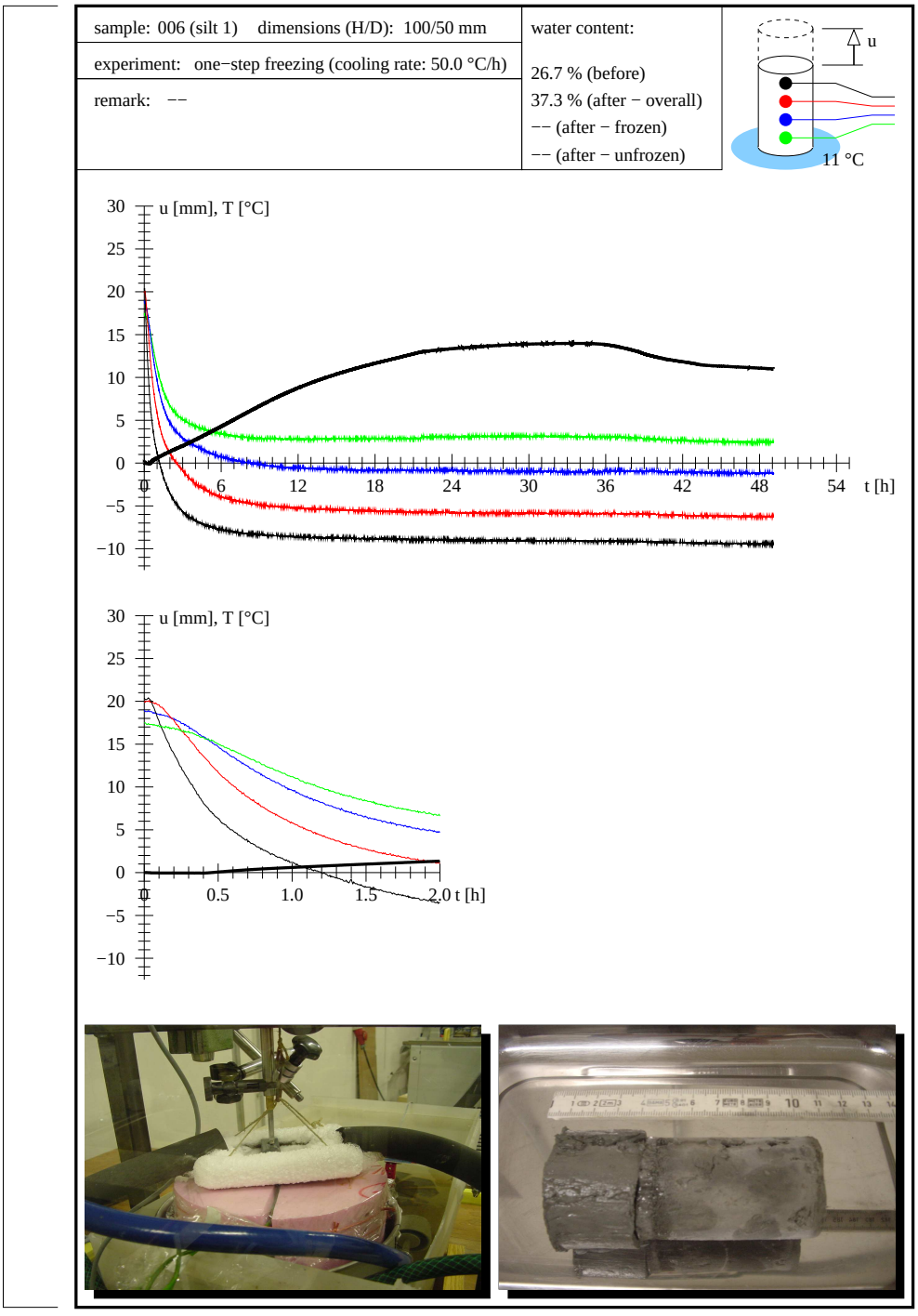

Figure 2: Results for experiment 6

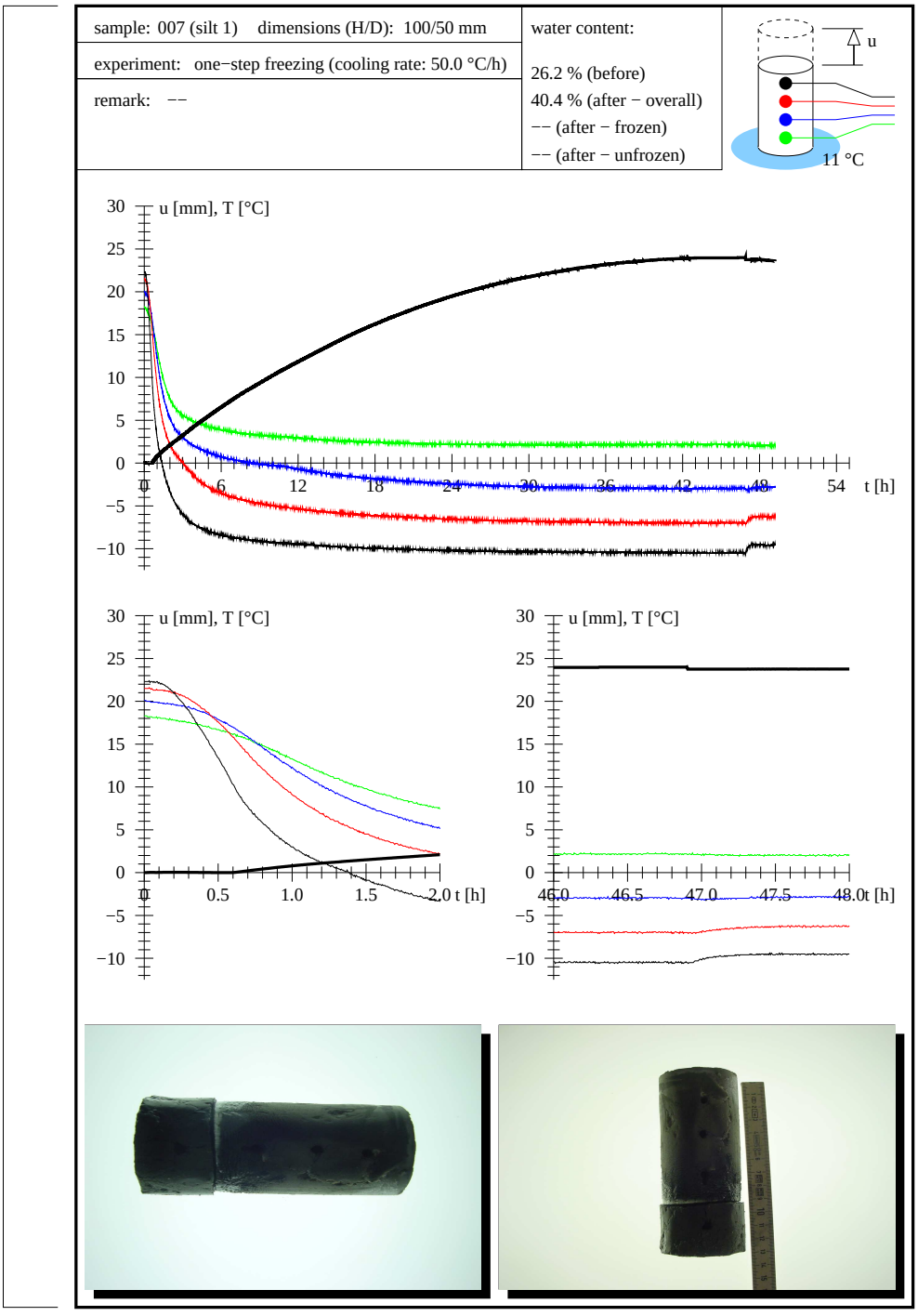

Figure 3: Results for experiment 7

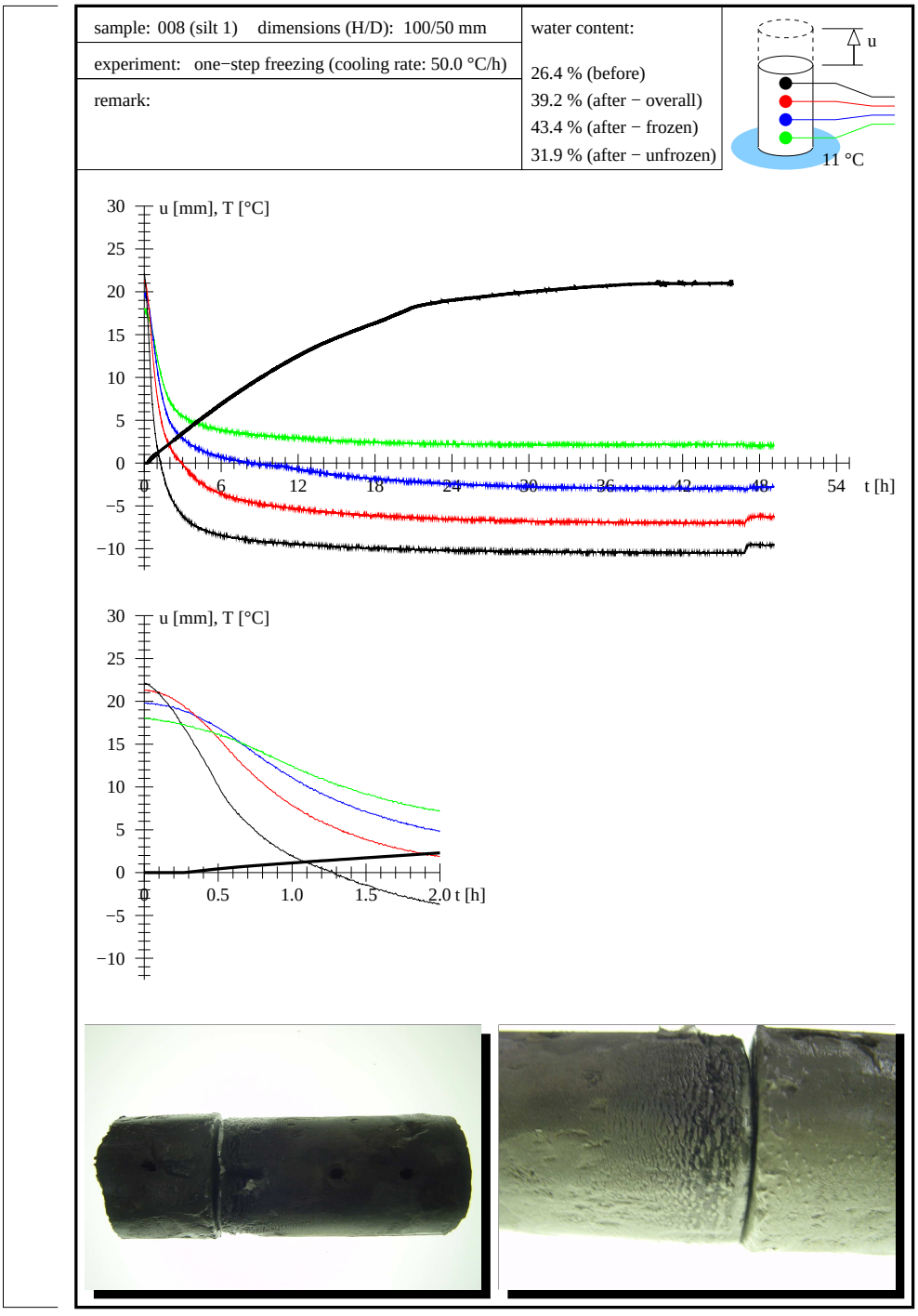

Figure 4: Results for experiment 8

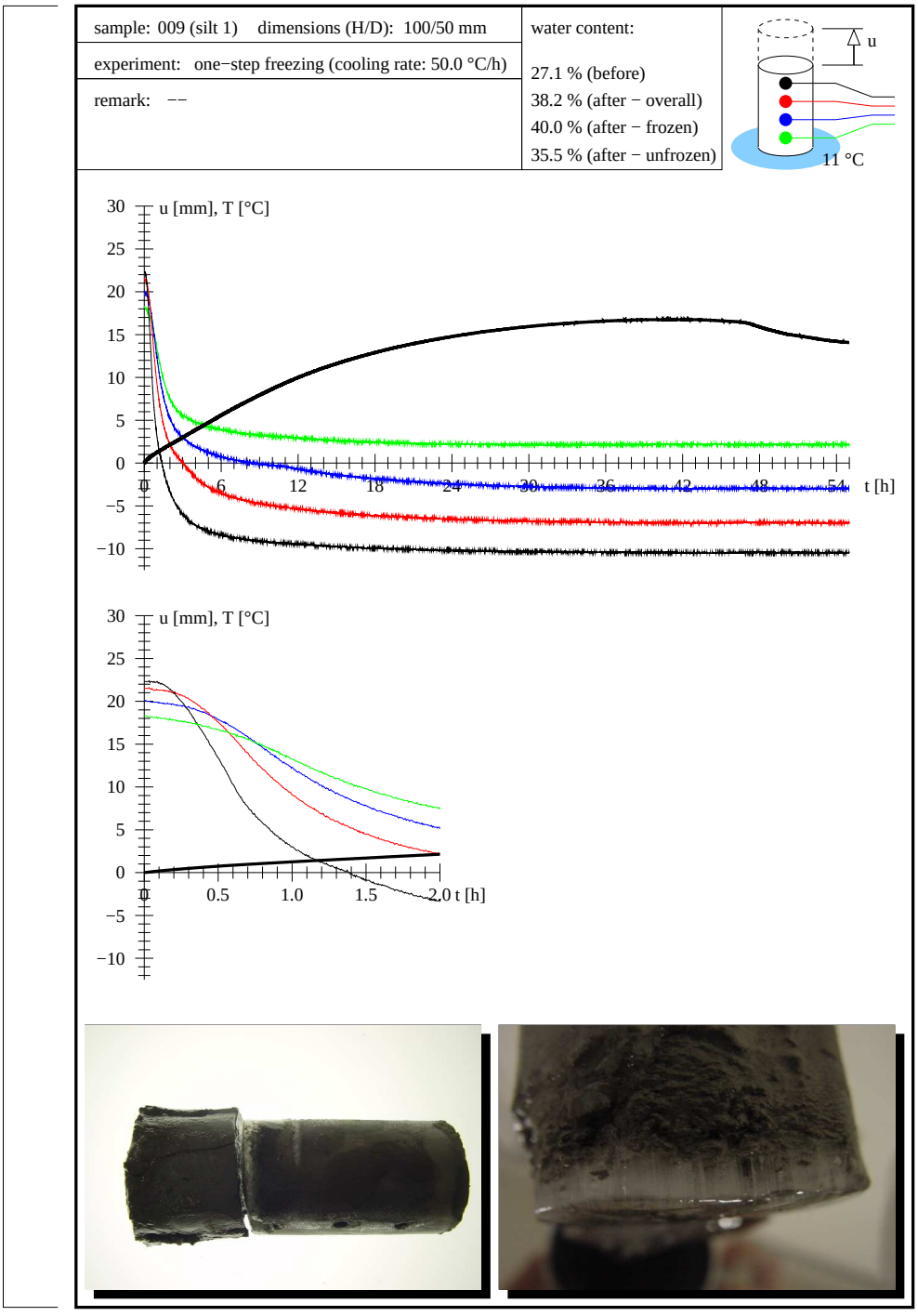

Figure 5: Results for experiment 9

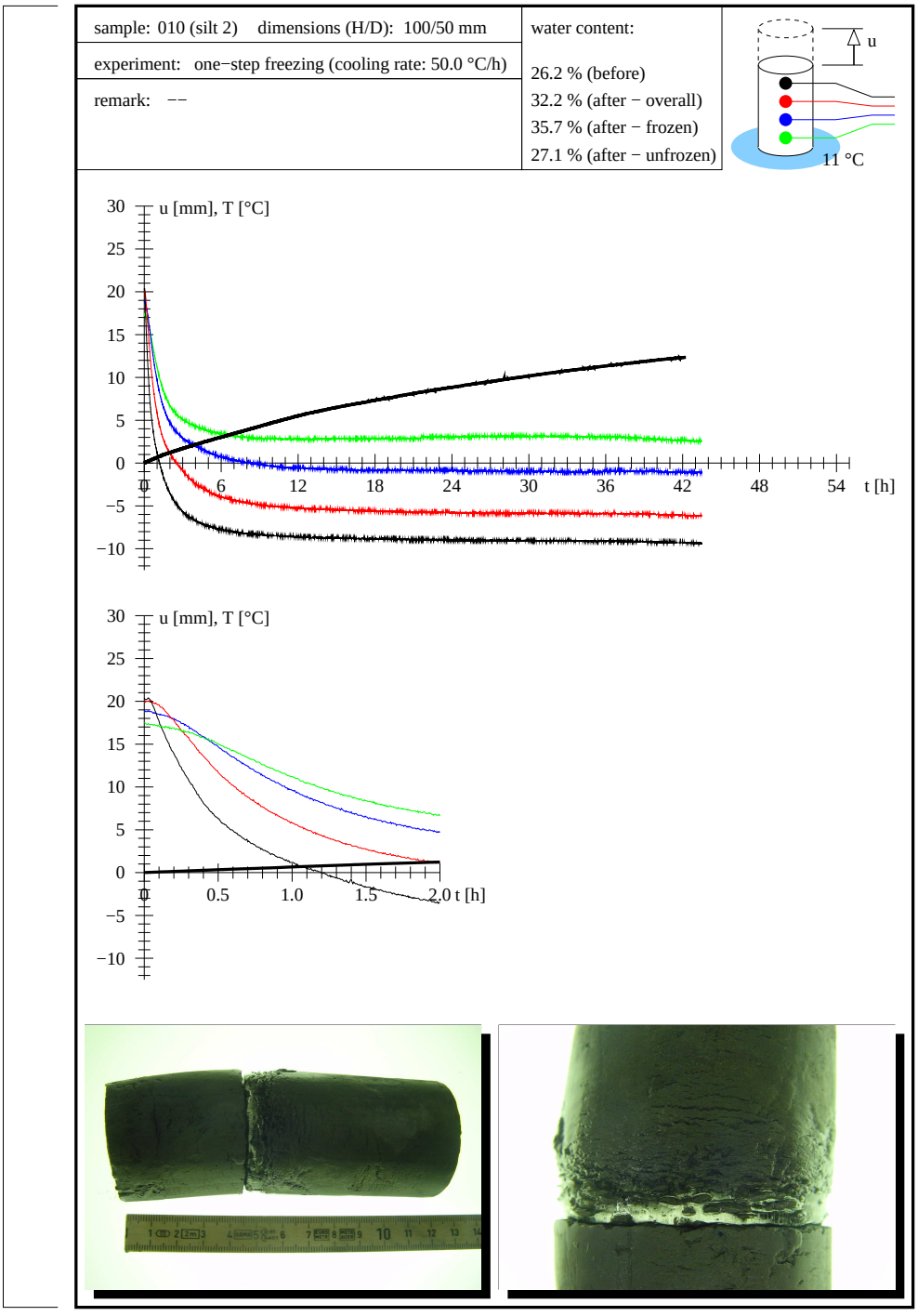

Figure 6: Results for experiment 10

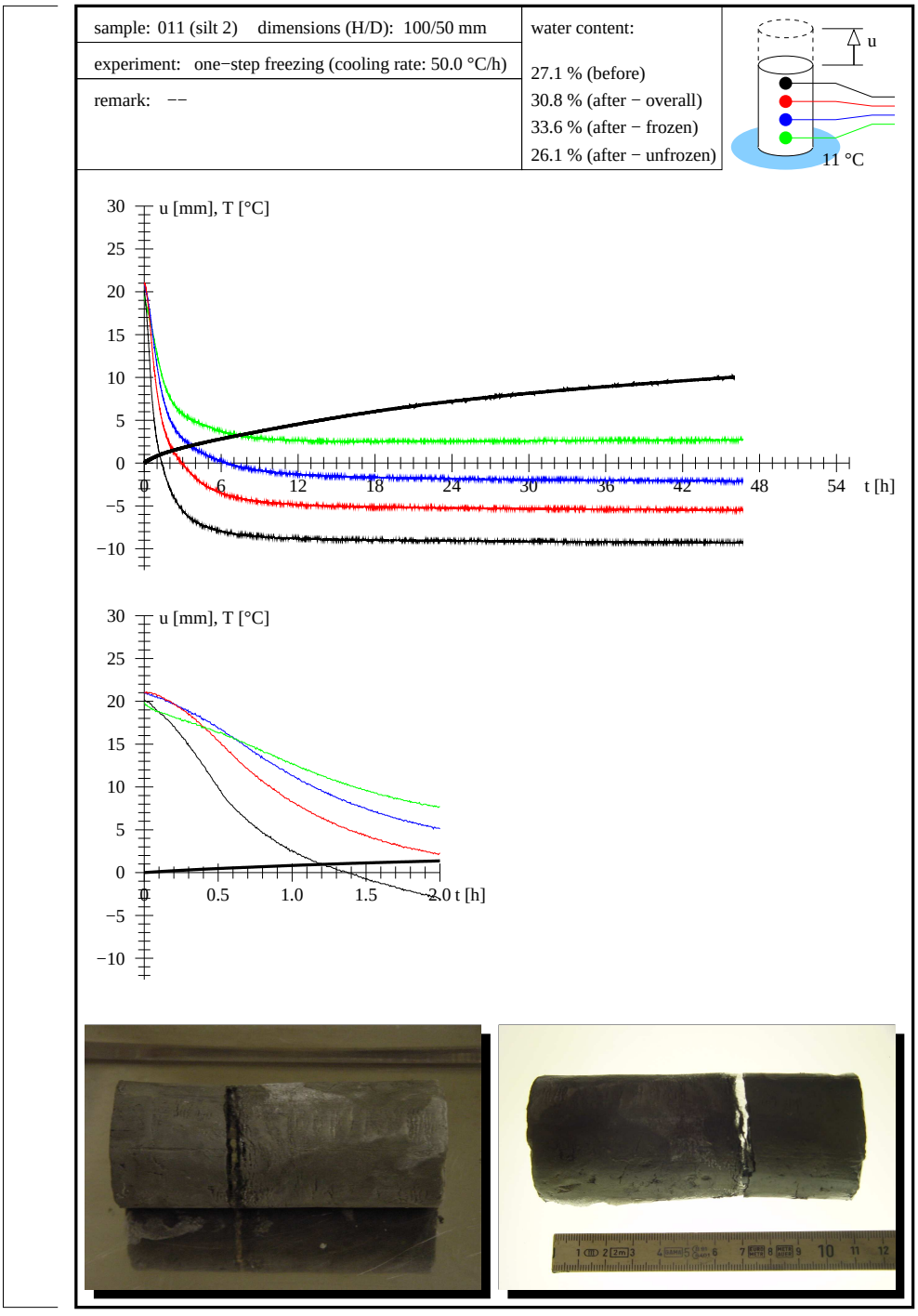

Figure 7: Results for experiment 11

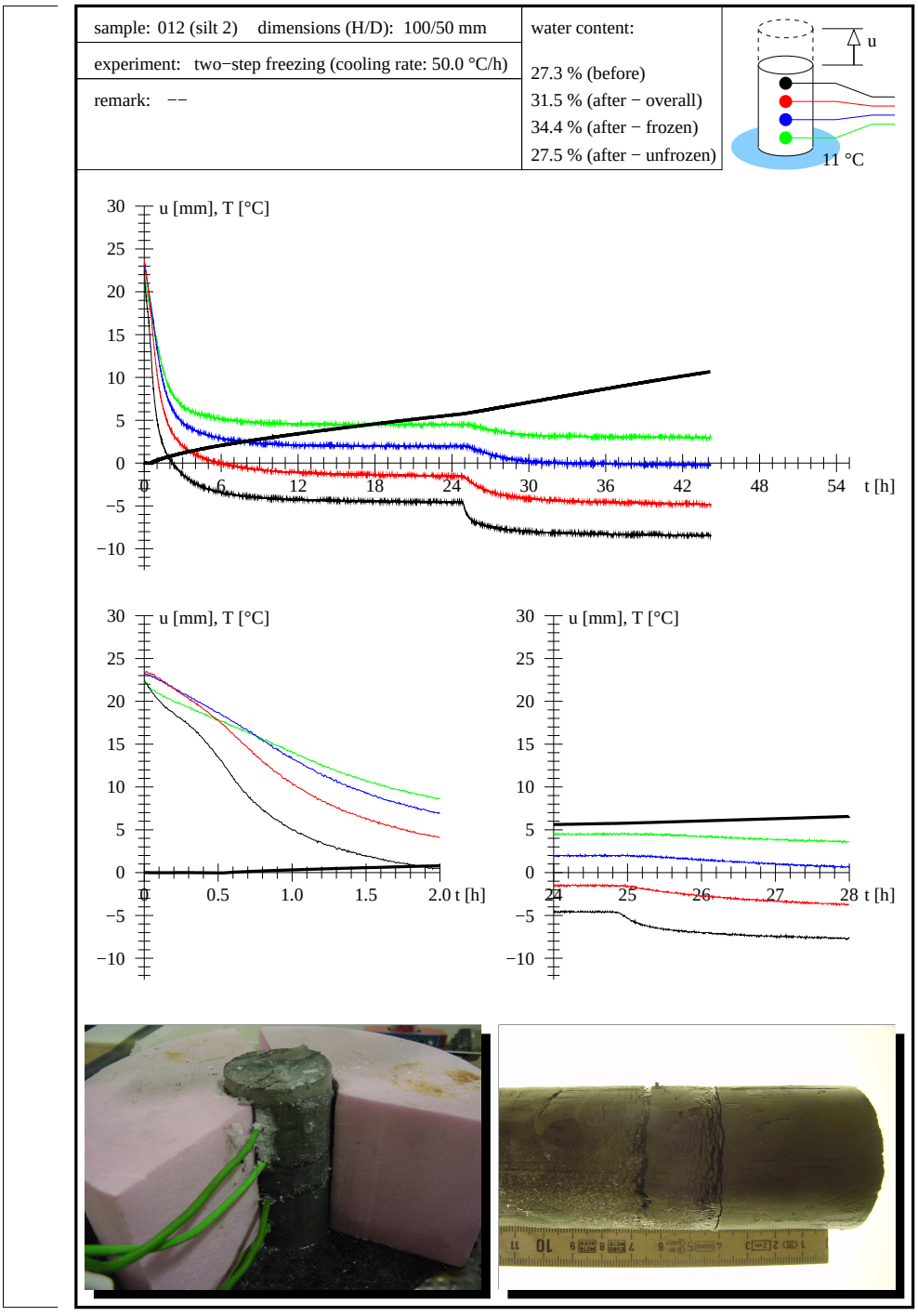

Figure 8: Results for experiment 12

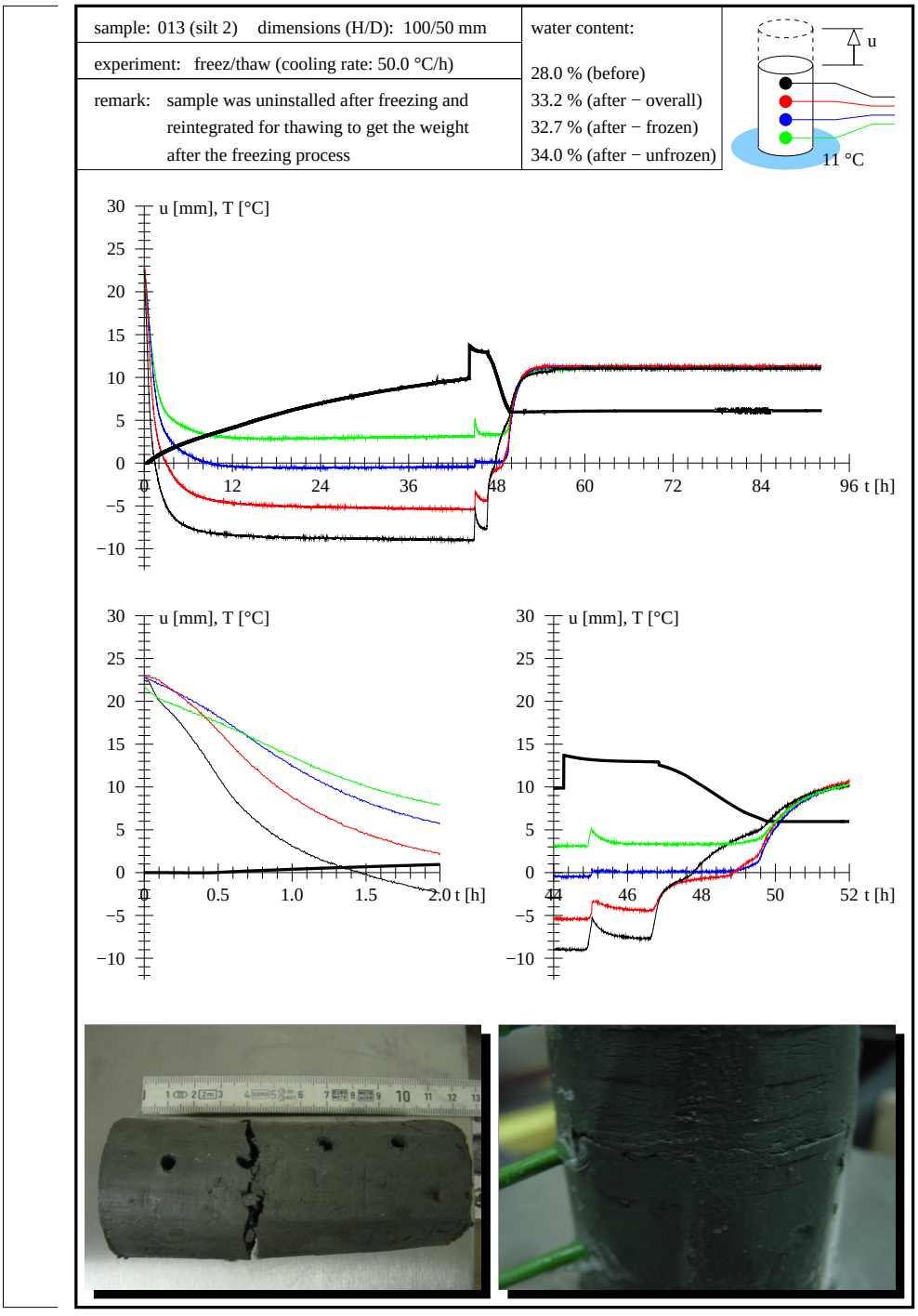

Figure 9: Results for experiment 13

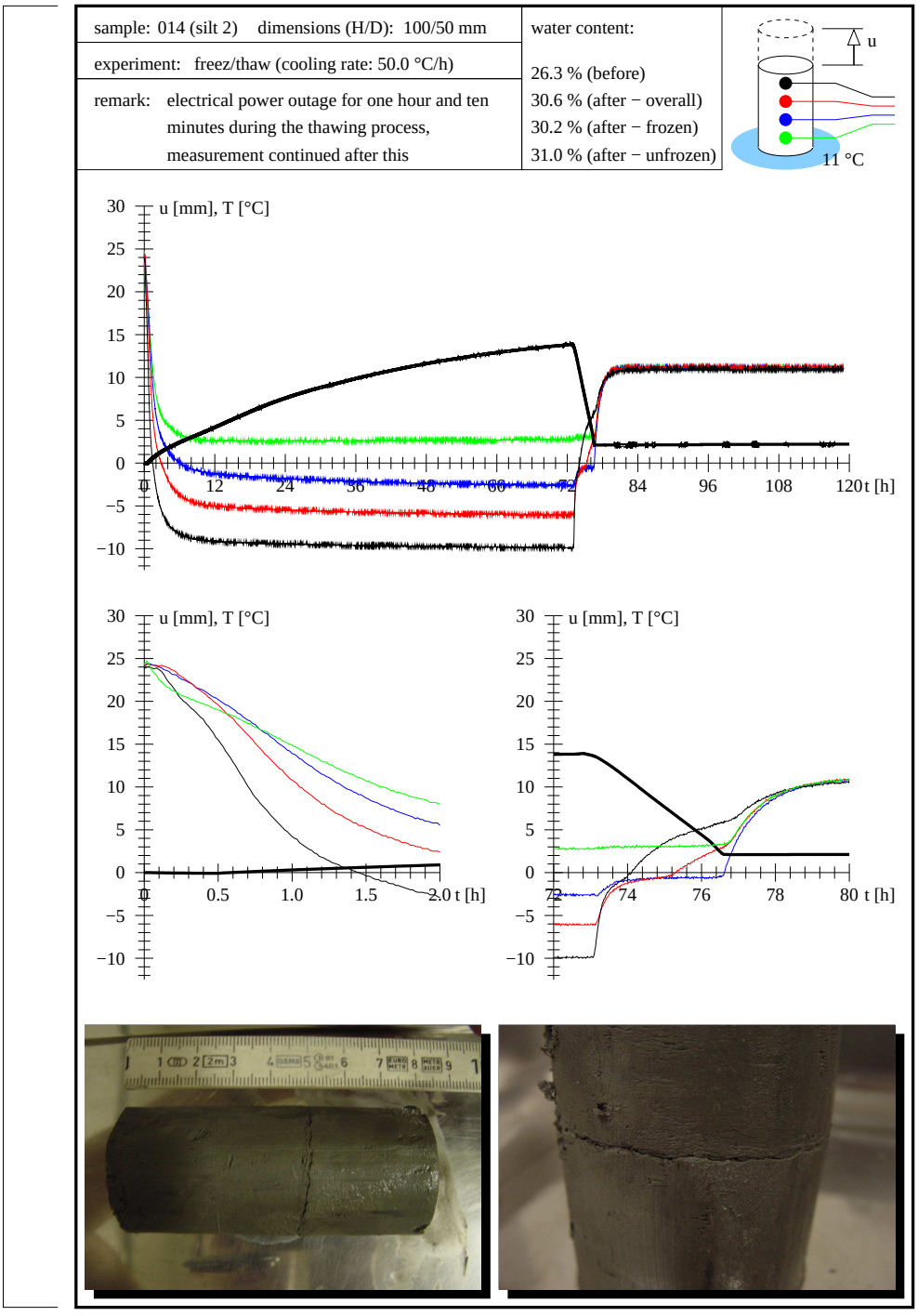

Figure 10: Results for experiment 14

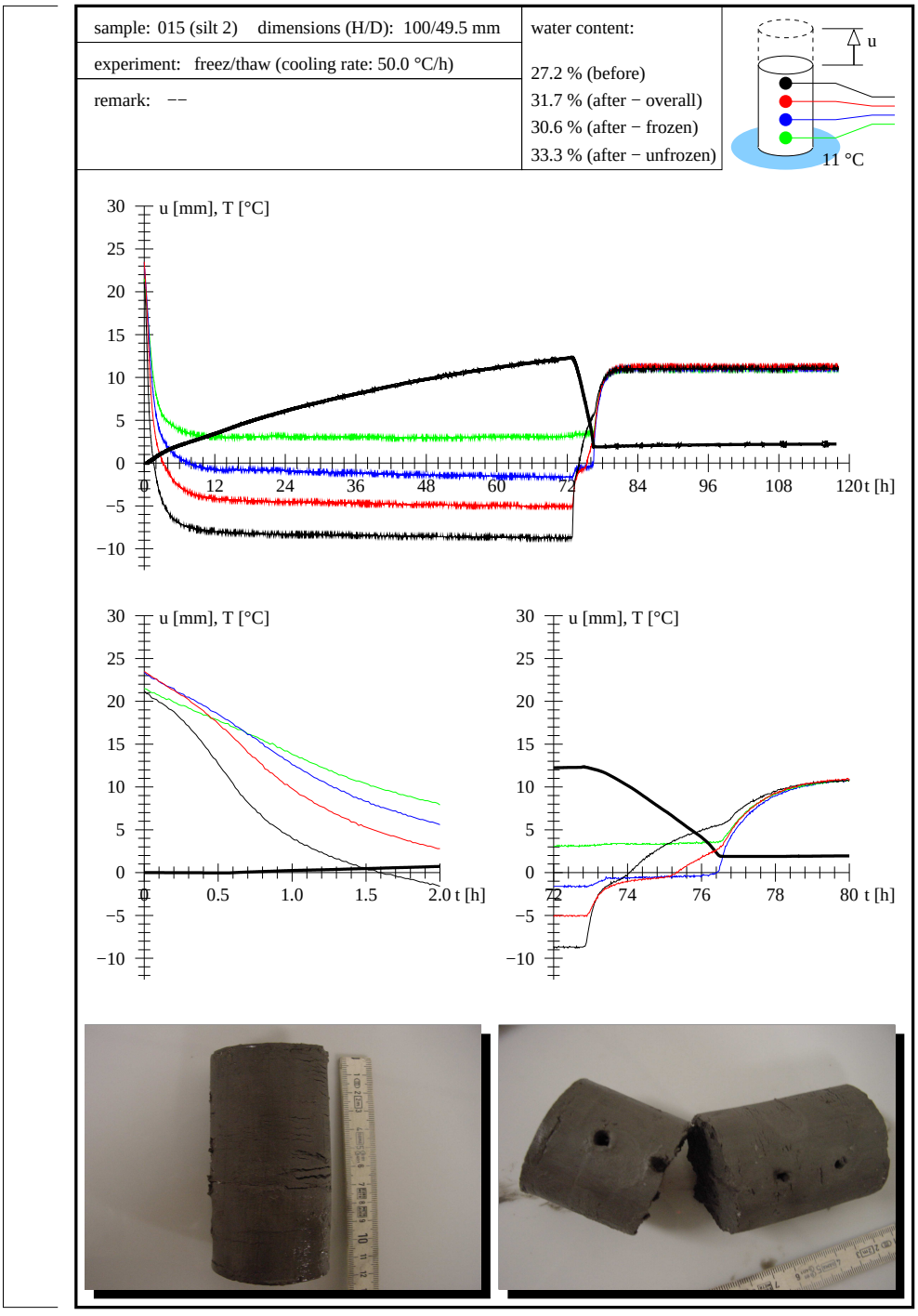

Figure 11: Results for experiment 15

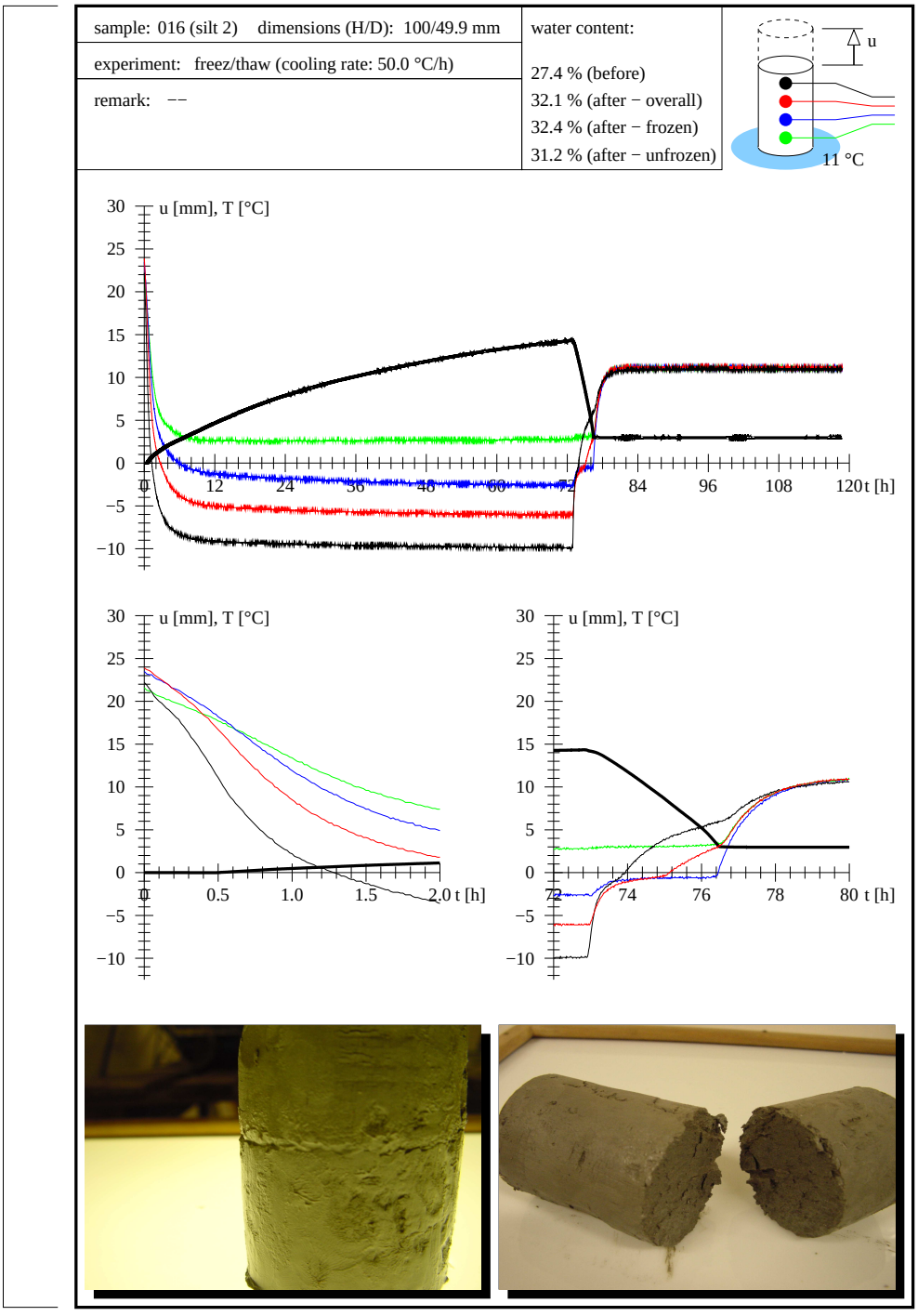

Figure 12: Results for experiment 16

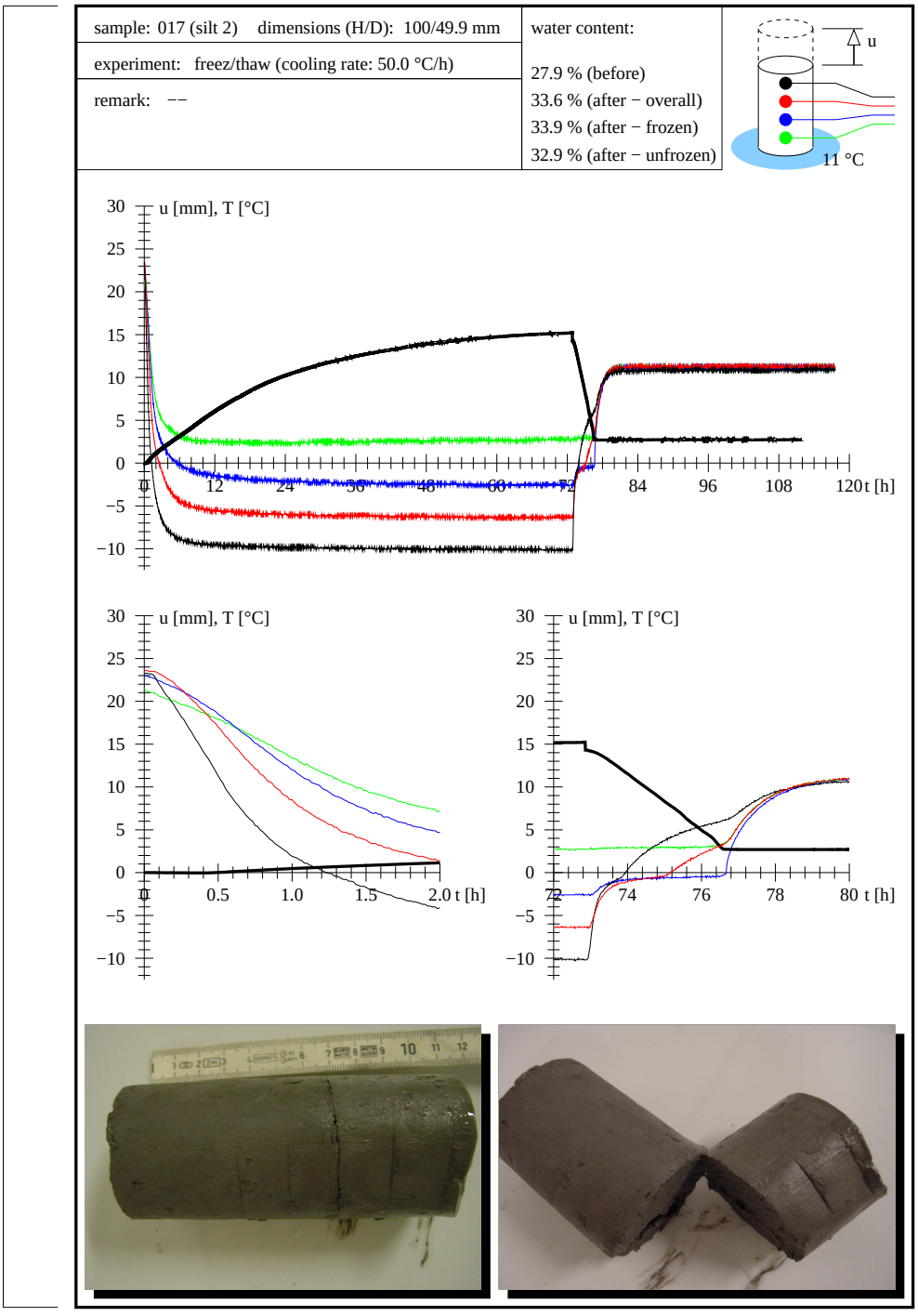

Figure 13: Results for experiment 17

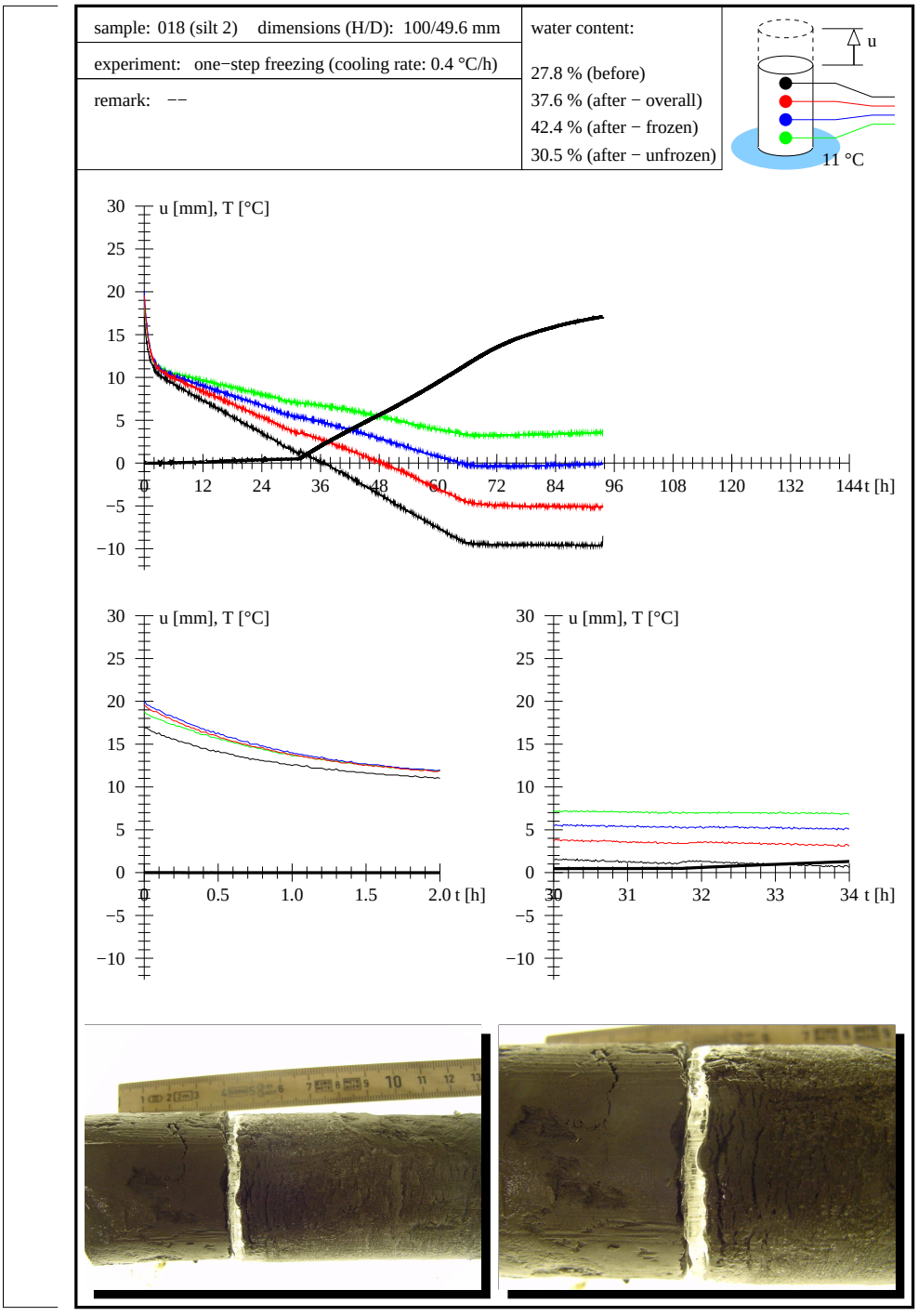

Figure 14: Results for experiment 18

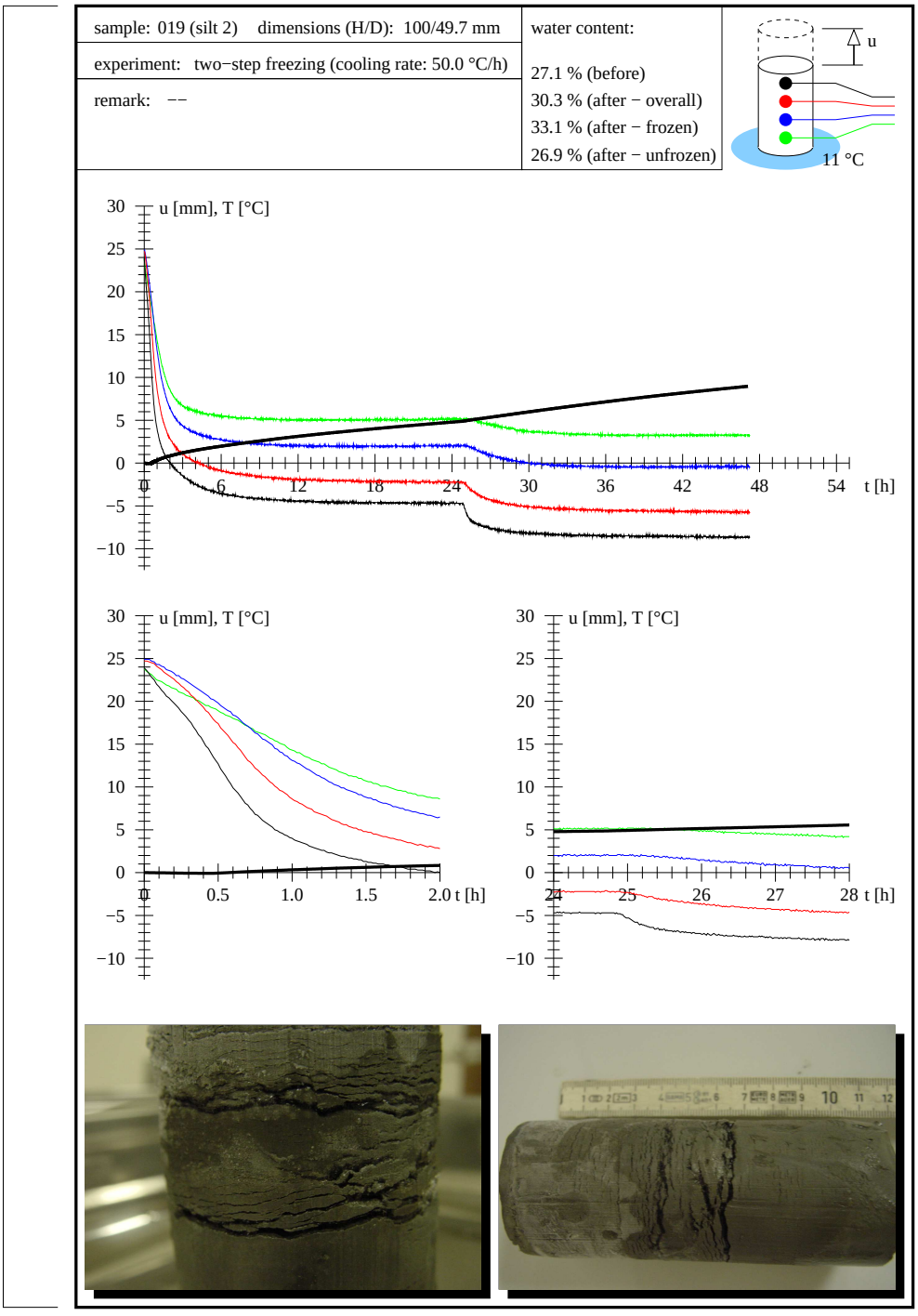

Figure 15: Results for experiment 19

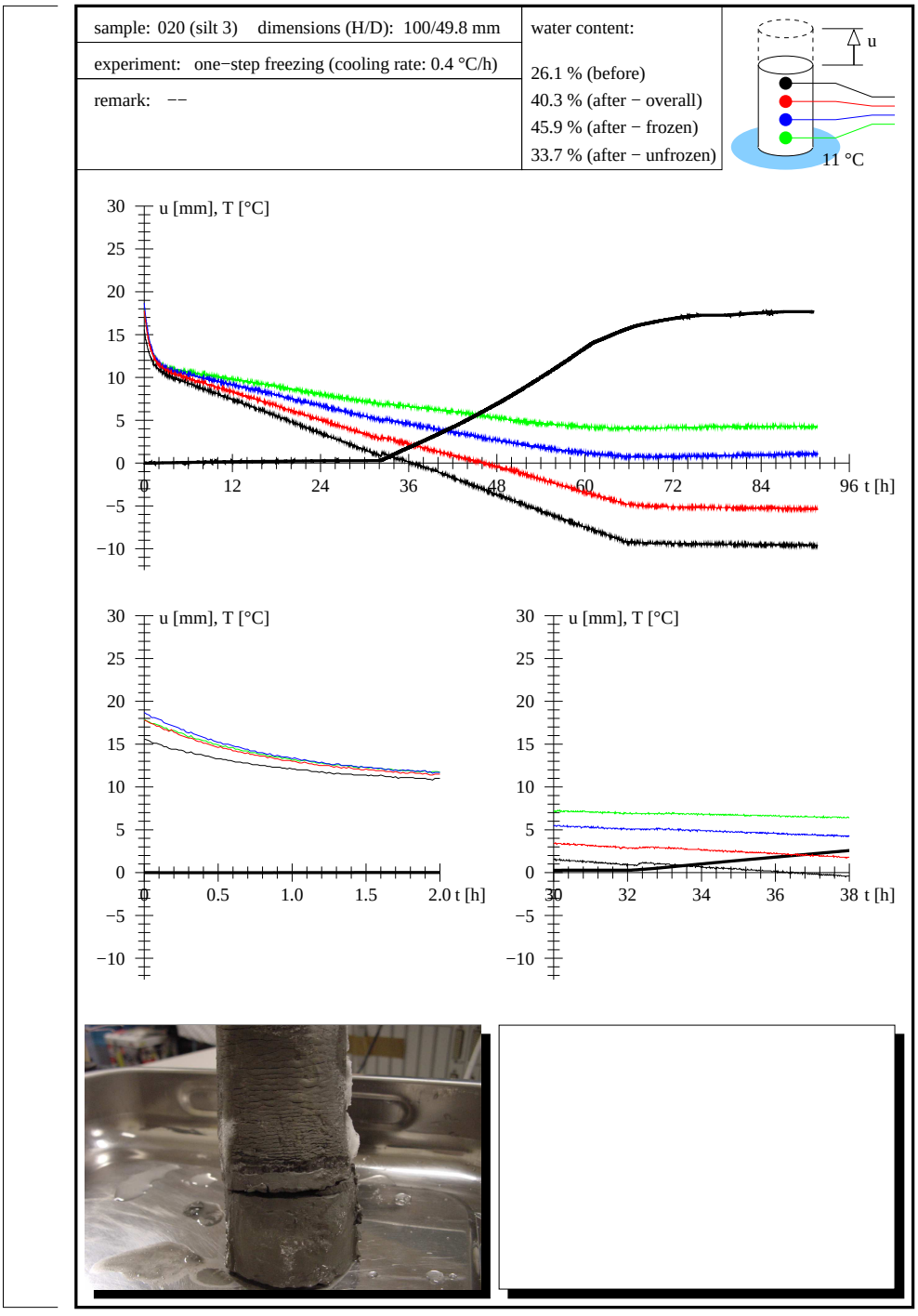

Figure 16: Results for experiment 20

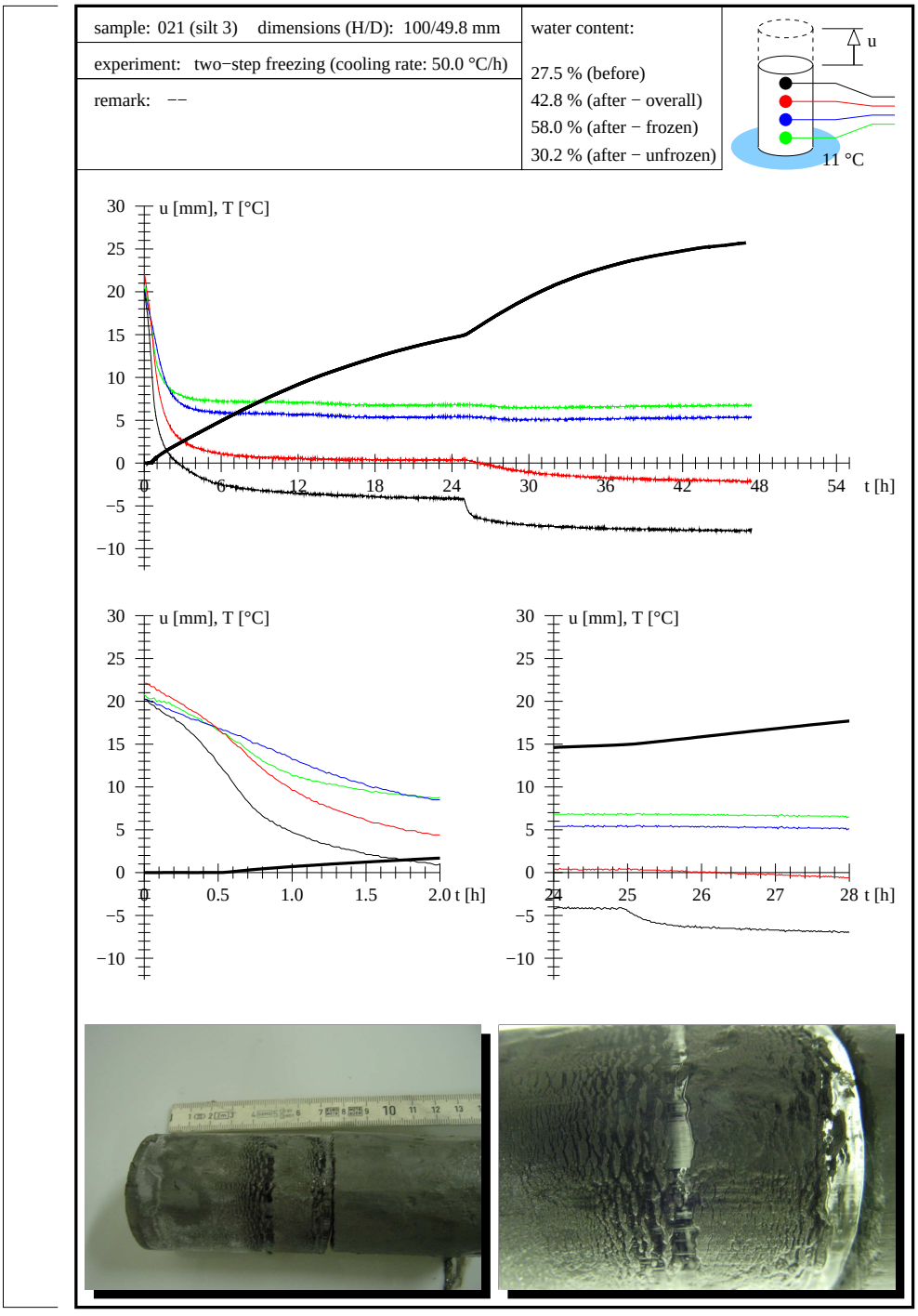

Figure 17: Results for experiment 21

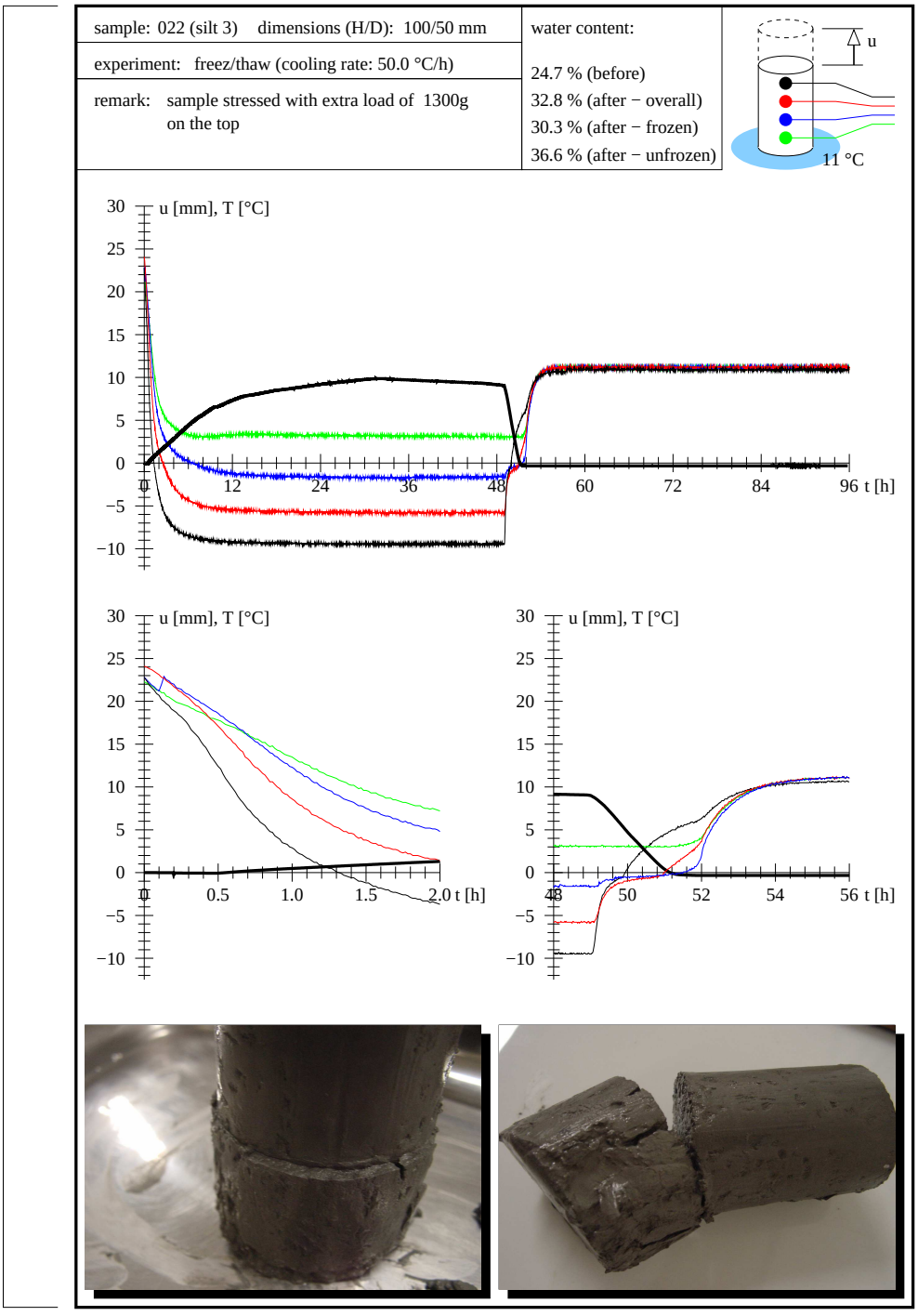

Figure 18: Results for experiment 22

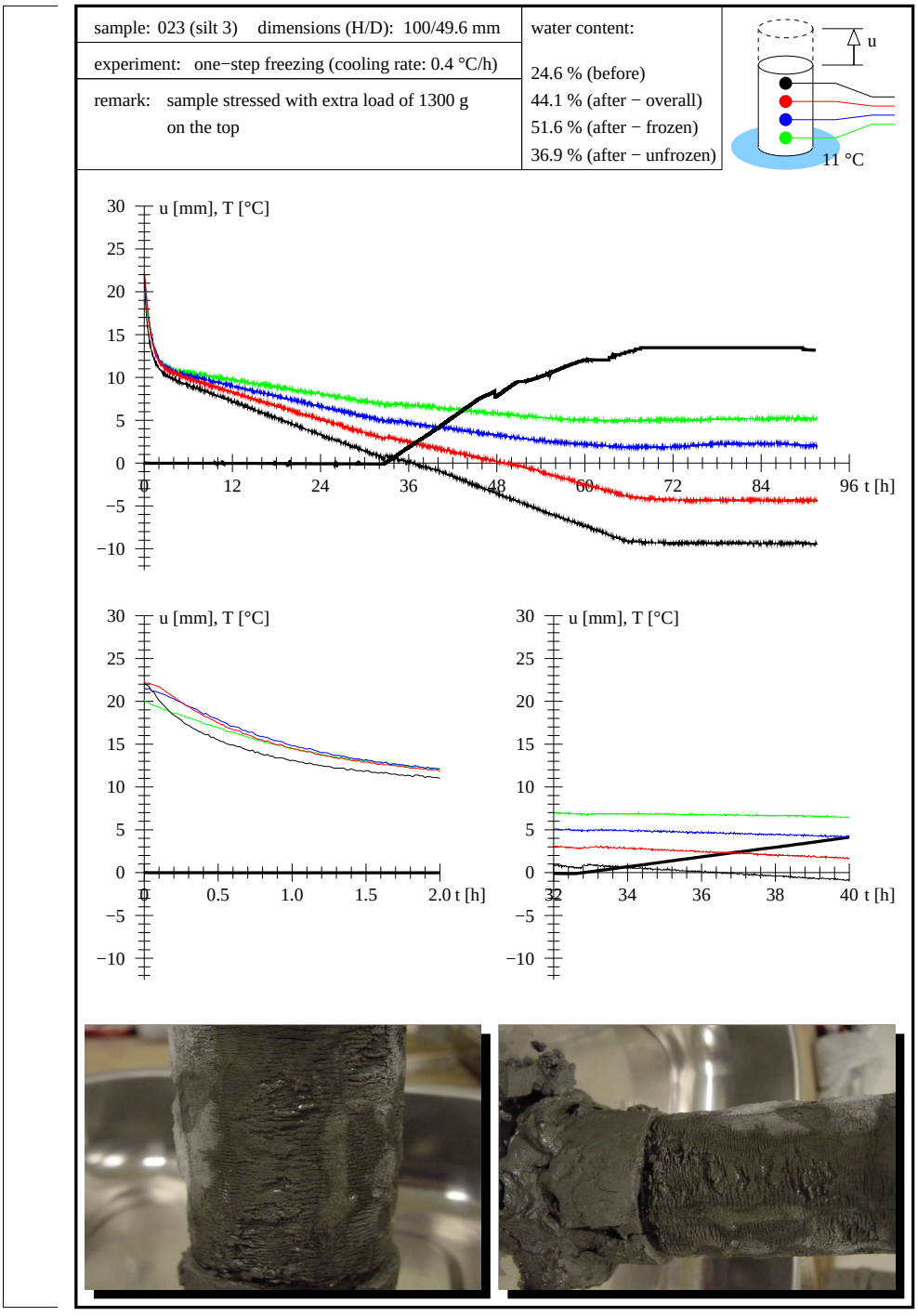

Figure 19: Results for experiment 23

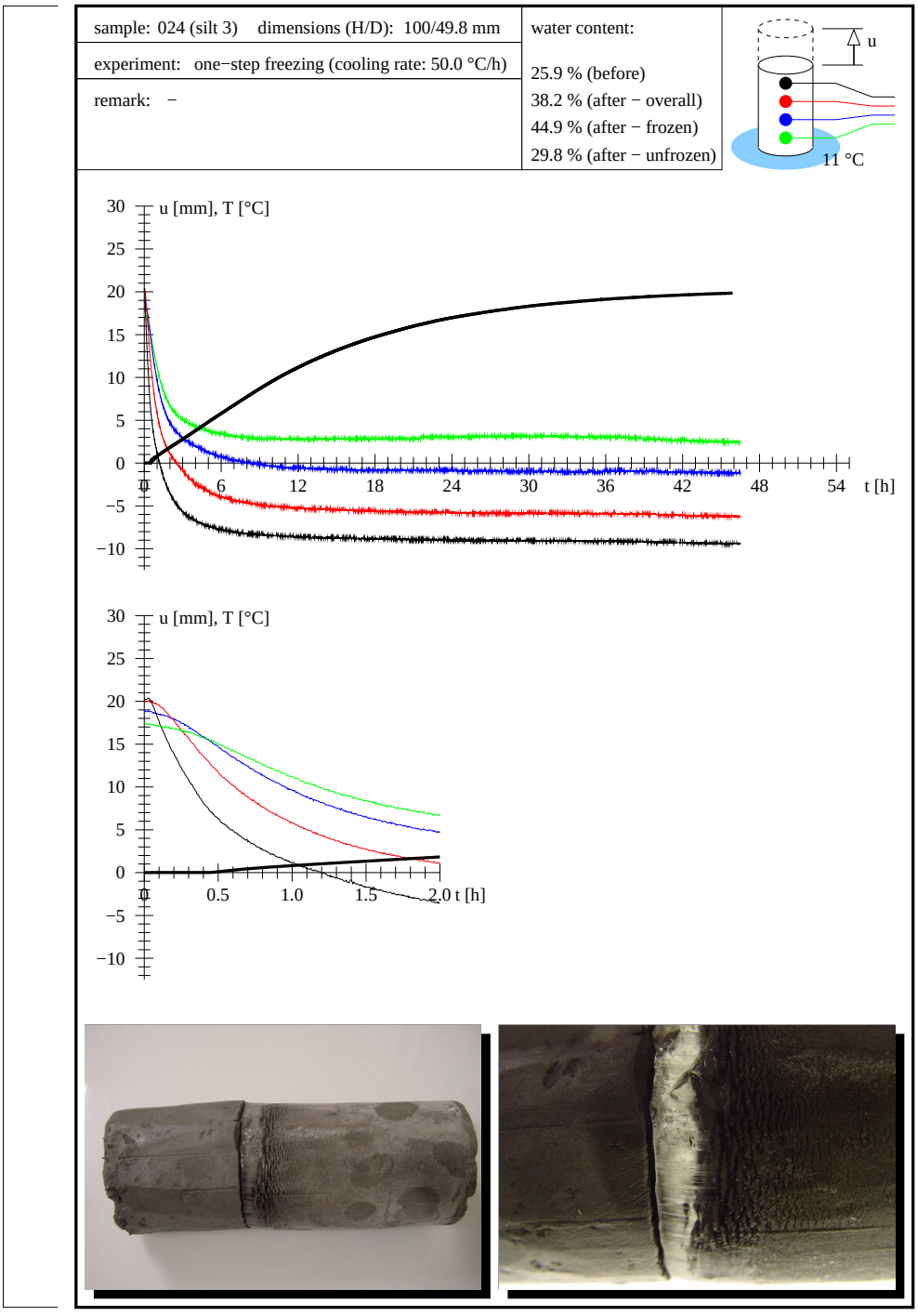

Figure 20: Results for experiment 24

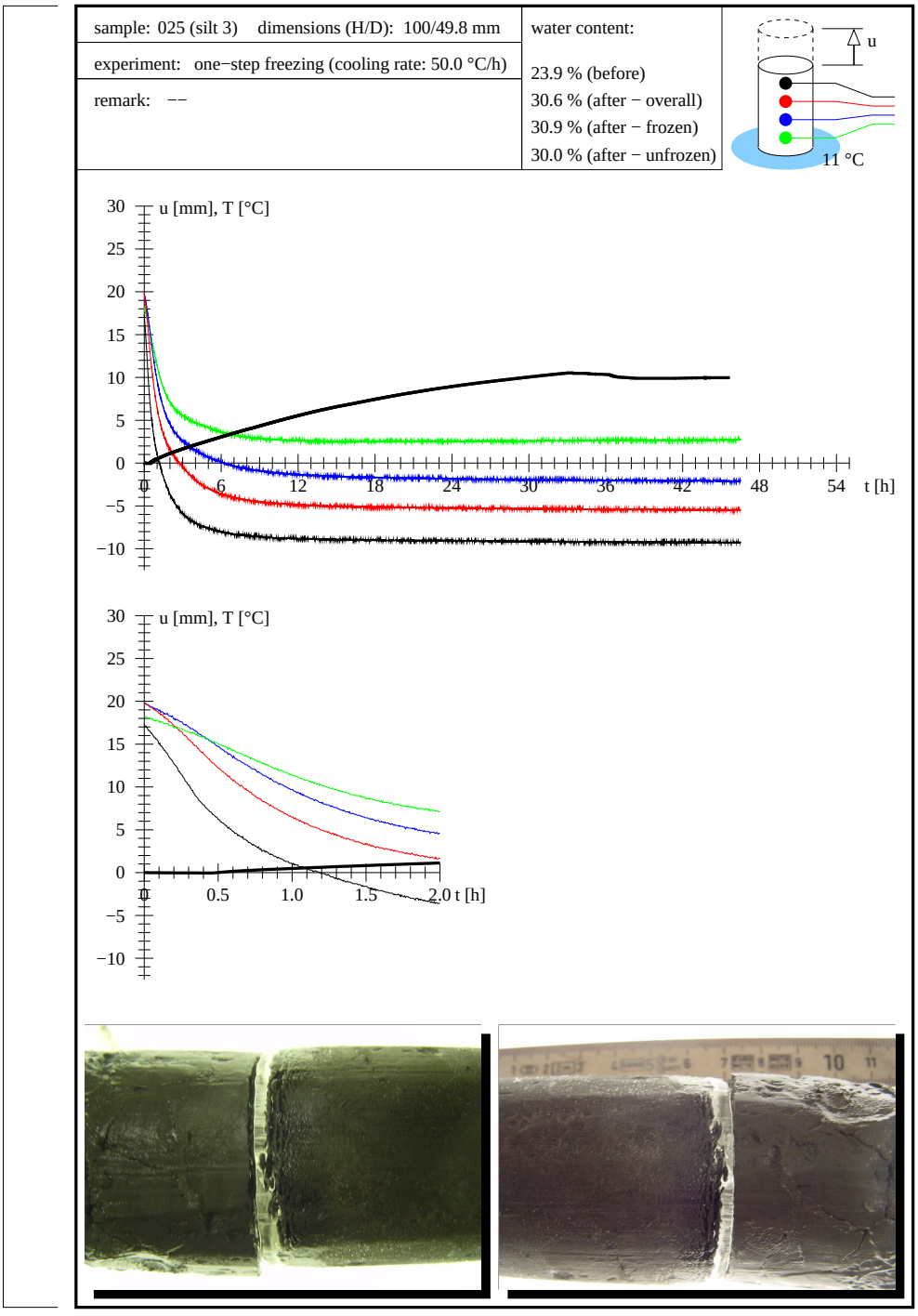

Figure 21: Results for experiment 25

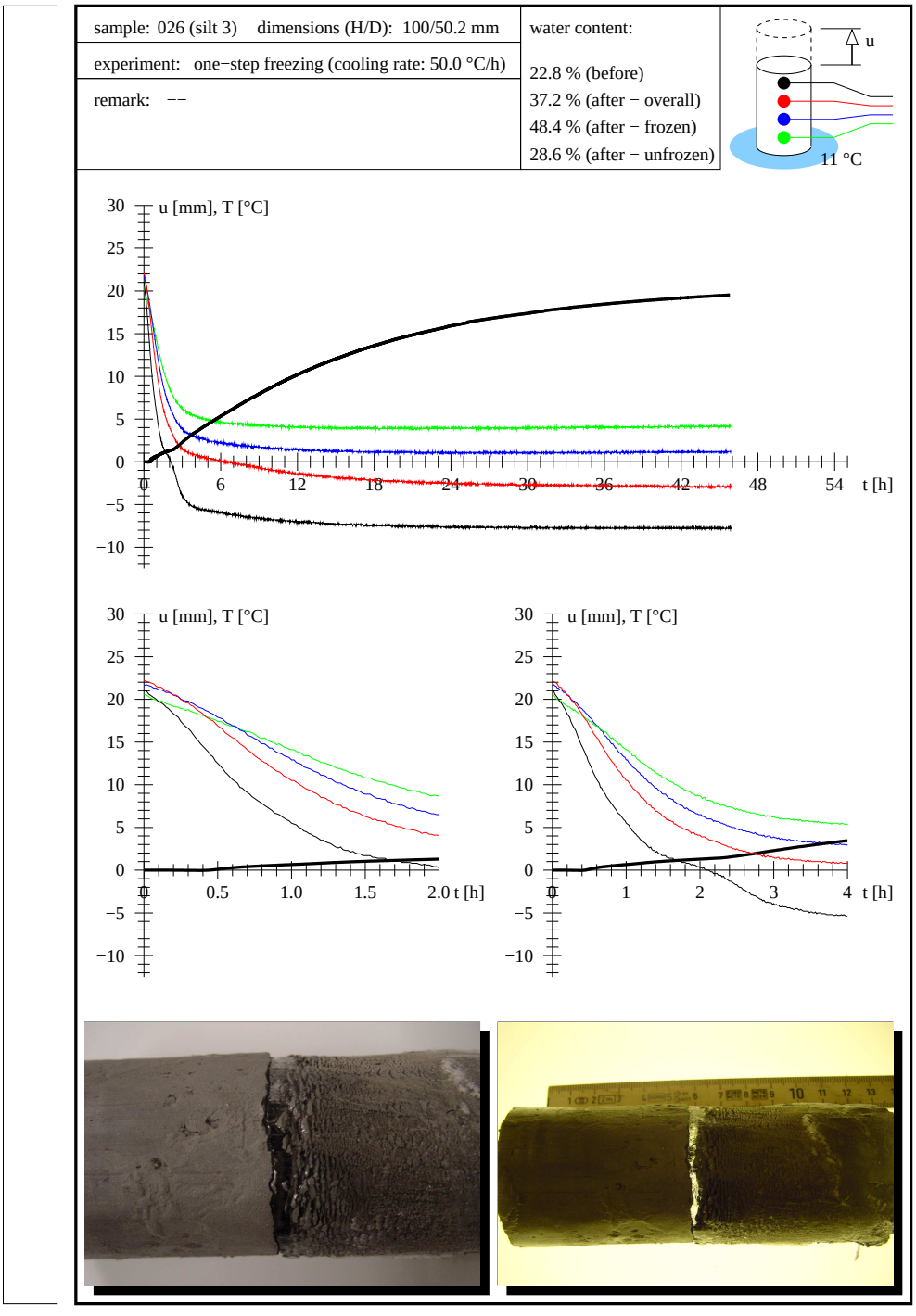

Figure 22: Results for experiment 26

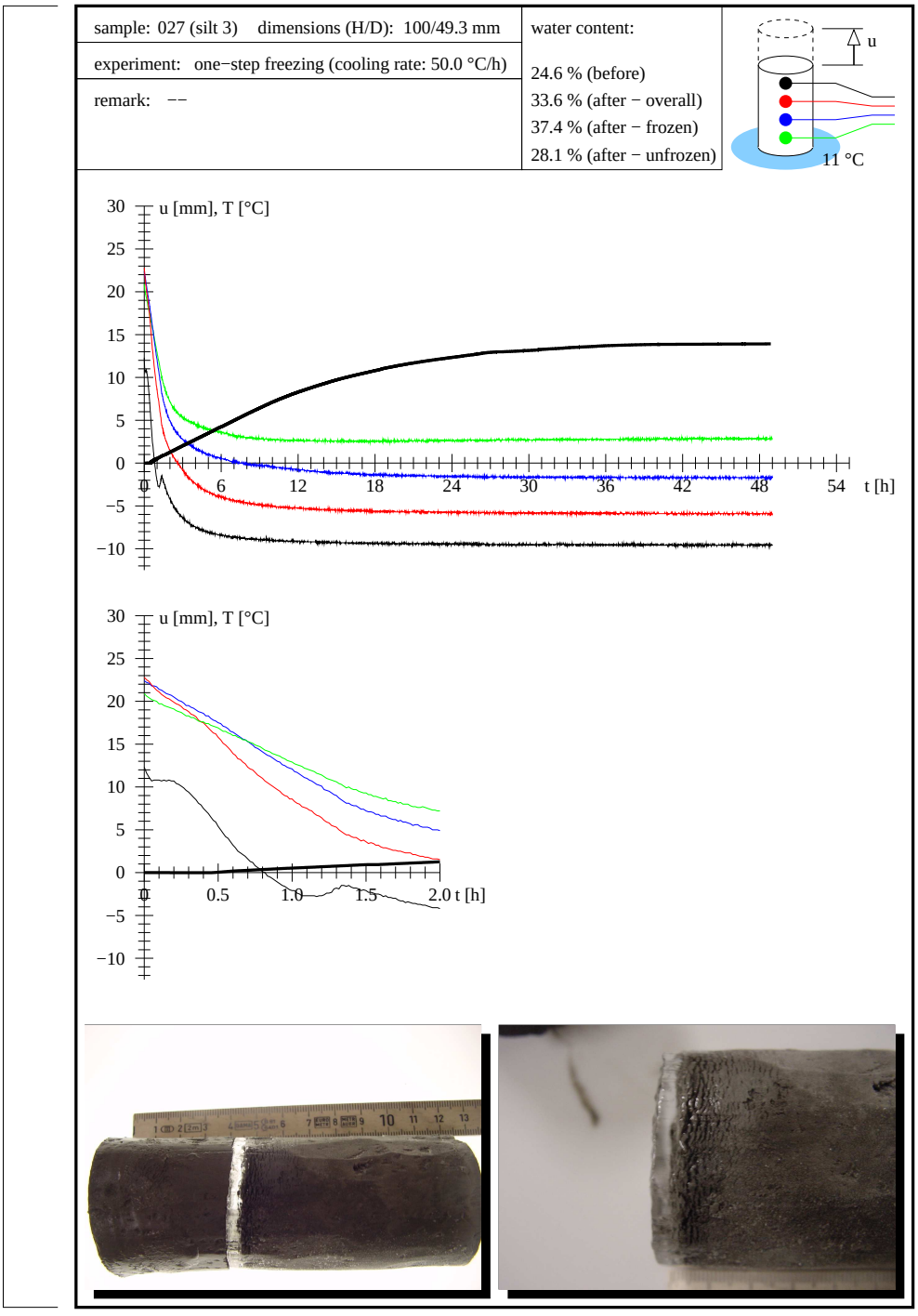

Figure 23: Results for experiment 27

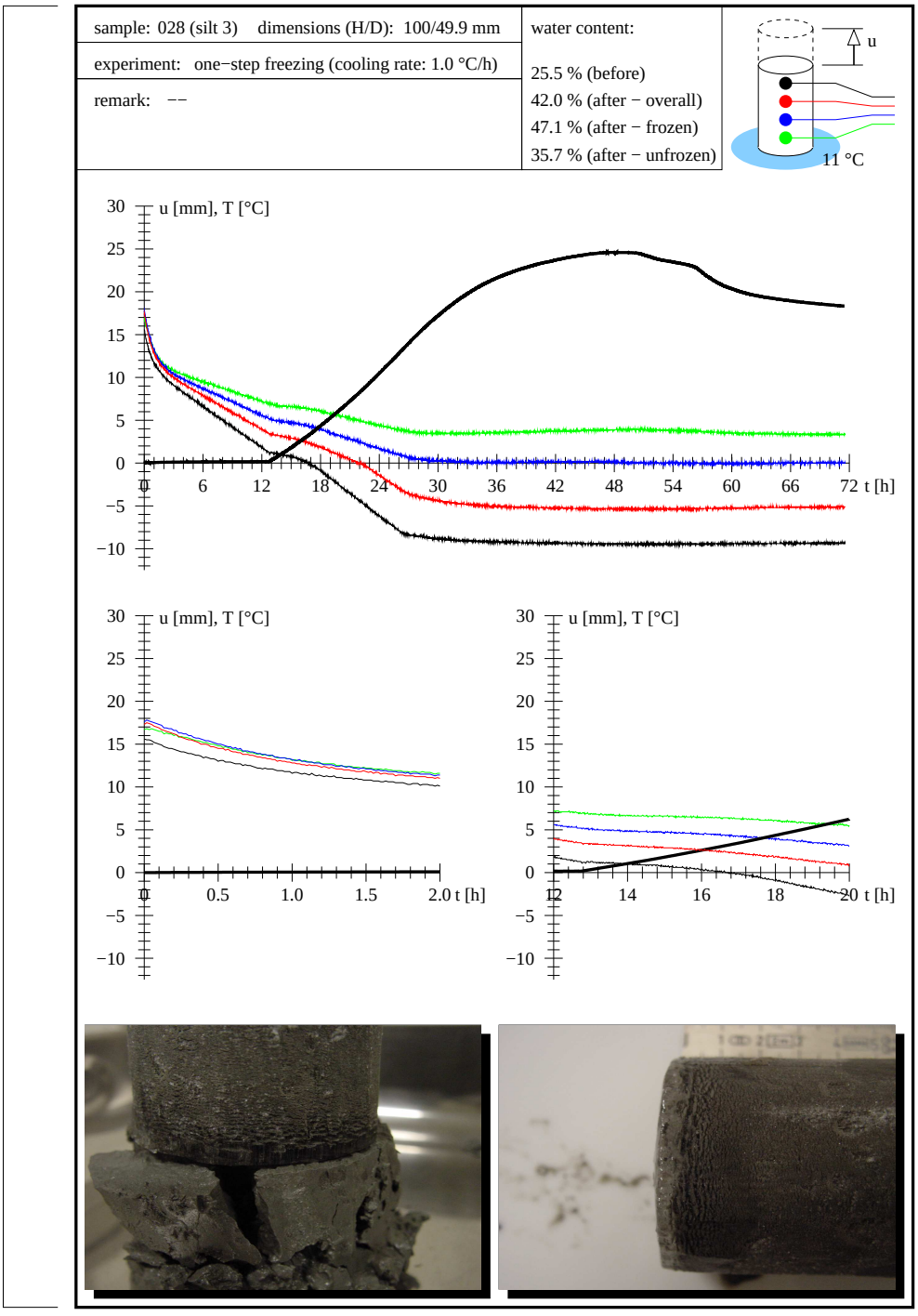

Figure 24: Results for experiment 28

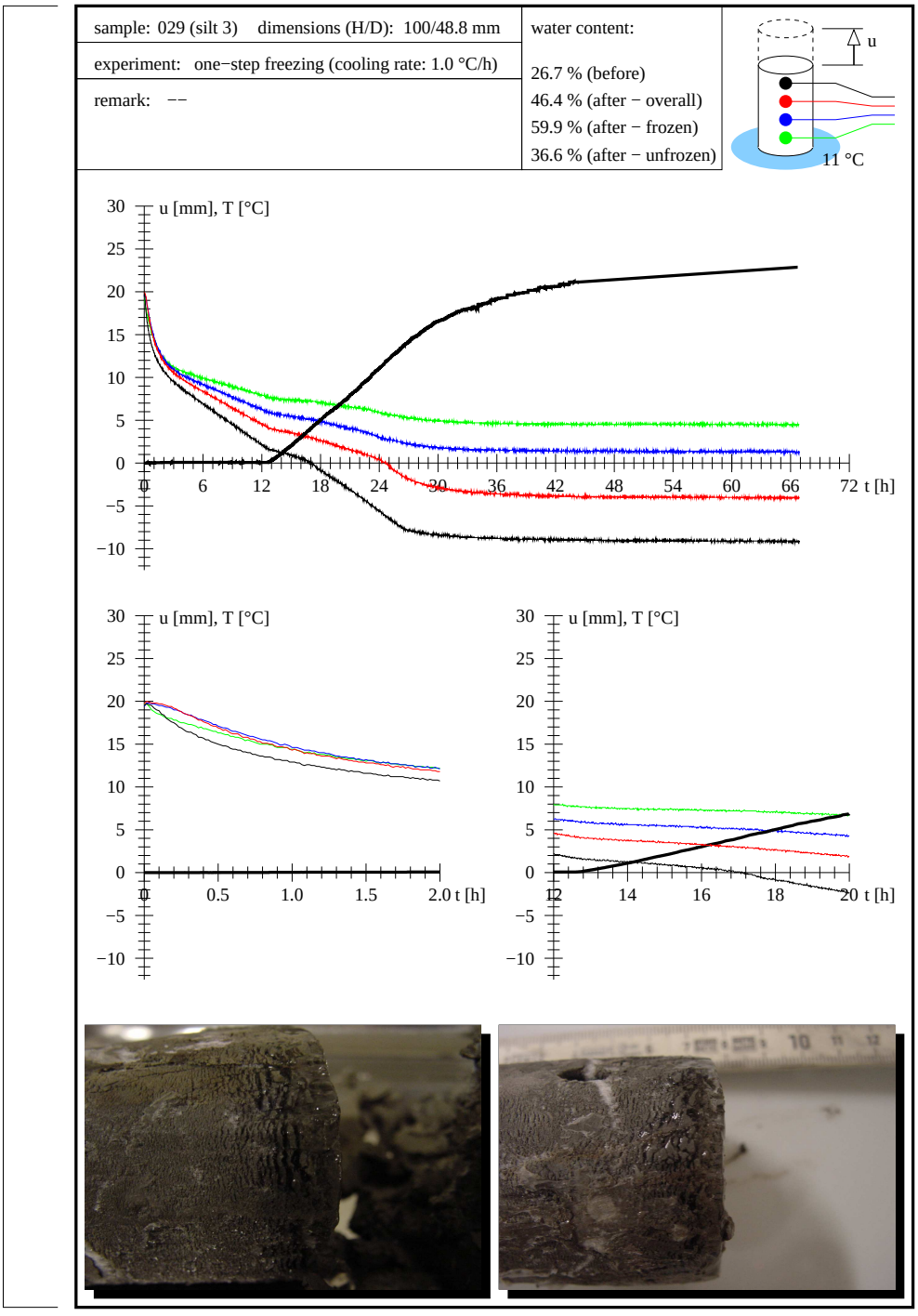

Figure 25: Results for experiment 29

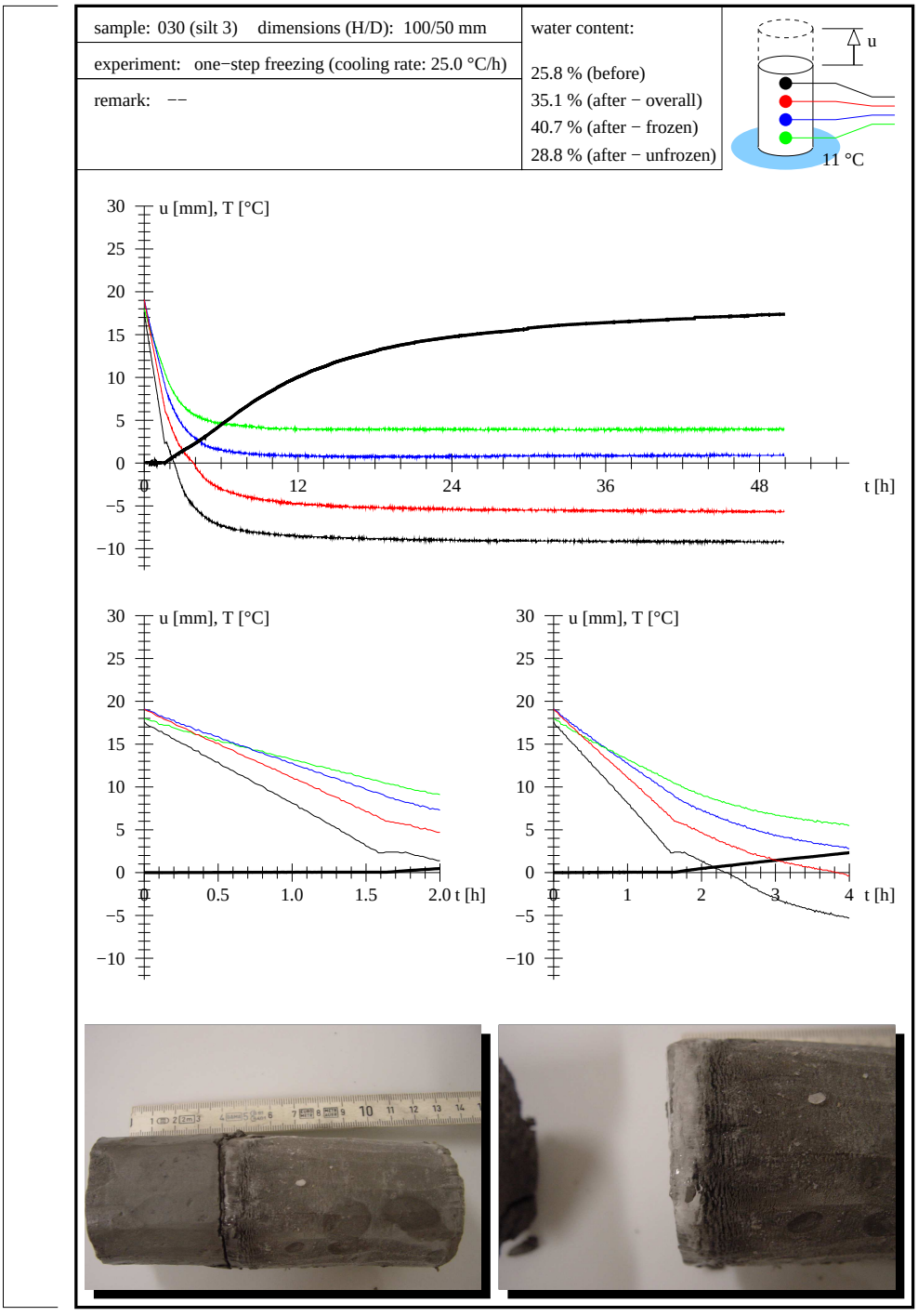

Figure 26: Results for experiment 30

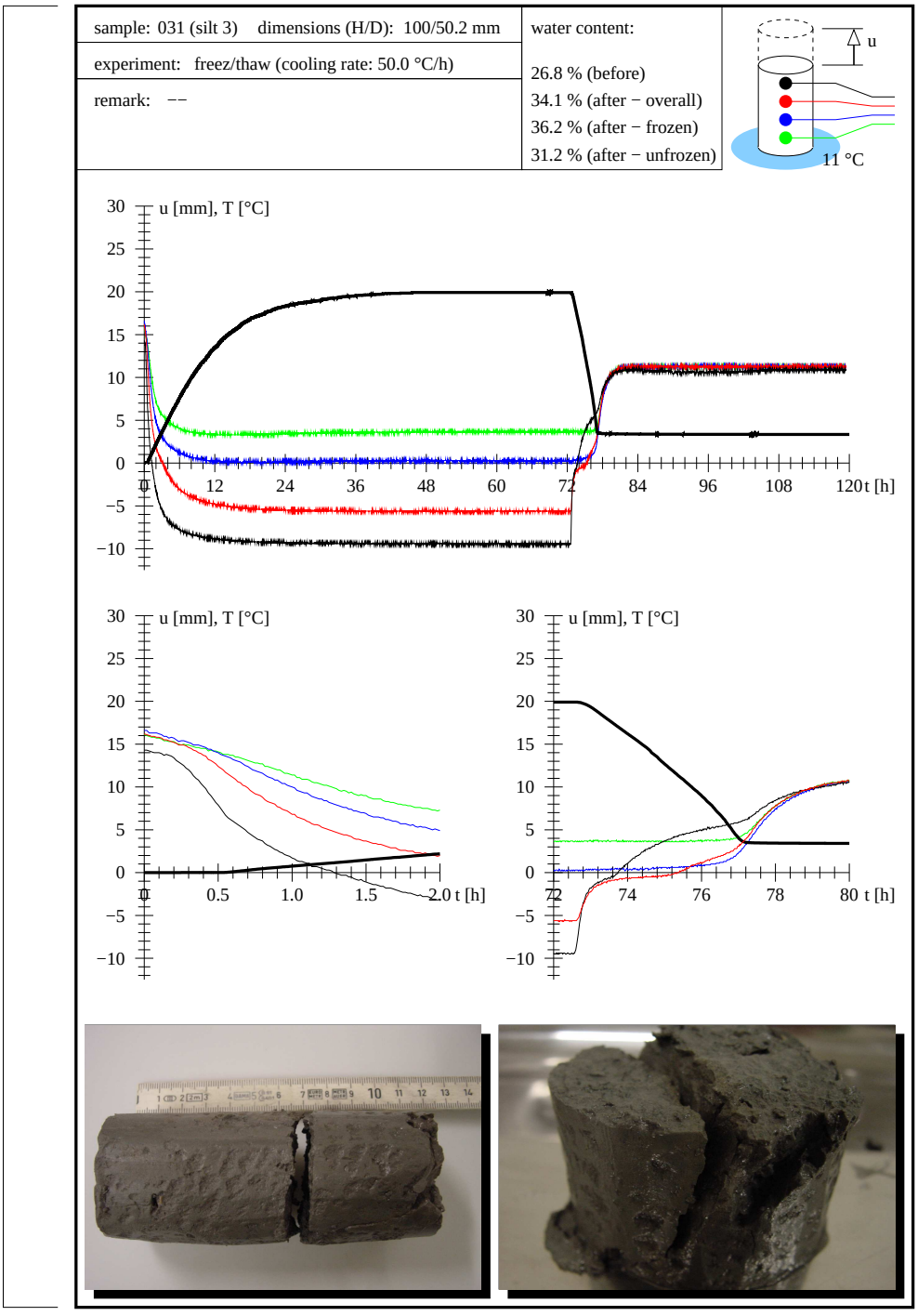

Figure 27: Results for experiment 31

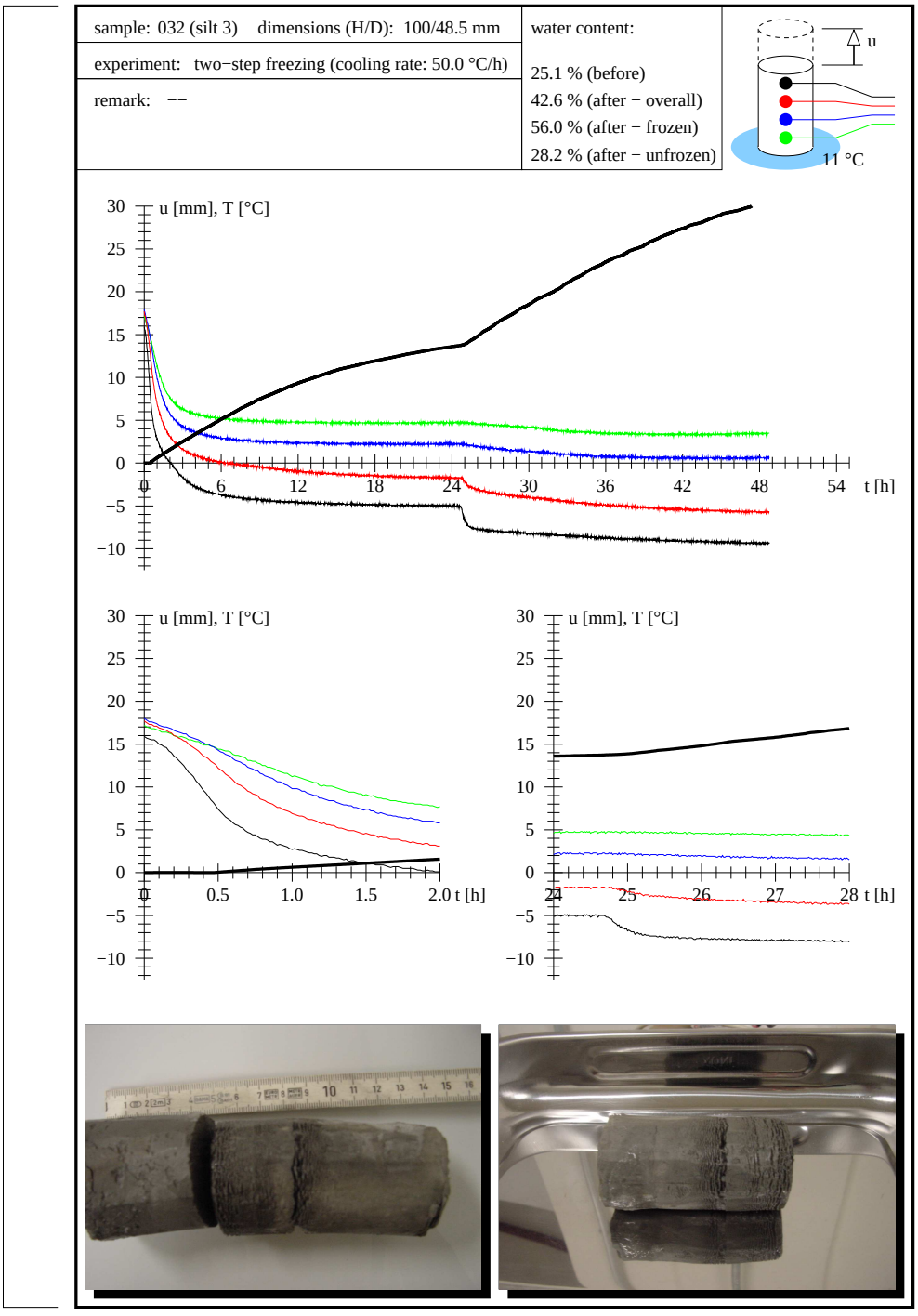

Figure 28: Results for experiment 32

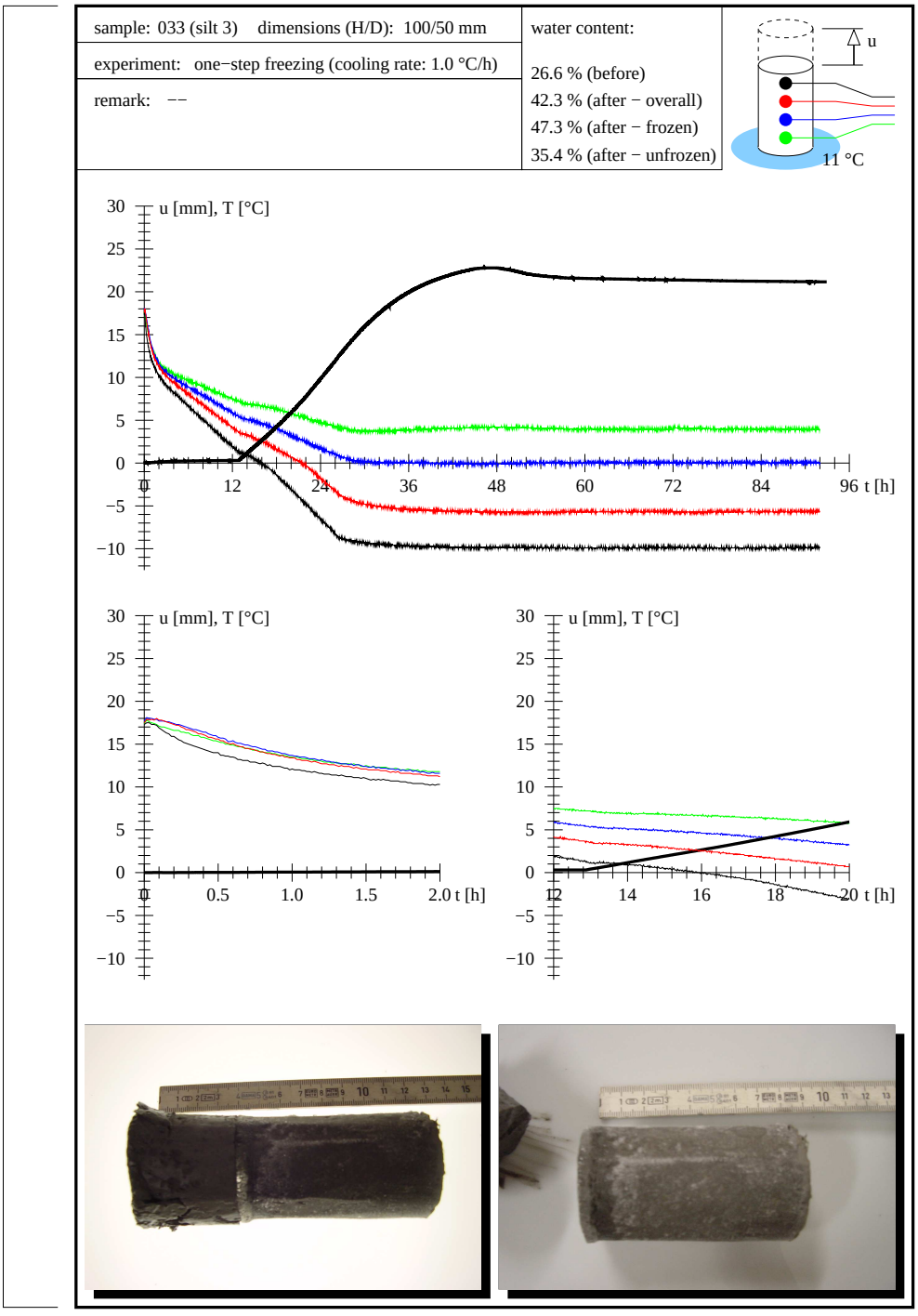

Figure 29: Results for experiment 33